UNIVERSITÀ DEGLI STUDI DI PADOVA

Dipartimento di Ingegneria Industriale DII

Corso di Laurea Magistrale in Ingegneria Aerospaziale

Design of a Vertical Test Bench for Hybrid Sounding Rocket Characterization

Relatore: Prof. Daniele Pavarin

Correlatore: Dr. Francesco Barato

Laureando: Tiziano Cecchetti, Matricola: 1156832

Padova, 11 ottobre 2019

Anno Accademico 2018/2019

Firma studente *Firma relatore*

Abstract

L'Università di Padova, assieme alla sua compagnia spin-off T4i, sta sviluppando un razzo-sonda spinto da un sistema ibrido che utilizza un grano di paraffina come combustibile e perossido di idrogeno come ossidante. L'obiettivo del progetto consiste nel lanciare il razzo all'inizio del 2020 fino a un'altitudine di circa 10 km allo scopo di validare la tecnologia ibrida messa a punto finora. L'autore di questa tesi ha partecipato alla progettazione di alcune parti del motore. Poiché lo sviluppo del razzo deve anche includere dei test di alcune componenti e dell'intero motore, sono necessari appositi banchi da test. L'apparato da test per il motore, disposto orizzontalmente, è già stato sviluppato e utilizzato più volte dalla T4i. Tuttavia, alcuni sottosistemi necessitano di essere testati separatamente: la linea fluidica, la cui funzione è immagazzinare il perossido di idrogeno e iniettarlo nel motore, e il reattore catalitico, la cui funzione è decomporre il perossido di idrogeno prima di iniettarlo in camera di combustione. L'obiettivo di questa tesi è quello di fornire una descrizione dettagliata di requisiti, design e dimensionamenti di due banchi da test verticali, uno per la linea fluidica e uno per il reattore catalitico del razzo-sonda. La tesi è divisa in sei parti: l'introduzione fornisce una descrizione generale di razzi-sonda, sistemi a razzo ibridi e banchi da test; il capitolo successivo descrive il razzo-sonda, ponendo particolare attenzione al design della linea fluidica e del reattore catalitico; nel terzo capitolo sono spiegati gli obiettivi, i requisiti e le procedure della campagna di test; nel quarto capitolo sono descritti in dettaglio design e dimensionamenti dei due banchi da test; lo stato del progetto e i suoi sviluppi futuri sono discussi nel quinto capitolo; infine, la conclusione riassume i risultati della tesi.

Abstract

The University of Padua, together with its spin-off company T4i, is developing a sounding rocket propelled by a hybrid system using a paraffin grain as fuel and hydrogen peroxide as oxidizer. The aim of the project is to launch the rocket at the beginning of 2020 up to an altitude of about 10 km in order to validate the hybrid technology developed thus far. The author of this thesis participated in the design processes of some of the motor parts. Since the rocket development must also include tests for some of its components and for the entire motor, specifically made test benches are needed. The motor test stand, which has a horizontal layout, has been already developed and repeatedly used by T4i. However, some subsystems need to be tested separately: these subsystems are the fluidic line, whose function is to store the hydrogen peroxide and inject it into the motor, and the catalytic reactor, whose function is to decompose the hydrogen peroxide before injecting it in the combustion chamber. The aim of this thesis is to provide a detailed description of requirements, design and sizing processes of two vertical test benches, one for the fluidic line and one for the catalytic reactor of the sounding rocket. The thesis is divided into six parts: the introduction provides a general description of sounding rockets, hybrid rocket systems and test benches; the next chapter describes the sounding rocket, paying particular attention to the designs of the fluidic line and the catalytic reactor; in the third chapter goals, requirements and procedures of the test campaign are explained; in the fourth chapter the design and sizing processes of the two test benches are described in details; the status of the project and its future development are discussed in the fifth chapter; finally, the conclusion summarizes the results of the thesis.

INDEX

Chapter 1

Introduction

1.1 Sounding Rockets

A sounding rocket (also known as research rocket) is a sub-orbital rocket used for scientific measures and experiments [1]. Sounding rockets have been used since the late 1950s and were originally utilized for meteorological and upper atmosphere studies. These rockets take their name from the nautical name “to sound”, which means “to take measurements”.

They are generally made up of 3 major parts: the propulsion system (generally solid or, recently, hybrid), the service system (rate control, telemetry module, recovery system), and the scientific payload (carrying the instruments to conduct measurements or experiments).

As previously mentioned, sounding rockets are sub-orbital carriers, which means that they do not end up orbiting around the Earth, but follow a parabolic trajectory from launch to landing [2].

In the last 30 years sounding rockets have become increasingly popular for the following reasons:

- *They provide unique conditions for scientific research*: the parabolic motion at high altitude is useful for peculiar scientific experiments and measurements (as in geophysical and meteorological research). Generally, after depleting all the propellant, the propulsion system separates from the payload and falls to the earth, while the latter continues to fly in space. It is during this flight (generally lasting between 5 and 20 minutes) that experiments and measurements take place. The presence of low microgravity environment also provides optimal conditions for many of those tasks (vibration-free conditions). Data are often collected and transmitted to Earth by

telemetry systems. On top of that, often the payload lands safely on Earth by means of a parachute and is therefore recovered.

- *They provide a relatively easy, quick and cheap access to space*: since the payload doesn't go into orbit, a sounding rocket doesn't need particularly complex propulsion system and telemetry. For example, a hybrid liquid-solid propulsion system can be used instead of a more performing, solid-only motor: the former has separated oxidizer and fuel, reducing risks of explosion, which translates into a safer (and therefore cheaper) system. For all these reasons mission costs and development times are considerably lower than those for launches into orbit. On top of that, payload recovery is possible, meaning that experimentation and payload development costs can be spread over multiple missions.
- *They are useful for devices validation and new technologies development*: sounding rockets provide an efficient way to test new systems and devices. Relatively low costs also promote innovation: non-sufficiently developed instruments and technologies are generally too risky to be tested in an expensive, full-blown satellite-program, so they are previously tested on a sounding rocket.
- *Learning*: sounding rockets are excellent learning opportunities for students and novice engineers to follow a research project in all its phases, building precious experience for a future career [1].

1.2 Hybrid Propulsion

Three main types of chemical rocket exist: liquid, solid and hybrid. The subdivision is related to the phase of the stored propellant. In a liquid rocket the liquid oxidizer and the fuel are stored in the respective tanks and injected in the combustion chamber. In a solid rocket the fuel and oxidizer are mixed together in a solid matrix that is stored directly in the combustion chamber. Systems where the propellant is stored in a gaseous or gelled form and then injected in the combustion chamber are assimilated to liquid systems.

In a hybrid rocket one component is stored as a liquid (or a gas or a gel) in a tank and the other is a solid placed inside the combustion chamber. Usually the liquid is the oxidizer and the solid is the fuel (the so-called classical configuration). However also reverse hybrid could exist where the liquid is the fuel and the solid is the oxidizer. Up to now (and almost certainly in the future) the classical scheme is the most utilized because liquid oxidizers have higher energetic

content than solid ones. Exceptions are cryogenic solid oxidizers like solid oxygen, the solidified version of liquid oxygen. However solid cryogenic storage is even more complex than its liquid counterpart. Moreover, almost infinite combinations of solid fuels exist for hybrid propulsion while generally the choice of oxidizer is much more limited (both in solid and liquid phase) and in this case the manufacturing of the grain requires a binder. No advantages seem to come from the reverse approach.

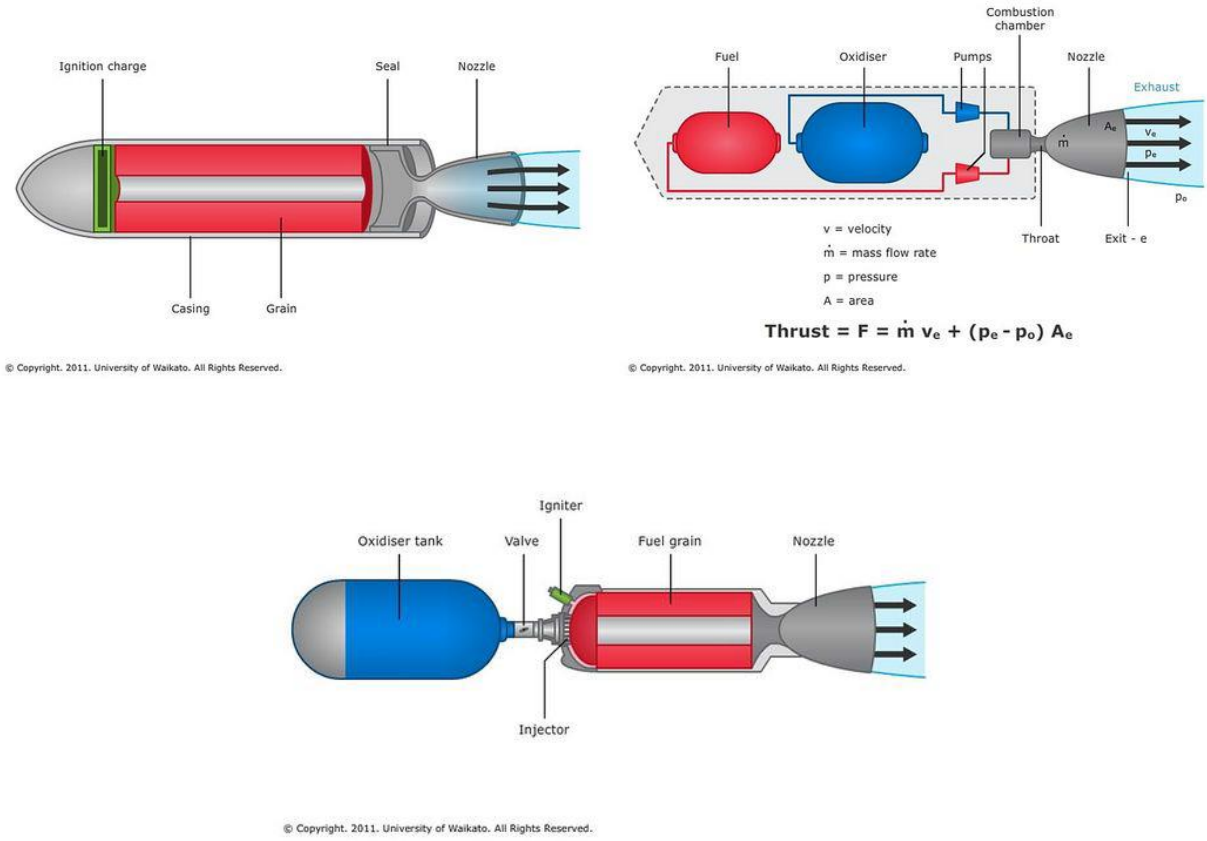

Figure 1.1 - Solid (upper left), liquid (upper right), and hybrid (bottom) rocket schematics.

Solid and liquid motors have monopolized the military and commercial market up to now, leaving only a limited room in research programs (and more recently in amateur/academic activities) to hybrid ones. The reason for that is related to the peculiar characteristics of the three propulsion systems coupled with the requirements of the cold war era.

Solid rockets are very simple, ready to launch and could reach the highest value of impulse density making them ideal for volume constrained applications such as military weapons,

sounding rockets and boosters. Liquid rockets can reach the highest specific impulse; they can be stopped and started multiple times in flight making them ideal for launchers and spacecrafts.

Hybrid systems have long been considered an intermediate case between the two, not showing a clear advantage relative to either extremes in a performance-oriented environment.

Moreover, the greatest advancement of rocket propulsion was done in the 50s-60s. During that period almost every solution was designed and tested. After an initial assessment only the most promising technologies were chosen for extensive further work. Some hybrid issues were still not solved at that time (and partially today). Hybrid rockets maturity, as well as other propulsion technologies, still suffers nowadays for being excluded from that choice. After the golden age of space, investments have decreased, preventing today's hybrid systems from making a considerable step towards maturity.

However, the space business has been slowly changing in the last decades (and it is expected to change even more in the future, hopefully). Today more attention is paid towards safety, reliability, cost and environmental friendliness. This in turn has paved the way for a renewed interest for hybrid propulsion favored by its inherent characteristics.

First it is necessary to highlight that hybrid rocket combustion is much different from solid or liquid rocket combustion. In a solid rocket the fuel and the oxidizer are intimately pre-mixed in the grain at a specific oxidizer/fuel (*O/F*) ratio. The propellant burns with a thin flame next to the surface (few μm). The amount of propellant depends on the linear regression of the grain surface that in turns generally depends on chamber pressure. In a liquid rocket the oxidizer and the fuel are injected in the combustion chamber. The average *O/F* ratio is dependent simply on the ratio between the two mass flows. In a hybrid rocket the oxidizer is usually injected at the head end of the combustion chamber, mixing later with the pyrolized fuels in a macroscopic turbulent diffusion flame. The regression of the fuel is dependent on the convective heat exchange from the flame to the surface.

In a liquid rocket the total mass flow and *O/F* ratio can be perfectly (at least nominally) controlled. In a solid rocket the *O/F* ratio is fixed by the grain composition, so the propellant mass flow, being dependent only on the chamber pressure, can be defined with a proper design of the fuel grain. For both propulsion systems the motor *O/F* ratio and propellant mass flow are independent variables.

On the contrary only the oxidizer mass flow can be directly controlled in a hybrid rocket, while the fuel mass flow is dependent on the complex physics of its coupled fluid

dynamic/combustion. The regression rate in a hybrid varies with time and space. The motor *O/F* ratio and total mass flow are not independent variables. This complex coupling between motor parameters, the difficult prediction and scaling, the dependence on space of hybrid regression makes hybrid physics and design more complex and difficult to deal with. This added complexity has always hampered the realization of a competitive hybrid rocket unit. Moreover, in a liquid rocket motor the oxidizer and fuel are intimately mixed in the vicinity of the injector to form a combustible mixture. As previously said, in a solid rocket the two components are already mixed in a single solid phase. In both cases, therefore a uniform mixture is achieved in the combustion chamber. In a hybrid motor the oxidizer and the fuel enter the chamber from different sides, mixing slowly in the diffusion flame. This characteristic is also responsible for the usually lower performances of hybrid rockets. However, due to its peculiar characteristics, hybrid propulsion presents several advantages compared to solid and liquid systems.

Here's a general list:

- *Safety:* the fuel is inert and can be manufactured, transported, and handled safely as standard commercial products. The system is non-explosive because an intimate mixture of oxidizer and fuel is not possible. NASA classifies hybrid LOX-HTPB (liquid oxygen/hydroxyl-terminated polybutadiene**)** combination as 0 *TNT* equivalent. In case of an abort procedure the motor can be stopped turning off the liquid flow. Unlike solid rockets, fuel grain cracks are not catastrophic because burning occurs only when the fuel encounters the oxidizer flow. Hybrid combustion is diffusion controlled so it's usually not pressure-sensitive as in liquid and solid systems. This in turn makes hybrid propulsion less prone to catastrophic failures due to thermoacoustic instabilities or other parameters shifting outside nominal conditions. Hybrid failures are usually benign in nature.
- *Reliability*: a hybrid rocket requires roughly only half of the components of a liquid motor. Compared to solid motors, the grain is much more insensitive to defects. Being diffusion-controlled, hybrid combustion is more tolerant than in both solid and liquid rockets.
- *Mass flow control*: the engine can be throttled by modulating only the liquid flow rate. This is simpler than in liquid propulsion where two liquids have to be modulated simultaneously. This doesn't require only double plumbing but also synchronization

between the two flows. The engine can be started and stopped several times if a suitable ignition system is used.

- *Propellant versatility*: the selection of propellants is (nominally) much greater than with either solid or liquid systems. However, the focus has been directed to a narrower band of combinations. Liquid oxidizers are more energetic than solid oxidizers used in solid propulsion. Metals particles can be added easily in a solid matrix to improve performances; this doesn't apply to liquid systems, where the formation of slurries implies several drawbacks, such as sedimentation and issues in feeding-pressurization and atomization.
- *Temperature sensitivity*: because the temperature effect on the burning rate is small (as in liquid systems), ambient launch temperature variations have little effect on operating chamber pressure. Thus, the concern (typical for solid rockets) in designing for a maximum expected operating pressure (*MEOP*) is greatly reduced (this claim is partially negated in case of self-pressurized oxidizer).
- *Propellant specific impulse and density*: hybrid rockets have a theoretical specific impulse higher than solid ones and comparable to liquid ones, except for those using cryogenic fuels. With the addition of metals in the fuel grain the specific impulse of hybrid systems can be even higher than the one of liquid rockets of the same class. Indeed, the highest possible experimental I_{sp} has been achieved with a tribrid configuration. The density impulse is lower compared to solid systems, but nominally higher compared to liquid ones, particularly for metal loaded fuels.
- *Low cost*: considering the components composing the inert mass fraction of a rocket propulsion system the cost of a hybrid should stay between the more complex and expensive liquid systems and the simpler and cheaper solid ones. However, the total operational costs of a hybrid should take advantage of its safety characteristics and inert propellant. Manufacture of the fuel can be done in a commercial facility that does not require the large areas and many solid-propellant manufacturing facilities. Furthermore, the system can tolerate large design margins, resulting in lower fabrication costs. Transport and handling costs are greatly reduced.

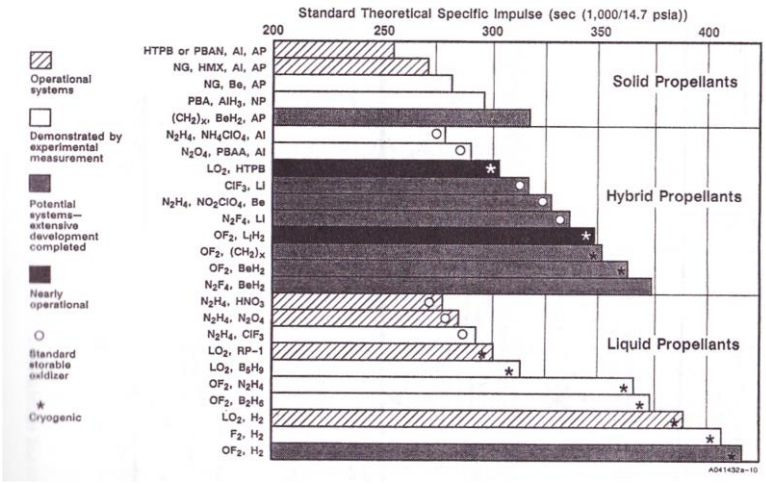

Figure 1.2 - Theoretical I_{sp} for solid, liquid, and hybrid rocket propellants.

- *Low environmental impact*: several low-polluting propellant combinations are possible for hybrid propulsion; many of them have been commonly used.

Unfortunately, hybrid rockets have also some distinct disadvantages, such as:

- *Low regression rate*: hybrid systems are generally characterized by low regression rates. This in turn requires a large burning area to achieve the required thrust. This large area could be obtained with a very long combustion chamber resulting in a too long motor. Moreover, the resulting web thickness is small concurring to a very poor volume loading (fuel volume/total volume). The problem is increased with scale-up for several reasons. First, the port area is proportional to the thrust while the web thickness is proportional to the product of the burning time with the average regression rate. Usually, burning time increases with scale-up much more slowly than thrust, resulting in a much higher ratio between internal diameter and web thickness. Moreover, hybrid regression rate decreases with scaling, exacerbating the issue. A better alternative is the use of a multiport grain. However, multiport design implies several other problems, like high residuals, deviations of regression rate for different ports, change of the port shape with time, structural issues (e.g. need for web support), generally higher *O/F* shift than single port design (even stronger if merging of ports is allowed), increased complexity and manufacturing costs. Several ways to increase the regression rate have been proposed and tested; almost no one has reached operational status, but some of them present an interesting potential for the future, particularly for up to medium scales.

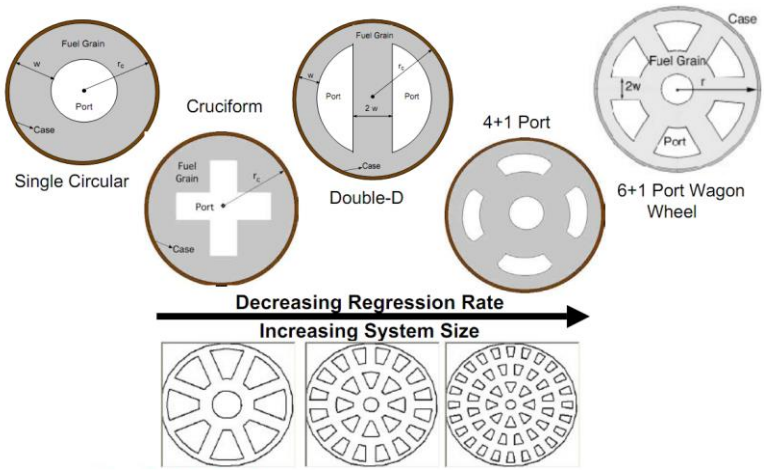

Figure 1.3 - Examples of multiport grain configurations.

- *Packaging issues*: in a liquid rocket the large part of the system is composed by the storage propellant tanks. This is increased particularly for low thrust to total impulse ratios (e.g. spacecrafts). Tanks can be easily packaged choosing different configurations in terms of tanks number, shape and positions. Solid rockets are composed mainly by the combustion chamber that encloses the solid grain (plus the nozzle). Several geometrical solutions are available for solid motors allowing to fulfill multiple different mission constraints (e.g. different *L/D* ratios), moreover the propulsion engineer can tailor the regression rate and the grain shape for the specific needs. In a hybrid rocket the liquid oxidizer can be easily packaged as in a liquid rocket. The hybrid combustion chamber geometry is dictated by the solid fuel envelope. Due to the complex dependency of the hybrid regression rate on several parameters (like oxidizer flux), it is not possible to easily alter geometries as in solid propulsion where the mass flow is readily related with the burning area. On the contrary in a hybrid motor the fuel mass flow changes even with a constant burning area. That's why a constant burning area (e.g. star shaped) grain produces a neutral burning in a solid while it's strongly regressive in a hybrid configuration [60] (inducing also a significant *O/F* shift for a constant oxidizer flow). For this reason, for hybrid rockets a star shaped grain is not an attractive option to increase the burning area and the volume loading as it is for solid ones. Usually hybrid combustion chambers tend to be slender. Often it is stated that this is related to the low regression rate and should not be a problem for low-thrust/long-duration applications. However, this is not completely correct. Considering a classical

design (single or multiport), even with a complete freedom on the regression rate it is difficult to design a performing system exceeding a certain ratio between the initial and final oxidizer flux (amount of *O/F* shift, max flux limited by flooding or exit Mach number, lower flux limited by chuffing etc.). This in turn fixes the ratio between the internal and external port diameter and consequently the required regression rate and *L/D* ratio (for a given motor *O/F*). Very "fat" hybrid motors are not likely possible for low-thrust/long burning time systems. An exception could be other alternative configurations like the vortex pancake which however bring its own problematics. Another important aspect compared to liquid rockets is that it is not possible to design a propulsion unit that can be used on different spacecrafts with different total impulse requirements because, again, the combustion chamber contains the solid fuel. On the contrary a liquid motor can be combined with different tanks to deliver different total impulses.

- *Combustion efficiency*: as previously said, a hybrid system tends to produce a rougher and less complete combustion compared to solid and liquid ones, causing a larger I_{sp} penalty compared to theoretical values.
- *O/F shift*: the impossibility to maintain the motor *O/F* ratio fixed at the optimal value leads to a decrease of the average specific impulse. Careful design can reduce these losses to less than 1%.
- *Slower transients*: ignition transients are generally slower for hybrid systems. The response to throttling is slower too. The combustion chamber of a hybrid is much bigger than an equivalent liquid because it must contain the solid fuels, moreover the chamber volume changes with time reaching its maximum value at the end of burning when the grain is consumed. Also, the thermal lag in the solid fuel changes with time and reaches its maximum towards the end. This prevents hybrid systems to be used when very accurate, repeatable, fast response is necessary (in which case hypergolic liquid mono-bipropellant operating in multi-pulse mode is preferred), but in general it should be no major issue.

The fact that, generally, theoretical hybrid figures (I_{sp}, ρI_{sp}) systems are intermediate between solid and liquid ones makes them less attractive when only few performance parameters must be maximized for a specific task. This was one of the reasons for the previously outlined discard of hybrid motors as main propulsion choice. The other fundamental aspect was the performance penalty caused mainly by the low regression rate

and related negative attributes. Finally, as already mentioned, the complex coupling of motor parameters makes hybrid rockets less attractive from an ideal design point of view. Other hybrid concepts have been conceived and (to a less extent) developed/tested to overcome conventional hybrid issues, but usually the added complexity or drawbacks of these solutions make them not sufficiently (or even less) attractive.

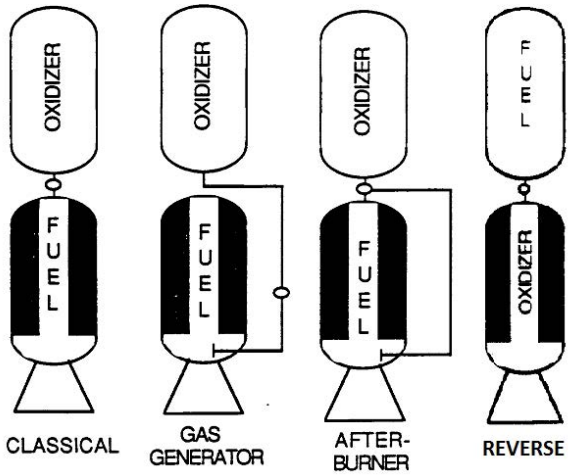

Figure 1.4 - Some alternative hybrid schematics.

One aspect to underline is that all the claimed advantages of hybrid propulsion are often not achievable for the same propulsion unit due to propellant choice or system configuration (this can be also partially attributed to the other two propulsion types to a less extent). Typical examples are the LEX sounding rocket or the *Firebolt* presented later. Moreover, some of the solutions proposed to solve specific hybrid issues negate other hybrid advantages. A typical example is the use of small amount of oxidizer in the fuel grain to increase the regression rate. Even if this solution is safer than a conventional solid propellant grain it loses the fundamental attribute of complete grain inertness.

It is also important to remark that the comparison between hybrid and liquid systems is often ill posed; for example, the ablative cooling of hybrid rockets is claimed simpler than regenerative cooling for liquid rockets. This comparison is a bit unfair because ablative-cooled liquid rockets exist, and a hybrid rocket could be also regenerative-cooled (even if it is less attractive for hybrid systems than liquid ones). Similar examples can be done for other aspects like the pressurization system.

However, it is worth noting that some hybrid characteristics like safety and simplicity could lead indirectly to a performance advantage. For example, a safe and simple propulsion system has more chances to exploit the advantages of air launch. Moreover, a simpler, safer, cheaper system can be tested much more times in a smaller timeframe. This in turn allows the possibility to continuously upgrade, optimize and improve the system with new state of art technology, for example in materials science. This fact is especially significant during a period of low investments like the current one.

An analysis of the technology used nowadays on launchers and spacecrafts shows that the state of the art for space systems is often far from being the real state of the art of the same technology. The reason for that is the following: the tremendously high costs of space (and the impossibility of repairing the failures) impose the need for a very high reliability. High reliability drives up costs that in turn increase the demand for high reliability. This phenomenon is called the space spiral. The required high reliability in a period of limited budgets induces a very conservative approach; a typical example is the fact that a common PC has more capability than the computers used in the ISS. Any improvement is introduced to operational level very slowly. This behavior has prevented the real birth of a large private autonomous space business limiting the great part of the activities to a relatively small number of governmental funded projects.

Figure 1.5 - The Space Spiral, how it is now (left) and how it should be (right).

Without the actual governmental support the space business would collapse (unlike the aviation segment for example). A dramatic reduction of the cost of space is deemed necessary to reverse the space spiral. A decrease of space costs coupled with less fragile and more flexible systems permits a lower demand of reliability that in turn requires less cost allowing an increased number of missions. More missions could guarantee a real sustainable business. It is hoped that hybrid propulsion could be one element (but for sure not the only one) that could help to reverse the space spiral. This could be possible only if hybrid systems could afford a significant

cost reduction, not being simply on the level of current liquid and solid ones. At the same time the exponential form of Tsiolkovsky equation allows only limited losses of performances. A larger penalty translates indirectly on high costs because of large size increase (these aspects have been highlighted by Grosse). To achieve this ambitious object classical hybrid issues must be fixed preserving its inherent advantages like safety and simplicity, guarantying high reliability and very low costs.

1.2.1 Hybrid Propulsion History

The early history of hybrid rocket development dates back to the '30s, the decade when the bases of modern experimental rocketry have been set. The first often claimed hybrid rocket (however sometimes referred as a liquid) is the GIRD 09 developed by a Soviet group of scientists (such as Korolev, the father of Soyuz family) and launched (only partially successfully) in 1933. It used liquid oxygen fed by its own pressure with gelled gasoline supported on a metal mesh.

Figure 1.6 - GIRD 09 combustion chamber (left) and complete rocket (right).

Afterwards other experiments were made by a few researchers using carbon as a fuel. They found a very low regression rate caused by the very high heat of ablation of carbon (in fact carbon-based material are often used as ablative protections). Further work was done during the '40-'50 at the Pacific Rocket Society, General Electric and Jet Propulsion Laboratory. These preliminary activities demonstrated the basic characteristics of hybrid rockets like low

regression rate, insensitivity to crack, regression rate dependency on oxidizer flow and consequently the possibility to modulate the thrust varying the oxidizer flow.

Remarking aspects are the first use of rubber-based fuels, the first catalytic-decomposed H_2O_2 hybrid rocket and the first (unsatisfactory) attempts of the reverse approach.

The following decade (the '60) has been probably the most prolific ever for rocket propulsion with a huge amount of investments on research and operational programs thanks to the space race initiated by the Sputnik launch in 1957 and culminated with the Moon landing in 1969. A great boost in hybrid rocket activity occurred as well, even if on a smaller scale compared to solid and liquid systems and without operational developments. However, the work done in that period has produced a great step in hybrid propulsion, defining the major part of the actual knowledge. A lot of experimental work was done in the United States, particularly at UTC. A wide variety of fuels and oxidizers were tested in different conditions defining the basis of hybrid rocket motor behavior.

The main finding was that hybrid regression rate data correlate well with the expression:

$$\dot{r} = aG_0^n L^m \tag{1.1}$$

Where G_0 is the oxidizer flux, L is the length, a, n and m are coefficient determined empirically. Using the previous equation, motor design studies were conducted and equations were developed to determine stoichiometric length and to predict thrust and *O/F* shift with time.

A significant accomplishment during that period was the development of a regression rate model by Marxman and coworkers. The key of the model was to relate the regression rate with the convective heat flux from the turbulent diffusion flame to the fuel surface. This successful treatment was favored by several advancements made in that period in the analytical description of combustion and in the study of the flow above blowing surfaces (this last work was pushed by the need of an ablative shield for ballistic missiles). The result of the model was an equation for the regression rate having the same structure of the experimental developed correlations. In particular the model was able to describe the blocking effect, which is the reduction of the heat flux on a blowing surface. This effect was responsible for the low sensitivity of hybrid regression rate to the thermochemical parameters of the propellant combination.

Several aspects of the theory were investigated with the use of Schlieren photographs of a slab burner.

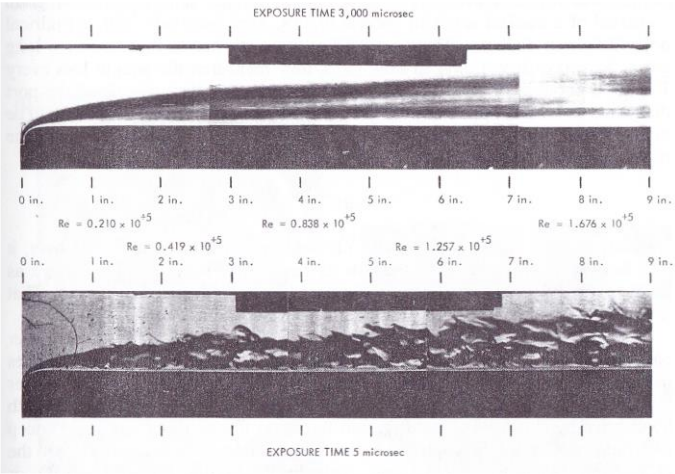

Figure 1.7 - Hybrid combustion boundary layer Schlieren photographs.

In 1967 there was the first attempt to scale up hybrid technology with the test of a large motor (180 kN) using the multiport configuration. This solution was conceived to compensate for the low regression rate. The wagon-wheel grain design paved the way to the larger works made two decades later.

In the mid-1960s NASA sponsored a series of study about high-energy combination for space engines. One concept was based on the reaction of lithium with fluorine, elements at the opposite ends of Mendeleev's periodic table. A large eleven port motor (1.07 m diameter) was tested using 70% FLOX (70% fluorine, 30% oxygen) as oxidizer and a mixture of lithium and lithium hydride incorporated on a HTPB binder. The ignition was hypergolic and the combustion was smooth. Probably the high reactivity of the propellants helped the vaporization and burning of the incoming oxidizer. This throttleable system exhibited high performances with an I_{sp} efficiency of 93% corresponding to a delivered vacuum specific impulse of 380 s at an area ratio of 40.

Another approach called tribrid was conceived. The name indicates that three propellants were used, one of which in the solid phase. The motor should have burned liquid hydrogen, liquid oxygen and beryllium powder placed in a solid matrix (HTPB). The principle was to burn the beryllium with the oxygen to produce a large amount of heat used to accelerate a low molecular

weight fluid (the hydrogen). This solution should have provided the highest possible I_{sp} for a chemical rocket (more than 500s). Both programs were cancelled because of the very dangerous characteristics of the propellants used (Fluorine ad Beryllium respectively). The same destiny was shared with almost all the exotic propellants tested in that period (e.g. boranes).

At the same time in Europe two important activities were performed, culminating with successful ground and flight tests of hybrid sounding rockets. One was done in France by ONERA, that developed the Lithergol Experimental (LEX). The oxidizer was nitric acid while the fuel was based on amine consisting of meta toluene diamine/nylon. The ignition was hypergolic. A diaphragm was placed in the midst of the grain to increase regression rate and efficiency. An automatic system was developed to fill the oxidizer tank immediately before launch. The rocket was launched a few times reaching more than 100 km with 10 kg of payload and an initial weight of 70 kg, a record at that time and still an impressive feat. A larger version (LEX 04) was ground tested successfully 12 times afterwards.

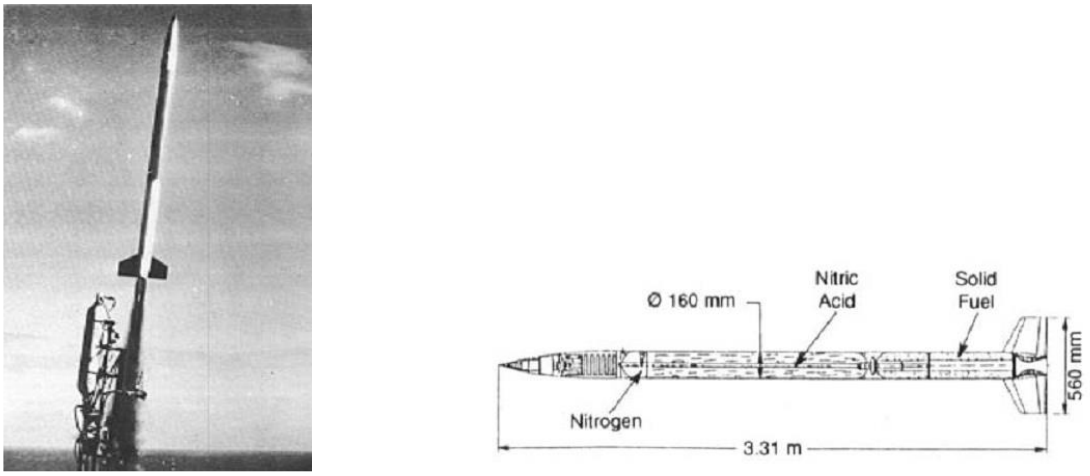

Figure 1.8 - LEX sounding rocket.

Similar design and propellant combination were used in Sweden by Volvo Flygmotor. They developed fuels called Tagaform (PB plus an aromatic amine) and Sagaform. After the successful flight test of small rockets, two large sounding rockets called SR-1 and SR-2 were planned but never launched. Both programs were abandoned in the '70.

It is worth to remark that the LEX sounding rocket was one of the highest performing hybrid rockets ever developed, achieving very high combustion efficiency and propellant mass

fraction and competing with solid rockets. However, the use of a toxic propellant combination with the consequent handling complications and the lack of synergy with other (military) programs were probably the reasons of the discard of the hybrid solution in favor of solid rockets.

A peculiar series of programs about hybrid target drones covered three decades from the '60s to the '80s. In the mid-1960s UTC and Beech Aircraft began to work on the Sandpiper under an USAF contract following a requirement for a unit capable to be launched from an altitude of 12 km, accelerate to 30 km at Mach values between 2 and 4 and fly for 300 s.

The system required a propulsion unit able to guarantee a short boost/long sustain thrust profile with a throttle ratio of 8:1. Hybrid propulsion was considered an optimal candidate for this objective. The Sandpiper used the storable liquid oxidizer MON-25 (25% NO, 75% N_2O_4) and was pressure-fed with a Nitrogen tank. The solid fuel was composed by PMMA loaded with magnesium. The system flew six times.

Later another program called High Altitude Supersonic Target (HAST) followed. In contrast to the Sandpiper the propellant changed to IRFNA (inhibited red fuming nitric acid) and PB/PMMA and the oxidizer was pressurized by a ram air turbine that provided also electrical power. The grain configuration was changed from a single cylindrical port to a cruciform one using four liquid injectors. Unlike the Sandpiper, which was expendable, the HAST was recoverable by use of an onboard drogue parachute and retrieved in midair by a helicopter. The thrust range was controlled by a throttle valve providing a 10:1 range. This work later became the Firebolt target missile system produced by Teledyne Ryan Aircraft (with CSD as the motor manufacturer). 40 units have been delivered.

These drones were the only hybrid flight programs built to military specifications. However, no follow-on contract for Firebolt production was awarded, presumably because it was significantly more expensive than the simpler expendable liquid fueled AQM-37. It is worth noting (and an ironic paradox) that both LEX and Firebolt were discarded not for their (excellent) performances but for reasons of cost and complexity. This is in contrast with the common view that hybrid rocket motors are cheap, but poorly performing.

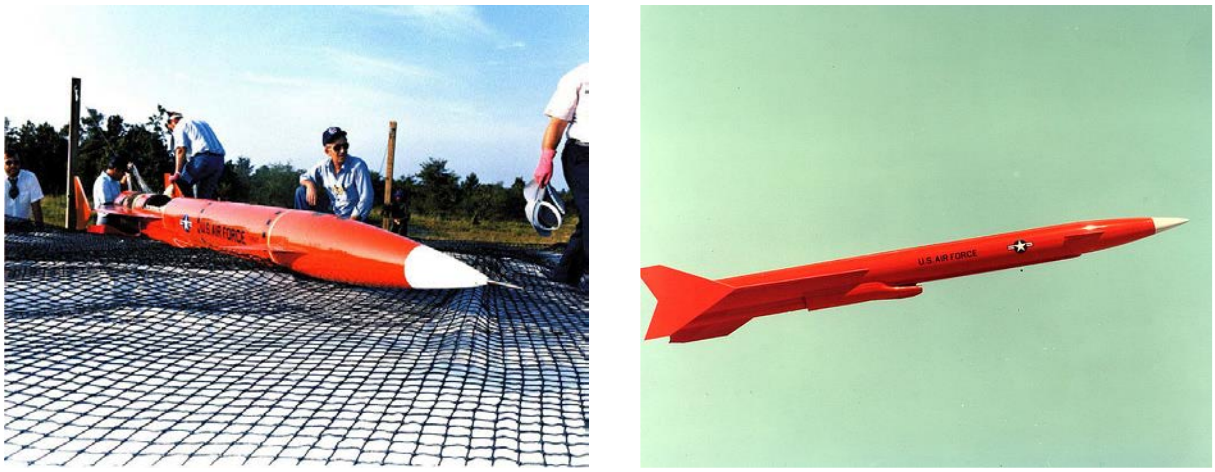

Figure 1.9 - Teledyne Ryan AQM-81 Firebolt Drone.

After a decade of stagnation there was a revival of the interest in hybrid propulsion in the '80s. The growth of the commercial satellite market and the increased international competition prompted the search for a low-cost access to space. Two private ventures selected the hybrid approach as a way to reduce development and launch costs. The company STARSTRUCK was created to develop a large sounding rocket named Dolphin. The selected propellant combination was LOX-PB. A sea launch of this vehicle was attempted on 1984. Unfortunately, a thrust vector LOX valve froze in the closed position causing a pitch over and a subsequent command termination. The company was subsequently reorganized in 1985 and renamed AMROC (American Rocket Company). With private funding, AMROC began developing a low-cost launcher called AQUILA. The Aquila was composed by 4 LOX-HTPB common core boosters, a small solid upper stage and a final hybrid stage (N_2O-HTPB) for accurate orbit insertion. The basic philosophy was to use high design margins to reduce development and production costs and to increase the reliability of the system. The inert characteristics of hybrid propellants were perfectly suited for this kind of approach.

AMROC fired the largest hybrid motors ever tested up to that time. They relied on a multiport configuration to achieve the necessary burning area and had to face several stability issues. That work laid the foundation of our modern know-how on large hybrid systems. As an intermediate step the sea launch of a large sounding rocket called SET-1 was planned on 1989. Again, a similar fate affected the new attempt. A LOX valve froze in a partially open position resulting in insufficient thrust for lift-off.

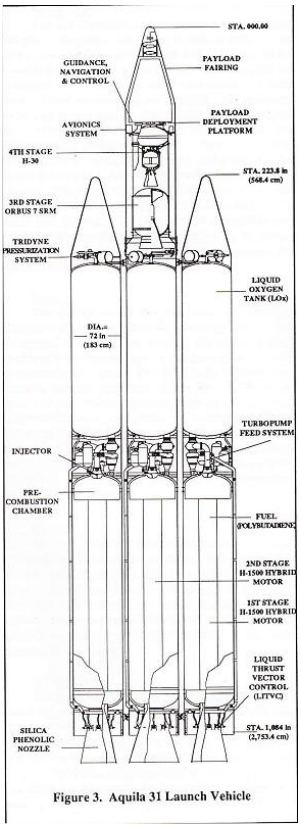

Figure 1.10 - Aquila Launch Vehicle.

The failures of both Dolphin and SET-1 were a negative setback; however, they demonstrated an important hybrid feature: the damage made by the two accidents was very limited, proving the safety and nonexplosive characteristics of hybrid systems also at large scales. This attribute of hybrid propulsion gained more attention after the disaster of the Shuttle Challenger on 1986 when NASA became interested in a possible replacement of the Shuttle solid rocket boosters (SSRM). Hybrid systems were seen has an interesting option because of their larger grain manufacturing tolerances, their benign failure modes and their possibility to stop the motor in flight. Several design studies were made to assess the use of hybrid motors for large boosters.

Meanwhile AMROC continued its work testing a 250000 lbf (1.1 MN) hybrid motor at the beginning of the '90s. A new sounding rocket called HyFlyer using this motor was conceived.

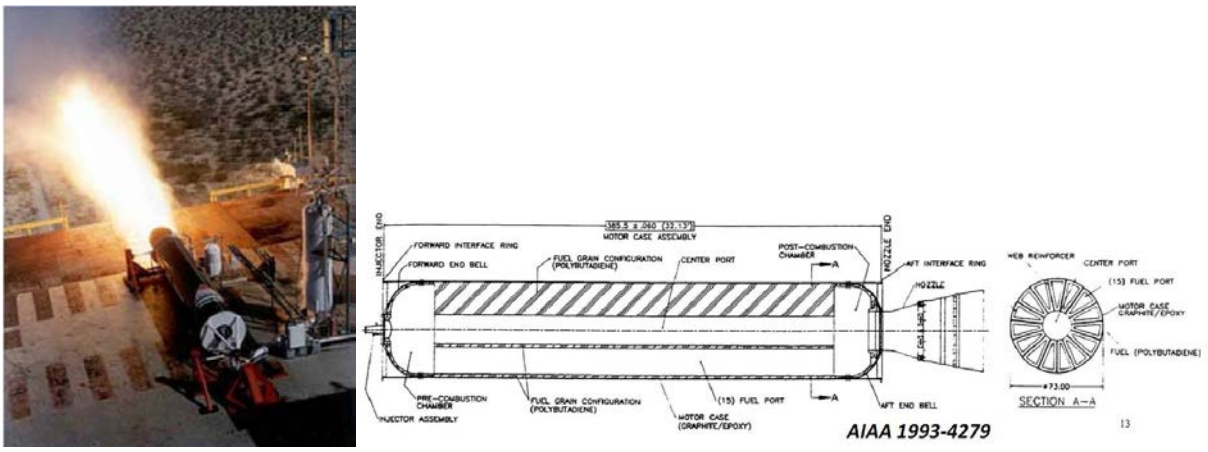

Figure 1.11 - Large scale test firing of AMROC Motors.

Because AMROC had insufficient founding to pursue the program on their own a new group was formed with support from NASA. The project was renamed Hybrid Technology Option Project (HyTOP) and included the companies AMROC, Martin Marietta and CSD. AMROC lost its sponsor and failed in 1995. The work continued within the Hybrid Propulsion Demonstration Program (HPDP) with a new member (Thiokol) replacing AMROC in the consortium. New tests were done on a configuration slightly different from the previous ones. Some improvements were made but the basic limits remained. The multiport design chosen to overcome the low regression rate suffered from several drawbacks (as previously cited), resulting in a poor volume loading and fuel utilization. Moreover, the instabilities related to the difficult LOX vaporization and the flow unbalance between different ports were never completely understood, slowing the development and leading to a more complex injector pre-chamber design. Often it was necessary to add an external heat sources to help LOX vaporization, like the injection of a pyrophoric fluid (e.g. TEA) or the use of small hybrid gas generators.

In the frame of the HDPD program, Environmental Aeroscience Corp (eAc) designed, manufactured and tested the Hyperion sounding rocket using N_2O and HTPB as propellants. Four flights took place between 1996 and 1997, reaching a maximum of 36.5 km. These flights demonstrated a safe non-pyrophoric/non-pyrotechnic ignition, inexpensive component manufacturing, simple launch operations and a quick launch turnaround time. They represent also the first time a self-pressurized oxidizer was successfully employed in a flight.

During the '90s hybrid research began to gain more attention also in the academic world and between small companies following the shifting from the performance dominated cold war era

to a new period of increased attention for safety, cost and environmental friendliness. New (or sometimes forgotten) ideas were conceived and tested in order to improve the low regression rate of hybrid systems because it was seen (properly) as a major show-stopper for hybrid propulsion.

One of the most successful solutions proposed was the swirl or vortex injection. In this configuration the oxidizer is injected tangentially to the chamber walls in order to create a rotating flow field. This strong swirling flow inside the combustion chamber enhances the mixing of reactants, improving the efficiency. Moreover, the higher local mass flux due to the tangential component of the velocity, the stronger generated turbulence, the flame position nearer to the fuel surface due to centrifugal forces, all concur to a large increase of the heat transfer to the grain wall, leading to a noticeable improvement of the regression rate.

Yuasa experimented swirl injection wherein the oxidizer entered the combustion chamber at the head end as in a conventional hybrid. He obtained regression rate values several times higher than with a classical axial injection. In the US, at Orbital Technologies Corporation (ORBITEC), Knuth experimented the double vortex hybrid wherein the swirl oxidizer was located at the aft end (opposite to Yuasa) of the fuel grain, just upstream of the converging portion of the nozzle. Knuth discovered that this arrangement generated a pair of coaxial, co-rotating, bidirectional vortices in the combustion chamber. Following visualization experiments, numerical and analytical work confirmed this behavior. This configuration achieved a very high combustion efficiency and an impressive regression rate (even 7 times the classical values).

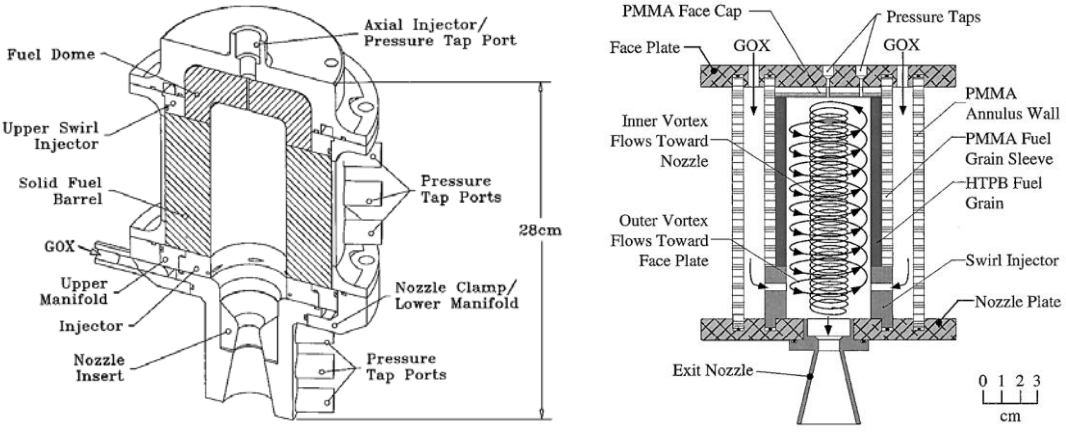

Figure 1.12 - ORBITEC Vortex Rocket Engine.

At the end of the decade the vortex flow pancake (VFP) concept was developed at Surrey. In this case the swirling oxidizer flow is generated between two fuel disks that end burn in opposite directions during combustion. A very smooth combustion and high efficiency were obtained.

More recently NAMMO Raufoss applied the head end vortex injection on a H_2O_2-HTPB hybrid motor. The great advantage of this solution consists in the possibility of catalytic decomposition of H_2O_2 prior to chamber injection. Indeed, most of the work with vortex injection has been done with the oxidizer in the gaseous phase (mainly GOX). However, in a real motor the oxidizer needs to be stored as liquid phase for performance reasons.

Liquid vortex injection has received less attention and the few works are not as impressive as for gaseous injection. Alternatively, the oxidizer can be gasified prior to chamber injection, but this usually adds complexity. H_2O_2 is an exception because it can be decomposed easily using a catalyst pack. In this way the full potential of gaseous vortex injection can be exploited on an operational motor.

NAMMO configuration resulted in a motor that is stable, throttleable, achieving a good efficiency and with a regression rate several times higher than a classical hybrid. Moreover, the hot products of H_2O_2 decomposition are able to ignite the solid fuel. In this way the motor can be started and stopped several times without a separate ignition device.

Meanwhile several research groups began investigating the regression rate and combustion characteristics of hybrid motors that employed cryogenic solid fuels in the frame of a preparatory program about the combustion of high energy density matter (HEDM). Many cryogenic (here the term cryogenic is used in an extended meaning) solid fuels (pentane, methane, ethylene, RP-1 etc.) were tested at Air Force Philips Laboratory in the '90s and by ORBITEC in the early 2000s. ORBITEC tested also a reverse cryogenic hybrid using solid oxygen for the grain. The experiments revealed an unexpected large regression rate, even an order of magnitude higher than HTPB. These results could not be explained by a lower vaporization enthalpy because the blocking effect reduces the sensitivity of the regression rate to the thermochemical parameters and it is responsible for the relative narrow range usually encountered. Later Karabeyoglu at Stanford University developed a theory explaining the anomalous high regression rate of cryogenic fuels. He postulated that an additional mechanism was present in the case of fuels forming a melting layer of low viscosity and surface tension (e.g. pentane or SOX). It has been shown that this melting layer could become unstable under

the influence of shear stress of the gas flow in the port resulting in the formation of liquid droplets that are subsequently entrained by the main flow. Afterwards he determined that a class of storable fuels like paraffin waxes (alkanes with carbon number between 25 and 60) could present the same behavior. Experiments at Stanford and NASA Ames confirmed the initial predictions. Regression rate 4 times higher than HTPB were obtained.

Moreover, the experiments showed also that the regression rate of paraffin wax is almost independent from the motor scale. This has the twofold advantage of making lab-scale testing more meaningful and to avoid the regression rate decay that classical fuels encounter when the motor is scaled up. Karabeyoglu later founded the small company SPG (Space Propulsion Group) which is developing paraffin-based hybrid motors under a contract for the Air Force. SPG is also collaborating with Stanford university and NASA Ames for the development of the Peregrine sounding rocket which is aimed to be a reusable and throttleable $paraffin\text{-}N_2O$ demonstrator able to lift 5 kg above 100 km. In recent years paraffin has begun to be used by several researchers, academics and amateurs worldwide (included CISAS).

After the HDPD experience Lockheed Martin started a new program in 1999 called HYSR. The object of this work was the development and flight test of a large hybrid sounding rocket, advancing readiness level of this kind propulsion and showing its positive attributes.

The three-year technology demonstration program was a collaborative effort between NASA and Lockheed Martin and had a total budget under $6 million. The oxidizer was LOX while the fuel was HTPB loaded with Aluminum. The motor had an initial thrust of 267 kN for 33 s of burning time.

In the frame of this project Lockheed Martin developed and patented two hybrid-based subsystems. The first consists in the use of small hybrid rockets fed by gaseous oxygen (GOX) to ignite the main motor and to maintain combustion stability for the entire burn. The second relates to the pressurization technique. For simplicity a pressure-fed solution was selected in order to meet the budget and time constraints. However, a special upgrade was conceived to limit volume and weight of the pressurization system.

In LM's patent the helium is stored at cryogenic temperature and moderate pressure. In this way the pressurant tank can be smaller and lighter. The helium is then mixed with the exhausts of a small GOX fed hybrid heater. Afterwards the hot helium mixture (94% He) flows through a minimal surface area heat exchanger to heat up the helium in the tank in order to minimize the helium residuals. Finally, the pressurant enters the LOX tank through a stainless steel

diffuser, which disperses the flow into the ullage. The use of a warm pressurant reduces the amount needed, decreasing further the total weight and volume of the pressurization system. The HYSR was finally launched from Wallops on December 2002 reaching an altitude of 42 km.

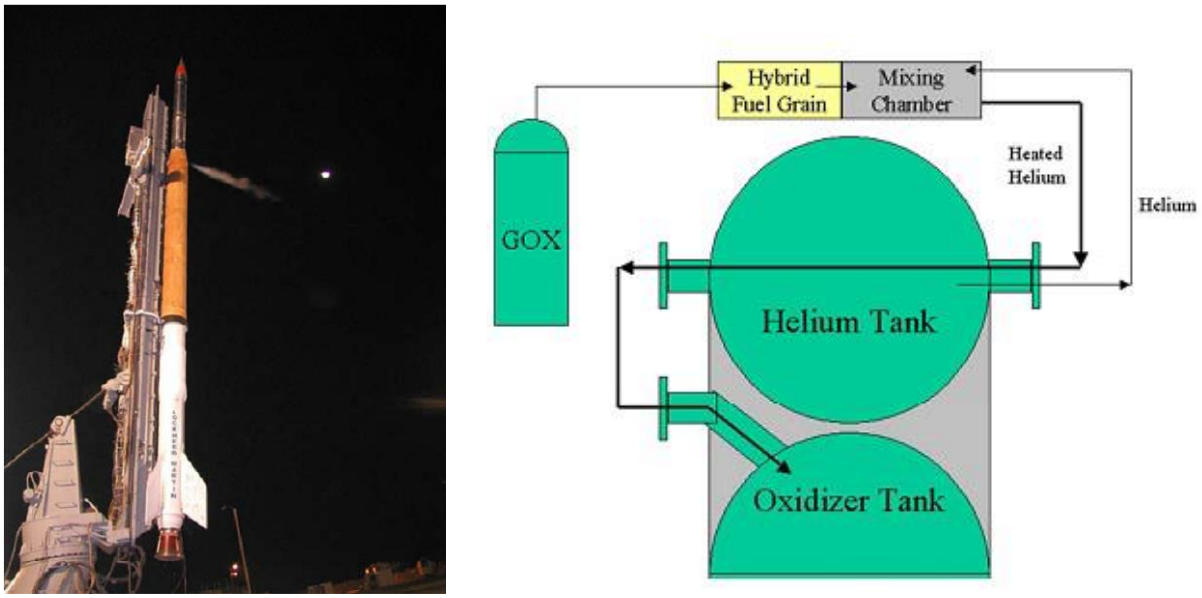

Figure 1.13 - HYSR Sounding rocket (left) and LM patented heated helium pressurization system (right).

Based on the previous experience Lockheed Martin participated to the DARPA Falcon Small Launch Vehicle (SLV) program aimed to develop and demonstrate an affordable and responsive space lift capability. LM claimed to have made several important improvements to the conventional design of large hybrid rockets. The first aspect is the use of a pump-fed pressurization driven by a gas generator where an amount of LOX is vaporized mixing with the exhaust of GOX-fed hybrid motor. The second fundamental achievement is a notable increase in the mechanical properties compared to the basic HTPB. This added strength allows a more complete consumption of the fuel without the need for leaving an overly thick residual or the use of web stiffener, reducing the inert weight and lowering the risk of potential fuel failure modes. Because of this it was possible to shift to a multi-row configuration in order to increase the volume loading. Thanks to its high strength the internal rows can be consumed until the ports merge. LM tested successfully a 3 rows/43 ports upper stage motor in 2005.

Figure 1.14 - Lockheed Martin DARPA Falcon hybrid rocket.

Doubtless the most famous hybrid success has been the victory of the Ansari X prize obtained by Burt Rutan's company Scaled Composites with its SpaceShipOne (SS1). The Ansari X Prize was a contest for the first commercial company to fly twice above 100km. Scaled Composites built a two-stage airplane to win the prize.

The first stage was an air-breathing plane called White Knight and was used as a carrier for the second stage plane, the already cited SS1 powered by an N_2O-HTPB hybrid rocket motor. Two companies competed for the hybrid motor: eAc developed a single port hybrid motor loaded with aluminum, while SpaceDev (which had acquired AMROC intellectual property in 1999) presented a 4 ports grain design. In the end, SpaceDev was chosen to build the hybrid grains for the flight vehicles, however eAc's design for some of the oxidizer system plumbing and valves was also adopted in the flight vehicle. The motor had a thrust of 74 kN for 87 s of burning time. Scaled Composites developed multiple unique and innovative solutions for its hybrid system. SS1 was completely built around the hybrid motor and the oxidizer tank, the latter bonded to the inside of the airframe. The N_2O valves were placed inside the oxidizer tank. This eliminates leak paths and allows the hybrid motor case to be bolted directly to the oxidizer tank in a cantilever configuration. The use of N_2O high vapor pressure eliminated the need of a pressurization system. The motor was made with a single piece of graphite-epoxy composite materials (CTN: Case Throat Nozzle). The tank was also made with a composite fibers

overwrap with an internal liner. The case had burn through sensors built into the motor (fiber optic wire), so that if unusual burning was detected the motor could be shut-off.

SS1 flew successfully in 2004 reaching more than 100 km and winning the X prize. Thanks to this accomplishment hybrid propulsion began to be known outside a restricted niche of propulsion engineers. The choice of hybrid propulsion by Scaled Composites confirmed its positive attributes like safety, good performance, system cost, quick turnaround and thrust termination. SS1's experience could indicate a path for the successful implementation of hybrid propulsion, mainly in the extensive use of composite materials, self-pressurization and integrated design.

Figure 1.15 - SpaceShipOne.

Today Scaled Composites together with Sierra Nevada Corporation (SNC, which acquired SpaceDev) is developing the hybrid motor for the successor of SS1, the SpaceShipTwo. This larger vehicle is able to accommodate six passengers and two pilots and would be used by Virgin Galactic for suborbital space tourism.

SNC is also developing the Dream Chaser under NASA Commercial Crew Development Program (CCDev). The Dream Chaser is a reusable composite spacecraft designed to carry from two to seven people and/or cargo to orbital destinations such as the International Space Station (ISS). The vehicle would launch vertically on an Atlas V and land horizontally on conventional runways. Its lifting body design guarantees a soft-reentry from space (1.5 g versus several g for conventional capsules). On-orbit propulsion of the Dream Chaser is provided by twin hybrid rocket motors developed from SS1. The motors allow the vehicle to be used also as a Launch Escape System in case of emergency, eliminating the need of a separate system (as it has been in previous manned capsules). Several milestones have been already achieved. If the

program would be completed successfully the Dream Chaser could be the first hybrid propelled orbital spacecraft.

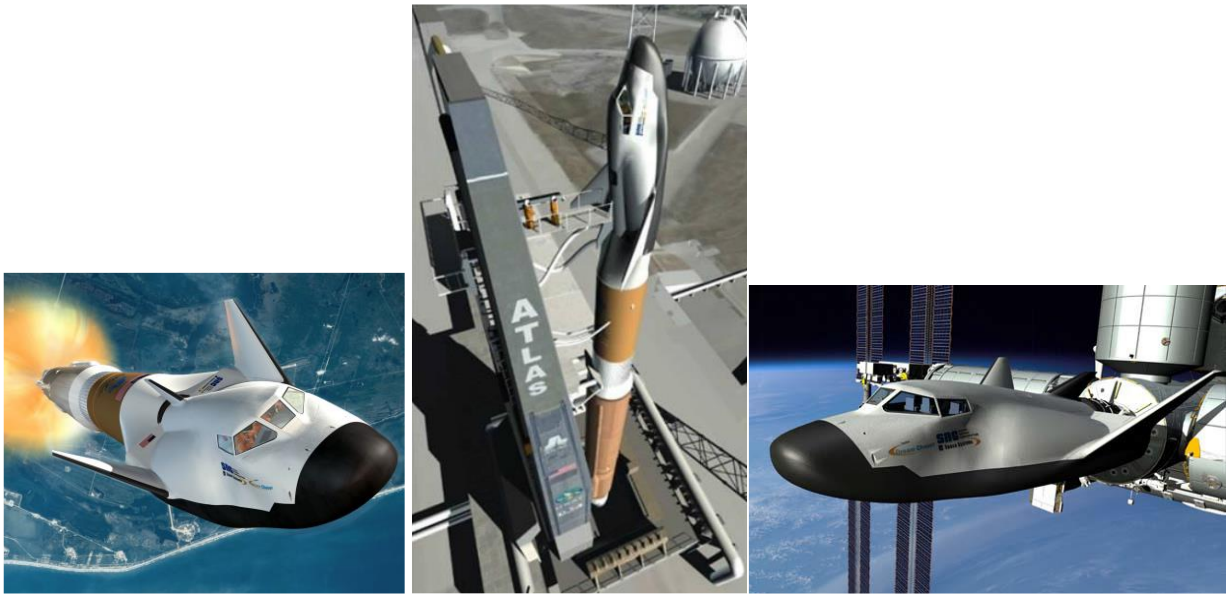

Figure 1.16 - Renderings of the Dream Chaser spacecraft.

Another event worthy to be cited is the launch of Atea-1 sounding rocket developed by the New-Zealand company RocketLab in 2009. The rocket was composed by a first N_2O hybrid booster and a second inert dart. The rocket had an empty weight of nearly 20 kg with a lift-off weight of 60 and was designed to reach more than 100 km of altitude. Unfortunately, the second stage was not recovered so actual performances have been not verified. However, it represents a demonstration that with a proper use of composite material a hybrid rocket could reach very good values of propellant mass fraction [3].

On September 2018 Nammo launched the hybrid sounding rocket Nucleus from Andøya Space Center in Norway. Reaching an altitude of 107.4 km, it was the first rocket powered by a Norwegian motor design to reach space and the first European hybrid rocket to do so in more than 50 years [4]. Nucleus was powered by a 30 kN motor using H_2O_2 as oxidizer and a solid rubber-like substance as fuel [5].

Finally, another important event is the test of the largest hybrid rocket ever fired outside the United States: all started in 2012 in the frame of the Bloodhound project. This project aims to break the land speed record with a supersonic car, powered by a combination of a jet engine (EJ200 from the Eurofighter Typhoon combat aircraft) with a hybrid rocket and designed to

reach 1,000 miles per hour (1,609 km/h). The pump-fed hybrid rocket motor burns 86% H_2O_2 with HTPB and it has a design average thrust of 111 kN (25,000lbf) for 20 seconds. The pump is driven by an F1 Cosworth V8 motor. After development stalled in October 2018, it was saved by Yorkshire-based businessman Ian Warhust in December 2018. Runway testing of up to 200 mph (320 km/h) occurred in October 2017. There are plans to make a 500 mph (800 km/h) test in October 2019 and a 1000 mph (1,609 km/h) test in 2020 [3].

1.3 Rocket Test Benches

The majority of test stands for rockets aim to test the entire propulsion system. There are mainly 2 types of configuration for these tests:

- *Horizontal test stand*: the rocket is tested horizontally. This configuration is the easiest to anchor, assemble and inspect, but it is also the furthest from the flight condition, which makes the test results less reliable compared to a vertical test. Injection and priming could also be more difficult compared to a vertical configuration with a pointing down nozzle.

Figure 1.17 - Nammo Nucleus tested horizontally [6].

- *Vertical test stand*: the rocket is tested vertically. This configuration has the advantage of being in a position more similar to the one during flight. The nozzle can be pointing down or pointing up: the former setup is the closest to the flight configuration, but requires a deflector below the nozzle to deviate the hot exhaust and is the most difficult

to anchor because the thrust could rip the anchoring away; the latter setup solves this problem, but is less similar to the flight configuration and could have injection and priming issues because fluids run against gravity.

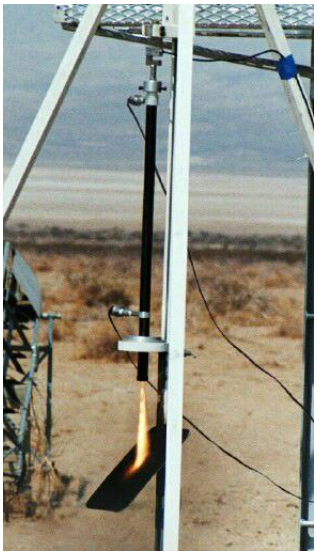

Figure 1.18 - RATTworks L1000 motor tested vertically with nozzle pointing down [7].

Figure 1.19 - Vertical test with nozzle pointing up (team Daedalus from Arizona State University) [8].

Compared to full rockets, in literature there are much less examples of tests for only catalytic reactors or fluidic lines. Nevertheless, the test bench configurations are somewhat similar: both horizontal [9] [10] and vertical [11] [12] setups are possible, both having similar advantages and disadvantages to the analogue configurations for full motors.

Figure 1.20 - H_2O_2 monopropellant test bench [9].

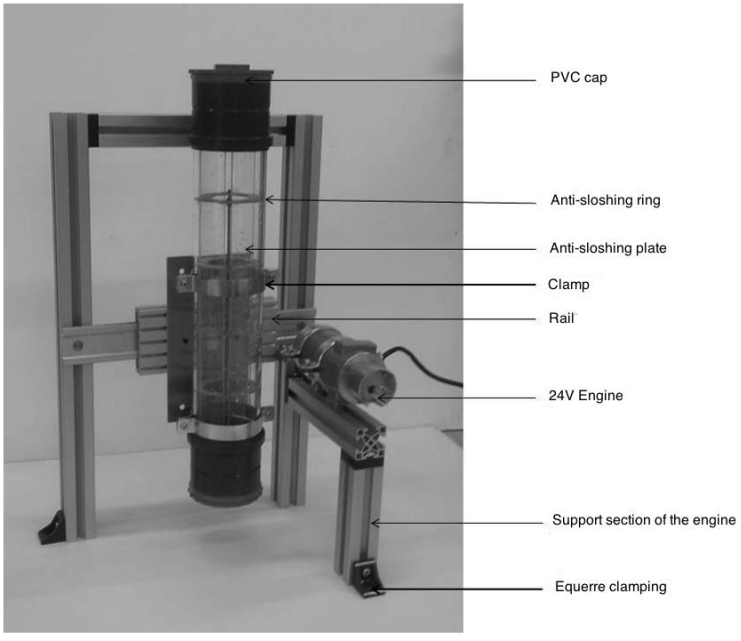

Figure 1.21 - Test bench for an anti-sloshing device for hybrid rocket oxidizer tanks [12].

Because the catalytic reactor alone produces a considerably smaller thrust than a full motor (half in our case) and because fluidic line alone does not produce thrust at all, a vertical configuration with downward discharge is particularly attractive for both types of test.

Chapter 2

Sounding Rocket Description

The sounding rocket to be tested has been designed by a team of students and employees of T4i, a spin-off company of the University of Padua. It is propelled by a hybrid system using hydrogen peroxide as oxidizer and a grain of paraffin as fuel. T4i has already designed and tested similar motors: the goal of the project is to validate the hybrid technology developed thus far. To do so, the rocket is expected to be launched the next year and reach an altitude of about 10 km.

It is worth to make known that many figures and of this chapter refer to older revisions of the project. They are only for explanatory purposes and do not necessarily represent the final design. Moreover, the project is still in development, therefore some configurations here described could be susceptible to change in future revisions.

2.1 General Characteristics

The general functional requirements of the rocket are:

- Thrust of 5 kN.
- Burning time of 20-30 s.
- H_2O_2 decomposed in a catalytic reactor and then injected into a single port, cylindrical grain of paraffin. Hot, decomposed gas must start the ignition, no igniter is required.
- Pressure-fed pressurization system using N_2 as pressurizer.
- External layout comprised of 3 main parts: nosecone, cylindrical body and 4 tail fins.
- External body, nosecone and fins made of carbon fiber reinforced epoxy composite.

- Oxidizer tank integrated with the external cylindrical body and without liner.
- Length not exceeding 6 m and diameter of about 180-200 mm.
- Recovery system with parachutes and inflatable float to retrieve the rocket after the mission.

The design process of the rocket has been divided into 4 main subsystems. Design efforts have been focused onto **motor**, **fluidic line**, **structures** and **recovery** subsystems. They have been individually taken care of by different teams of 3 people each. The subsystems and their respective branches of competence are listed below:

- *Propulsive system*: it has been additionally divided into two further subsystems:
    - *Motor*:
        - Catalytic reactor
        - Grain
        - Nozzle
        - Thermal protections
    - *Fluidic line*:
        - Pressurizer tank
        - Oxidizer tank
        - Feeding pipes and valves
- *Structures*:
        - Cylindrical cases
        - Nosecone
        - Fins
        - Junctions
        - Components assembly
- *Recovery system*:
        - Parachutes
        - Float
        - Controls and actuators
- *Payload*:
        - Avionics and telemetry
        - Diagnostics
        - Control

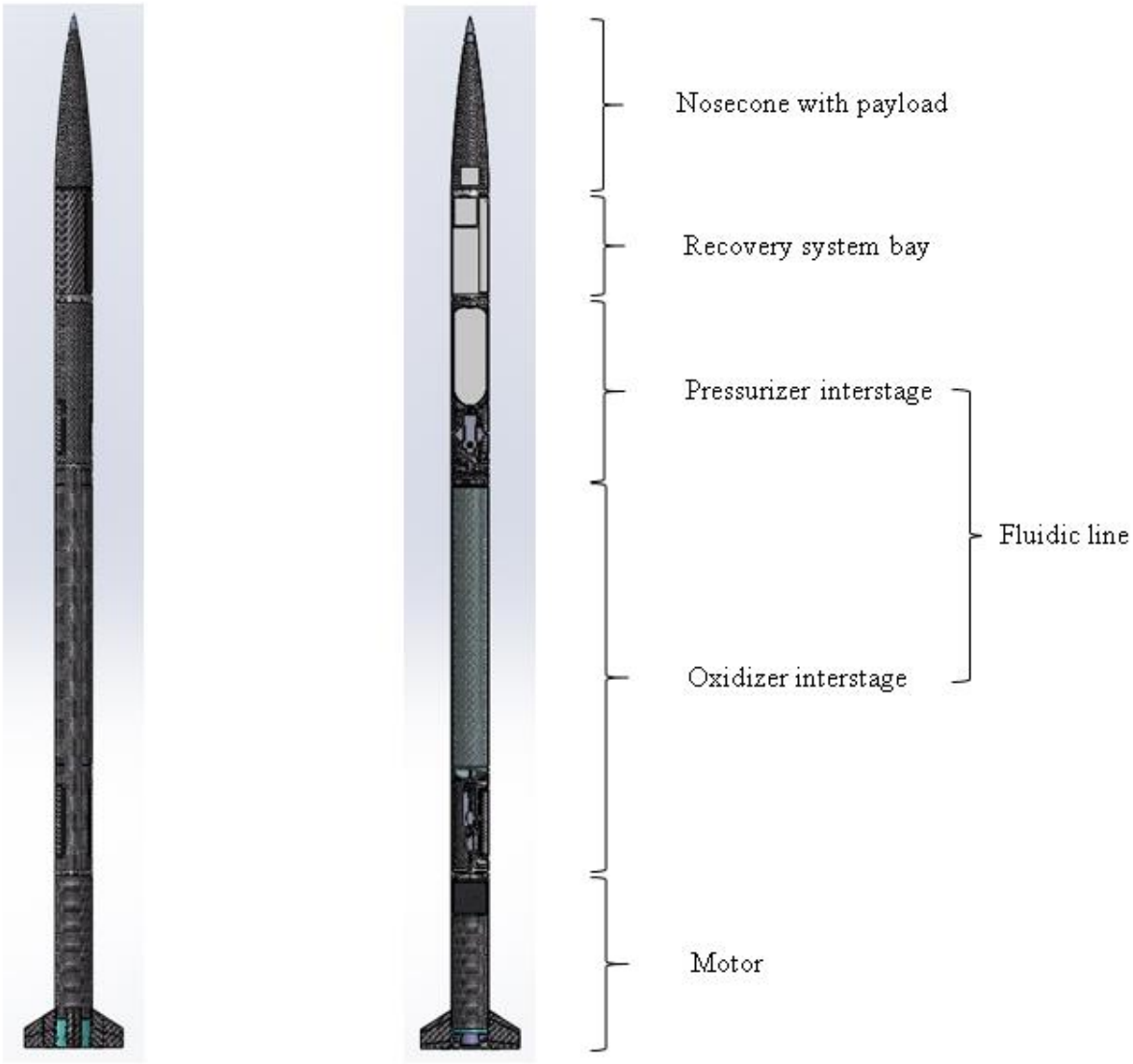

Figure 2.1 - Sounding rocket: exterior (left) and cross section with subsystems (right).

The author of this thesis participated in the design process of the motor, specifically in catalytic reactor and nozzle case sizing. Design details of the former are particularly interesting because it is the main subject of the tests described in this thesis. Before delving into that, a general description of the rocket design will be given.

2.2 Structures

Structures are the first subsystem to be described because they comprised the external shape and dimensions of the rocket, giving an idea of the general layout of the rocket as a whole.

Aerodynamic and trajectory studies are the basis for shape design choices, especially for nosecone and fins.

The rocket has a total length of 5.450 m and an estimated dry mass of about 75 kg. When the pressurizer and oxidizer tanks are filled, it should reach a mass of about 135 kg.

The **body** is a cylinder with an external diameter of 195.82 mm and a total length of approximately 4.5 m. It is made up of 4 cylinders of carbon fiber reinforced epoxy composite, with Ergal-made junctions. The composite is a 11 layers laminate with a total thickness of 2.91 mm. The layers are a mix of woven (using T300 fibers), unidirectional and biaxial (both using T700 fibers) plies. Each cylinder covers a different section of the rocket (see Figure 2.1 for reference); starting from the nosecone junction, the 4 sections are:

- *Recovery system*: 565 mm long. It has a 150×528 mm door to allow parachutes and float to operate (for more details see section 2.5).

Figure 2.2 - Recovery system exterior.

- *Pressurizer interstage (N_2 tank and fluidic line down to H_2O_2 tank)*: 910 mm long. It has 2 openings (90° wide and 285 mm long) in order to allow access to the fluidic line.

Figure 2.3 - Pressurizer interstage.

- *Oxidizer interstage (H_2O_2 tank and fluidic line down to catalytic reactor)*: 2100 mm long. The external cylindrical case functions as perimetral wall of the oxidizer tank.

There are 2 openings (90° wide and 380 mm long) in the lower part to allow access to the fluidic line.

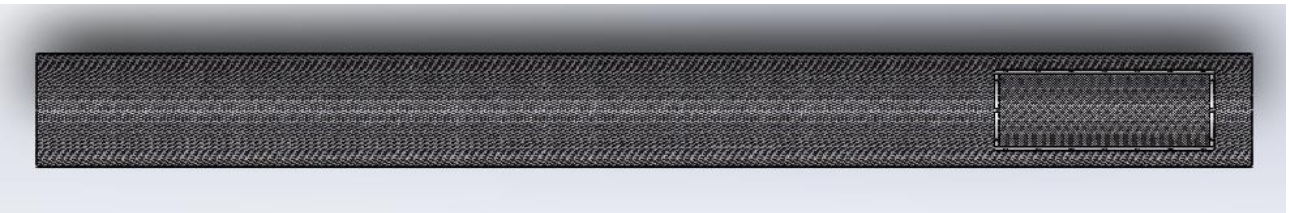

Figure 2.4 - Oxidizer interstage.

- *Motor (catalytic reactor, combustion chamber with paraffin grain, post-chamber and nozzle)*: ~920 mm long. The lower end is made up by a 148.7 mm long Ergal insert in order to fix the nozzle case without using fasteners on the composite.

Figure 2.5 - Motor exterior.

The **nosecone** has a Von Karman profile and is almost 917 mm long. It is externally made of carbon fiber reinforced epoxy, with a tip insert made of aluminum in order to withstand a maximum temperature of 300 °C. The insert is 134.3 mm long, of which 84.5 mm are exposed while 50.2 mm are inside the composite structure and serve for the bonding. The whole nosecone is designed to be easily removed or mounted in order to easily access the recovery system before launch.

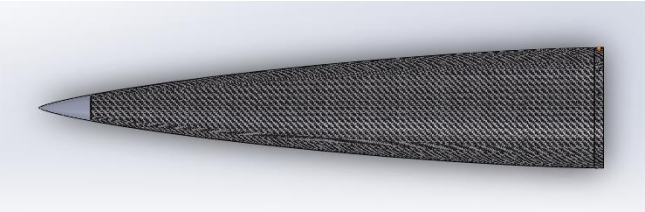

Figure 2.6 - Nosecone.

The **fins** have a symmetrical diamond profile. Each fin has a 160 mm span from tip to root. Root chord is 200 mm long, while tip chord is 100 mm long. Sweep back angle of the trailing edge is 0°, therefore the sweepback angle of the leading edge must be 57.99°. Maximum thickness, which is obviously at the mean chord, is 6 mm. The fins are made of composite material constituted by various laminas of T700 unidirectional carbon fiber and T300 woven carbon fiber, with a core made of Rohacell foam to increase the flexural modulus without significant weight increase. The 4 fins are bonded symmetrically around the nozzle-end of the rocket by means of epoxy adhesive.

Figure 2.7 - Fin.

2.3 Fluidic Line

The fluidic line purpose is essentially to store the oxidizer and inject it into the catalytic bed. The requirements that this subsystem must comply in order to carry out the mission are listed in the following table:

Oxidizer mass flow	$\dot{m}\ \left[\frac{kg}{s}\right]$	2
Oxidizer mass flow variation	$\frac{\Delta\dot{m}}{\dot{m}}$	10%
Burning time	$t_b\ [s]$	20-30
Minimum combustion chamber pressure	$p_{cc}\ [bar]$	20
Ullage of oxidizer tank	V_{ull}	5-10%
Internal diameter	$\phi_{in}\ [mm]$	190
Oxidizer type	90% H_2O_2	
Pressurization system type	Pressure-feed	

Table 2.1 - Fluidic subsystem requirements

In addition to them, there are also safety requirements. During the pre-launch phase, the take-off and the final operating phase it is important to avoid any failure of the system. Moreover, all the processes (rocket assembly, tests, launch) involve human interventions. That means that is mandatory to ensure safety every time these operations happen.

For these reasons, the designed fluidic line includes:

- A *by-pass line* to avoid a failure caused by the water hammer phenomenon.
- A non-reclosing, passive *pressure relief safety device* to let the tank pressure drop off without any human intervention or detection in case of unexpected H_2O_2 dissociation.
- A *pressure relief valve* to discharge the pressurization gas with no human intervention.
- *Redundant manual valves* after every main actuated valve to permit to operate on the rocket in safety conditions during the pre-launch phase.

In this section only a general summary of the flight fluidic line is provided. A more extensive description of procedures and fluidic line layout is found in chapter 3 exclusively for the test configuration, which is nevertheless characterized by design choices akin to those for flight configuration.

The fluidic line can be divided into **2 main lines**, one for the **pressurizer** and one for the **oxidizer**. The general layout of the whole line is illustrated in the following diagram:

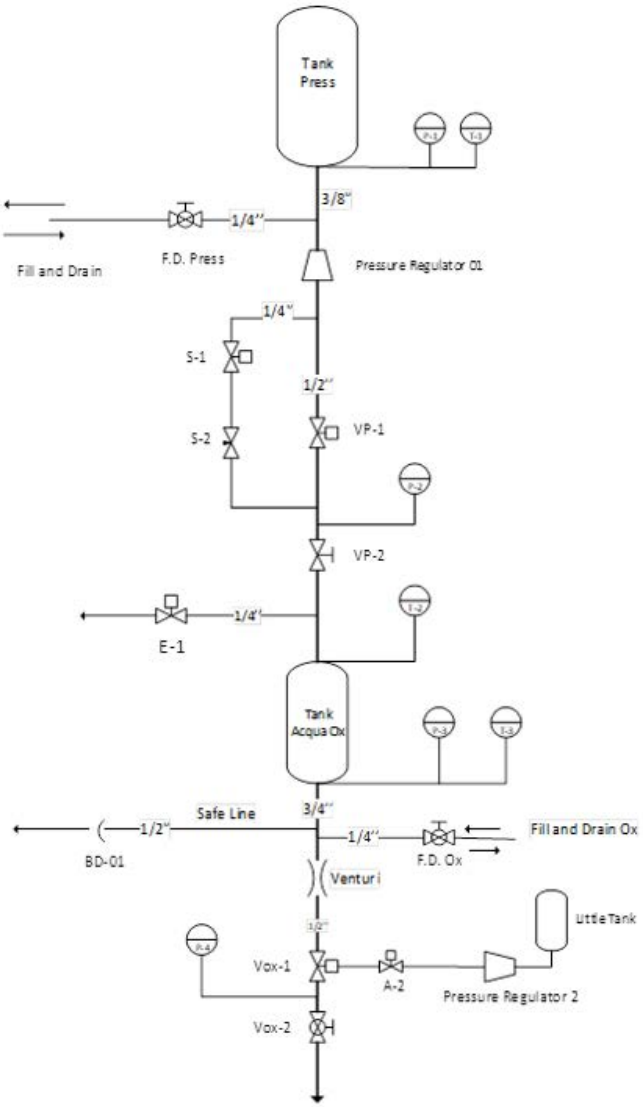

Figure 2.8 - Process flow diagram of the entire fluidic line.

The **pressurizer line** consists in a small tank filled with pressurizer gas (N_2) followed by a fluidic line.

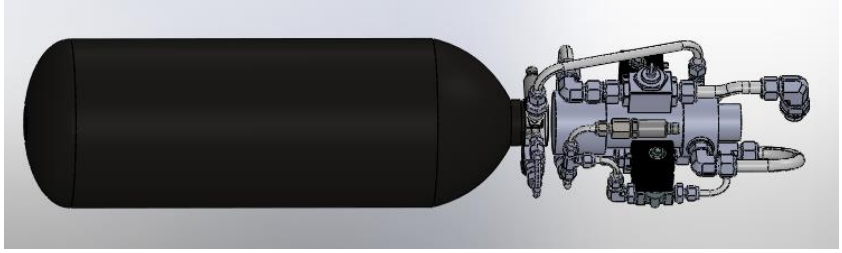

Figure 2.9 - Pressurizer line.

Here is the diagram of the line:

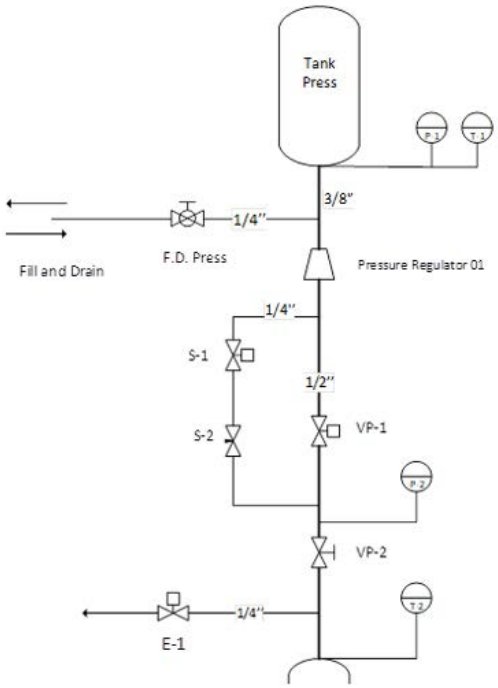

Figure 2.10 - Process flow diagram of the pressurizer line.

The *pressurizer tank* is a *CTS Ultralight*, has a capacity of 9 L and can withstand pressures of up to 300 bar.

Figure 2.11 - Pressurizer tank CTS Ultralight 9.0L - 300 bar.

The main components of the fluidic line are:

- *Manual ball valve 1/4" Ham-Let H6800 ("F.D. Press")*: a mechanical ball valve that allows the passage or the total blocking of the flow. It is used to fill and drain the pressurizing line.

Figure 2.12 - Manual ball valve 1/4" Ham-Let H6800.

- *Pressure regulator Tescom 44-1300 ("P.R.1")*: a control valve that reduces the input pressure of a fluid to a desired output value.

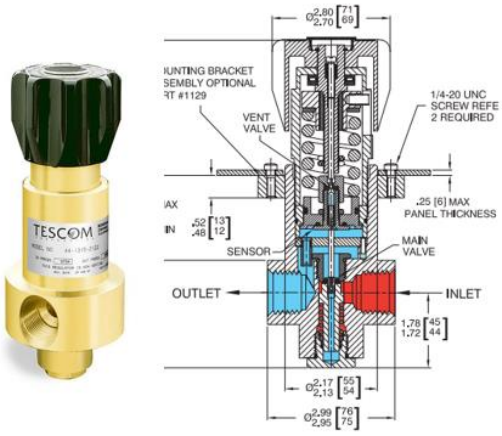

Figure 2.13 - Pressure regulator Tescom 44-1300.

- *Manual ball valve 1/2" Ham-Let H6800 with external actuator ("VP-1")*: an electric ball valve used to open the main line and pressurize the hydrogen peroxide tank.

Figure 2.14 - Manual ball valve 1/2" Ham-Let H6800.

- *Solenoid valve Tameson 75 Bar ("S-1")*: a solenoid valve used to open the bypass line in order to prevent high temperature due to the gas compression inside the oxidizer tank (ullage volume).

Figure 2.15 - Solenoid valve Tameson 75 Bar.

- *Calibrated orifice ("S-2")*: a calibrated orifice used to adjust the gas filling time to about 60 s.
- *Manual ball valve 1/2" Ham-Let H6800 ("VP-2")*: a mechanical ball valve that allows the passage or the total blocking of the flow. It is used as safety valve: it is opened before the pressurization and if *VP-1* or *S-1* fail it can stop the flow before reaching the hydrogen peroxide tank.

Figure 2.16 - Manual ball valve Ham-Let H6800.

- *Solenoid valve Tameson 75 Bar ("E-1")*: a solenoid valve that can be controlled remotely. It is used to drain the pressurant in case of emergency.

Figure 2.17 - Solenoid valve Tameson 75 Bar.

The **oxidizer line** consists in a tank filled with 60 kg of 90% H_2O_2 followed by a fluidic line.

Figure 2.18 - Cross section of the oxidizer line.

Here is the diagram of the line:

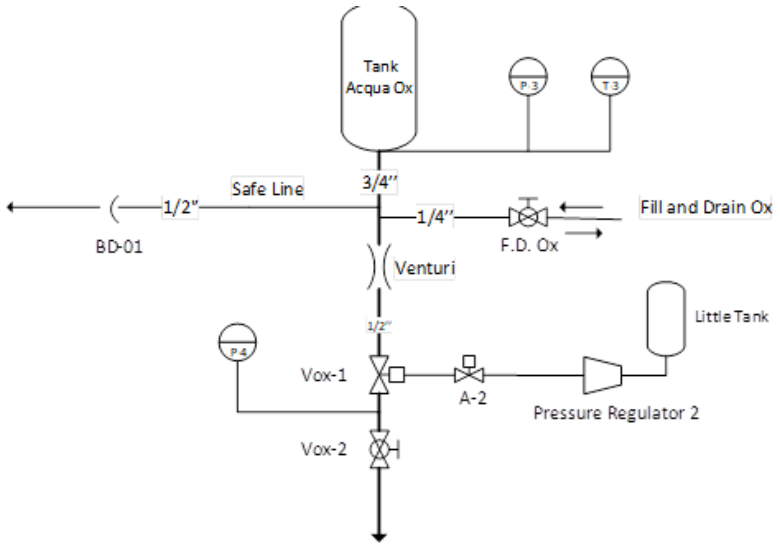

Figure 2.19 - Process flow diagram of the oxidizer line.

The *oxidizer tank* has a capacity of about 45 L, is 1636 mm long and its perimetral wall is the external composite cylinder (see section 2.1.1). The end-closures consist in carbon fiber composite domes, each with a steel insert at the center with a 3/4 G internal threaded hole.

The components of the fluidic line are listed in the following table:

- *Burst Disk ("BD-1")*: a burst disk which serves as safety in case of a high pressure inside the hydrogen peroxide tank.

Figure 2.20 - Burst Disk.

- *Manual ball valve 1/4" Ham-Let H800 ("F.D. Ox")*: a mechanical ball valve used to fill, drain and create vacuum inside the hydrogen peroxide tank.

Figure 2.21 - Manual ball valve 1/4" Ham-Let H800.

- *Cavitating Venturi ("Venturi")*: a nozzle used to fix or lock the flowrate of a liquid, making it not dependent on downstream conditions or fluctuations. This is similar to what a sonic nozzle does to a gas flow: the flowrate follows the inlet pressure and is not sensitive to downstream conditions. The cavitating Venturi, however, uses the liquid vapor pressure point to limit or lock the flow. The throat of a cavitating Venturi is sized so that the differential pressure generated from the inlet section to the throat reduces the liquid absolute pressure to its vapor pressure: in these conditions the liquid starts to vaporize or boil. Vapor bubbles begin then to physically block the throat passageway: this prevents any additional increase in flowrate. If the inlet pressure is increased, this also raises the throat pressure, taking the liquid at the throat out of its vapor pressure point. Additional flow may now pass through the Venturi which in-turn generates a higher differential pressure. This decreases the throat pressure to the vapor pressure again and a new higher fixed flowrate is found.

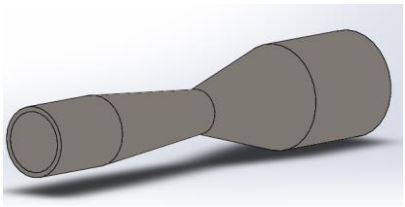

Figure 2.22 - Cavitating Venturi.

- *Manual ball valve Ham-Let H6800 with cylinder actuator ("Vox-1")*: a ball valve actuated with a pneumatic cylinder. It is used to start the sounding rocket.

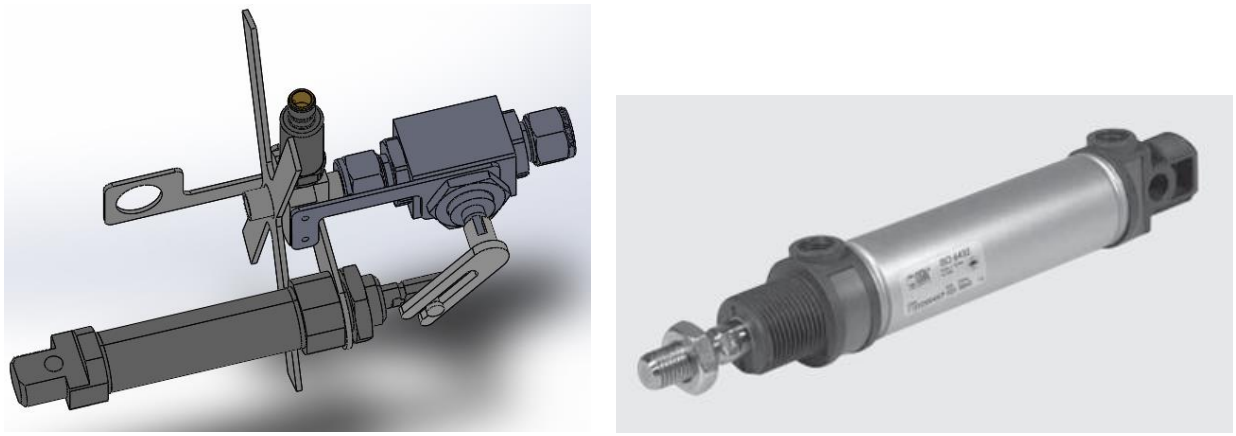

Figure 2.23 - Manual ball valve Ham-Let H6800 (left) with cylinder actuator (right).

- *Solenoid valve Ham-Let Z-SVD ("A-2")*: a solenoid valve attached to the actuator to create an electro-pneumatically actuated ball valve.

Figure 2.24 - Solenoid valve Ham-Let Z-SVD.

- *Miniature Pressure Regulator Tescom BB-1 ("Pressure Regulator 2")*: a control valve that reduces the input pressure of a fluid to a desired output value (in our case 5-8 bar).

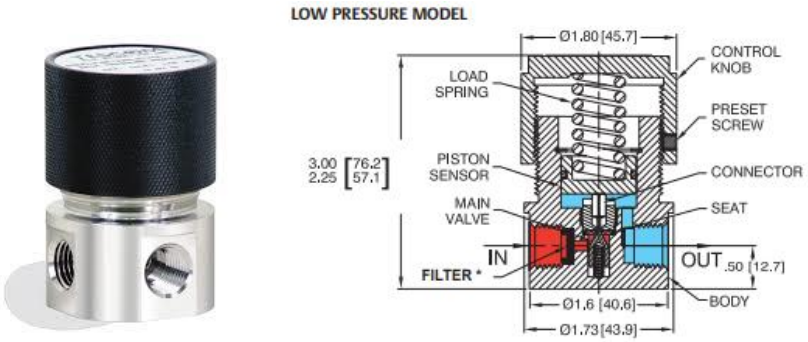

Figure 2.25 - Miniature Pressure Regulator Tescom BB-1.

- CO_2 *tank Ham-Let HSSC153BH ("Little Tank")*: tank filled with compressed CO_2 used for *Vox-1* actuation.

Figure 2.26 - CO_2 tank Ham-Let HSSC153BH.

- *Manual ball valve Ham-Let H6800 ("Vox-2")*: a mechanical ball valve which serves as safety valve. It is opened before the pressurization and if *Vox-1* fails it can stop the flow before reaching the catalytic reactor.

Figure 2.27 - Manual ball valve Ham-Let H6800.

2.4 Motor

The motor is the subsystem producing the thrust to propel the rocket. This subsystem is divided into:

- *Catalytic reactor*: it is a metal case containing disks of catalytic material which decompose H_2O_2 into gaseous O_2 and water vapor.
- *Combustion chamber*: it contains the paraffin grain, which burns reacting with the O_2 coming from the reactor. After that a post-chamber allows a more complete combustion of the products before the expulsion through the nozzle.
- *Nozzle*: it has a convergent-divergent layout in order to accelerate the exhaust gas to supersonic speed.

Each one of these parts will be summarily described. The catalytic reactor is an exception because it is one of the subjects of the tests described in this thesis, so it will be explained more thoroughly in section 2.4.1.

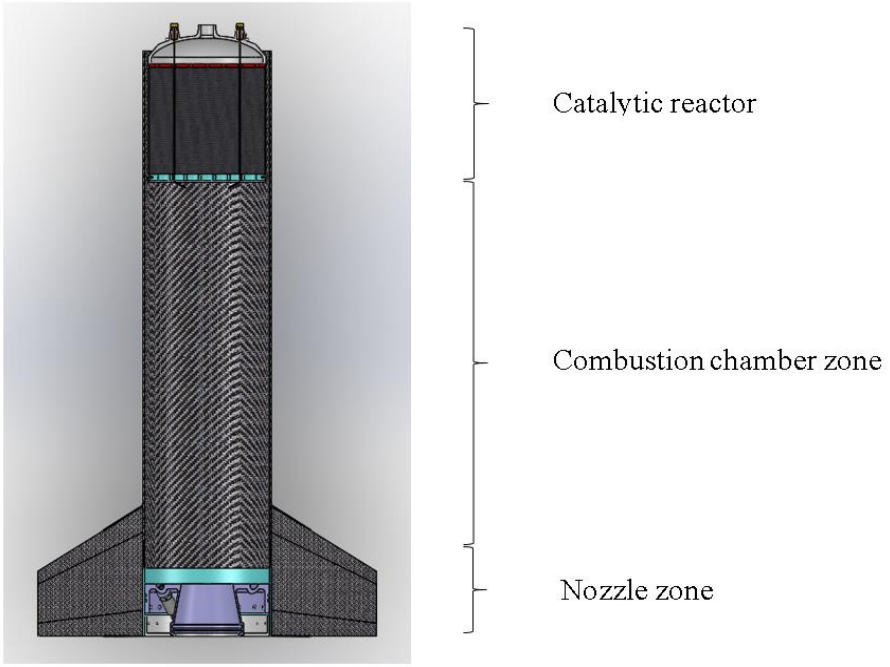

Figure 2.28 - Schematic cross section of the motor with its subsystems.

The **combustion chamber** contains a cylindrical paraffin grain with a single port. Additional HDPE (high-density polyethylene) thermal protections are placed at both ends of the grain. A cylindrical HDPE jacket encloses most of the motor, from the catalytic reactor to the nozzle, to protect the composite case from heat. The pressure in the chamber reaches about 25 bar. The post-chamber is divided into two sections by a mixer made of cotton-phenolic. It ensures a better mixing of the exhaust gasses.

The **nozzle zone** is made up of a titanium alloy (Ti-6Al-4V) case, cotton-phenolic protections and a graphite insert at the throat to reduce erosion. Pressure in the post chamber is measured by two pressure sensors *ifm PT5401* fastened into the titanium case.

2.4.1 Catalytic Reactor

The hydrogen peroxide is decomposed by the catalytic material contained in the case. The catalytic material is held in place by two plates: the injection plate and the catalytic stopping grid. The case itself consists in two parts: a cylindrical body and a dome welded on top of it. In the upper zone the metal case is in contact with the joint connecting the motor case to the oxidizer interstage case, whereas in the lower zone it is free from the rest of the system. Figure 2.29 shows a schematic cross section of the zone where the reactor is placed inside the rocket.

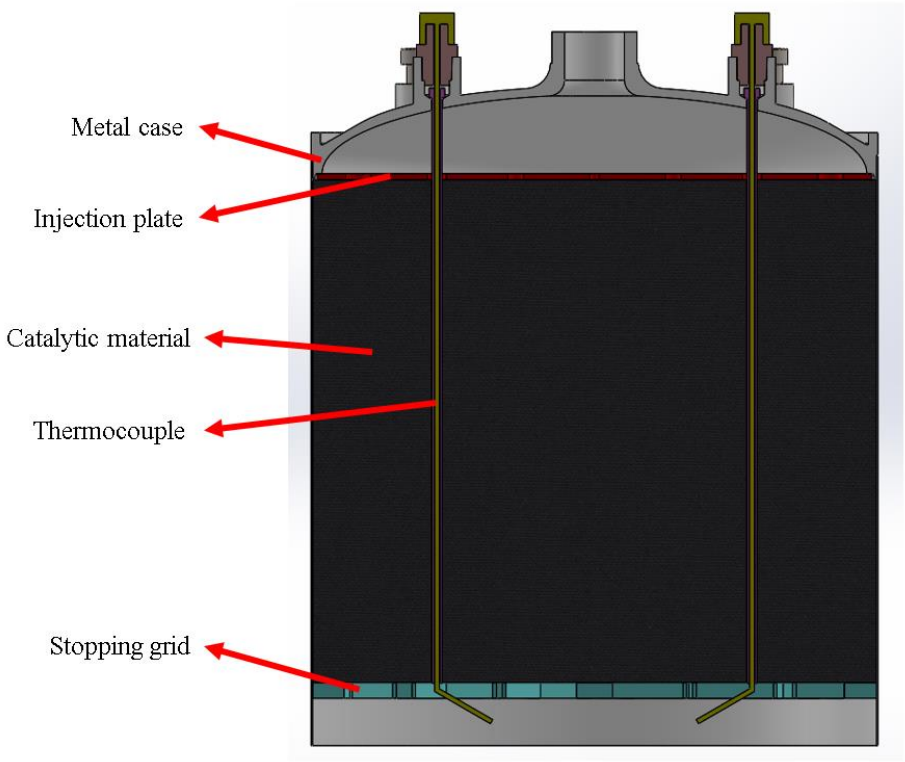

Figure 2.29 - Schematic cross section of the catalytic reactor zone.

Because of the high temperatures reached by the metal case (especially in the lower part, where the H_2O_2 is fully decomposed) the whole system has been placed inside the composite case without any direct contact between the hot parts of the reactor and the composite material or the joints. In the dome zone, where the reactor is connected with the rest of the system, there are no thermal problems since the H_2O_2 does not start to decompose until it reaches the catalytic material. On top of that, the regenerative heat exchanged with the cold, liquid H_2O_2 prevents the inlet zone from becoming hot.

The lower part of the reactor is not connected with any other component of the system; in this way the thermal dilatations of the metal case do not interfere with the other parts of the motor. This configuration has another advantage: the decomposed hydrogen peroxide is free to pass around the reactor metal case and almost counterbalance the inner pressure (the difference between the inner and the outer pressure is given only by the pressure gradient along the catalytic system), allowing the use of a thinner (i.e. lighter) metal case. The external composite case is then isolated from the hot gases by the cotton phenolic jacket used to enclose the motor (see section 2.1.3).

2.4.1.1 Cylindrical Body

Since the diameter-wall thickness ratio is higher than 20, Mariotte's law for thin-walled pressure vessels can be applied to verify the structural resistance of the cylindrical body:

$$t = \frac{pD}{2\frac{\sigma_c}{k}} \text{ [14]} \tag{2.1}$$

The chosen thickness t is 0.5 mm, therefore the formula could be rearranged in order to verify the safety factor on the material properties k:

$$k = \frac{2t\sigma_c}{pD} \tag{2.2}$$

p is the net pressure i.e. the pressure difference between the H_2O_2 in the inlet zone and the decomposed H_2O_2 after the reactor.

D is the external diameter of the case, equal to 180 mm as a requirement.

σ_c is the yield strength of the material. Since the catalytic material produces heat in the H_2O_2 decomposition process, values of yield strength at around 800 °C have been selected. The value for AISI 316 stainless steel is 110-124 MPa [15], which is not much. For this reason, Inconel 718 has been chosen instead, since it has a yield strength of more than 500 MPa at that temperature [16].

Substituting this value in Mariotte's formula, the safety factor *k* becomes 5.56.

2.4.1.2 Dome Sizing

One of the major restrictions to the catalytic reactor design was the dome filling time: an increase of the dome height would allow a lower thickness, leading to a reduction mass, but it would also determine an increase of the filling time. Consequently, the dome has been designed taking care that the filling time does not grow over 0.5 s.

The following geometric simplification has been considered: the dome has been assumed to be a perfect ellipsoid of constant thickness.

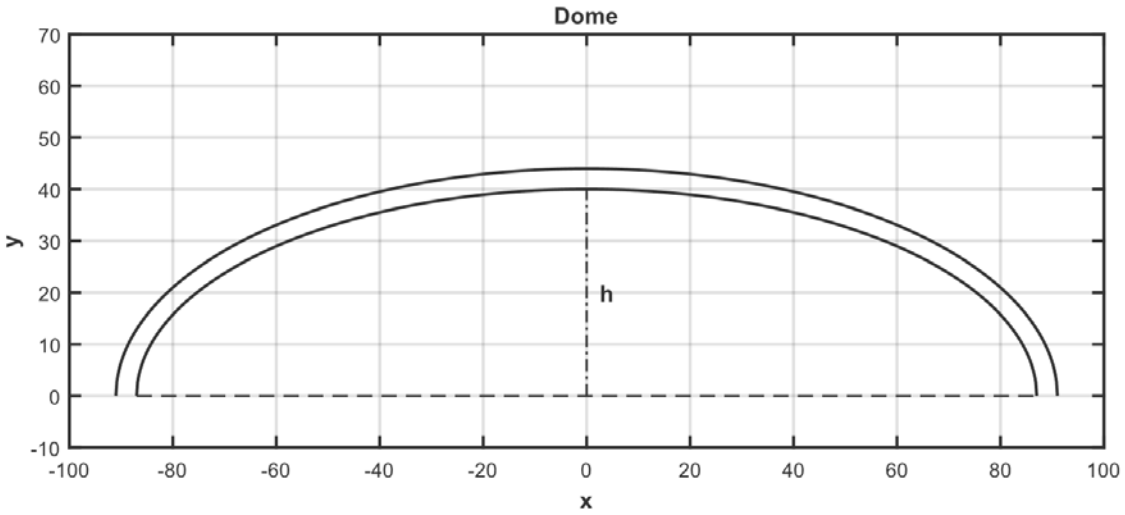

Figure 2.30 - Schematic model of the reactor dome.

In this case then, denoting:

- *th* = the dome thickness
- *h* = the semi-minor axis of the inner ellipse
- *R* = the semi-major axis of the inner ellipse

and considering the ellipsoid with a perfectly circular base, the inner volume can be evaluated as a half of an ellipsoid volume:

$$V = \frac{2}{3}\pi R^2 h \tag{2.3}$$

A further assumption has been made as regards volume filling. The hypothesis is that all the volume should be filled before the oxidizer begins to flow in the catalytic bed. Knowing the mass flow rate and the H_2O_2 density, the dome filling time can be evaluated as:

$$Q = \frac{\dot{m}_{ox}}{\rho_{ox}} = \frac{V}{t_{fill}} \tag{2.4}$$

which yields:

$$t_{fill} = \frac{2}{3}\frac{\rho_{ox}}{\dot{m}_{ox}}\pi R^2 h \tag{2.5}$$

A model for the thickness evaluation as function of dome height and internal pressure is the following:

$$th = \frac{p \cdot D \cdot K}{2 \cdot E \cdot \sigma - 0.2 \cdot p} \tag{2.6}$$

with:

$$K = \frac{1}{6}\left[2 + \left(\frac{D}{2h}\right)^2\right] \text{[17]} \quad (2.7)$$

E is a dimensionless welding efficiency coefficient. Its assumption is crucial, since the dome is welded to the cylindrical portion of the reactor case. A value of 0.6, which denotes a very poor-quality weld, has been assumed in order to have conservative results.

This led to the choice of the following dimensions:

Inputs		**Outputs**	
Pressure [bar]	25.0	Evaluated Thickness [mm]	2.67
H_2O_2 Density [kg/m^3]	1400	Minimum Actual Thickness [mm]	2.78
H_2O_2 Mass Flow [kg/s]	2.00	Evaluated Filling Time [s]	0.30
Internal Height [mm]	25.0		
External Diameter [mm]	180.0		
Inconel 718 Yield Strength [MPa]	248.2		
Safety Factor	2.0		
Maximum Filling Time (constraint) [s]	0.5		

Table 2.2 - Dome design results.

The actual design has some differences in terms of geometry. Having the dome perfectly elliptical would lead to a non-designable configuration, due to both the difference in terms of thickness with the cylindrical portion (whose design has been brought forward using the Mariotte's equation, as seen in section 2.4.1.2) and the fact that the external surface of the dome must interact with the case junction. Therefore, the actual design of the dome is summarized in the following figure:

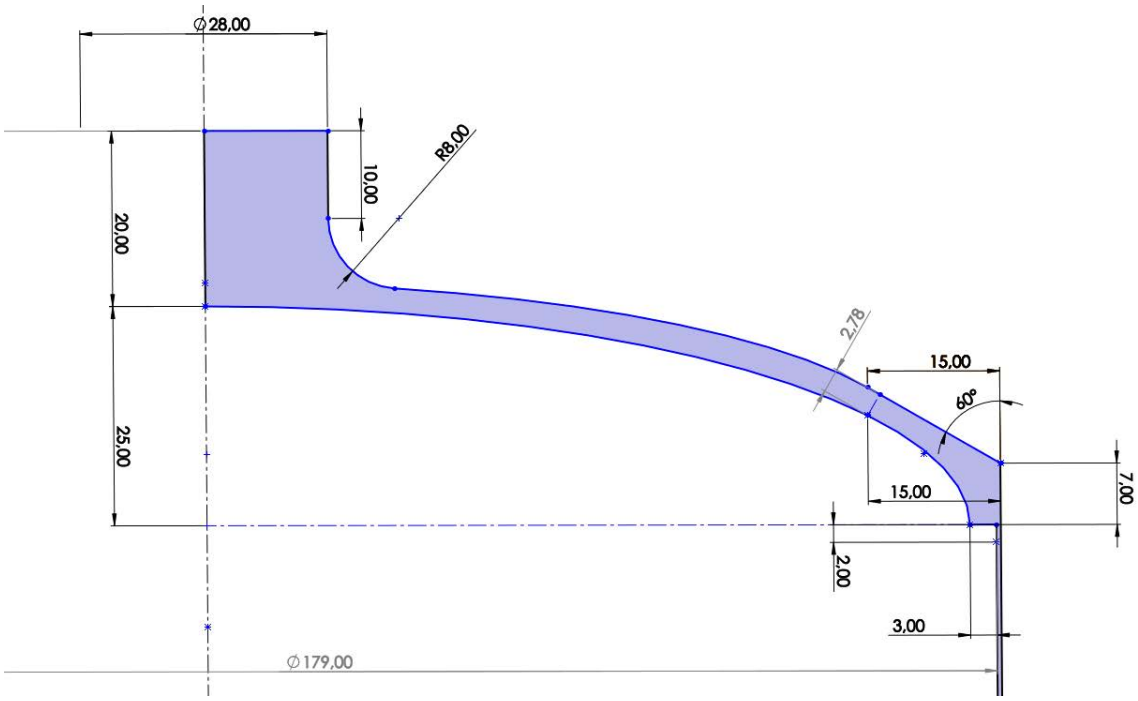

Figure 2.31 - Schematic of the reactor dome design.

The interaction with the case junction is needed in order to have a contact area through which the thrust could be transferred by the motor assembly to the rest of the rocket.

Again, another difference between the actual geometry and the "mathematical" one is in the fact that a G1/2 female threaded link has been placed on top of the dome to connect the reactor to the above fluidic subsystem.

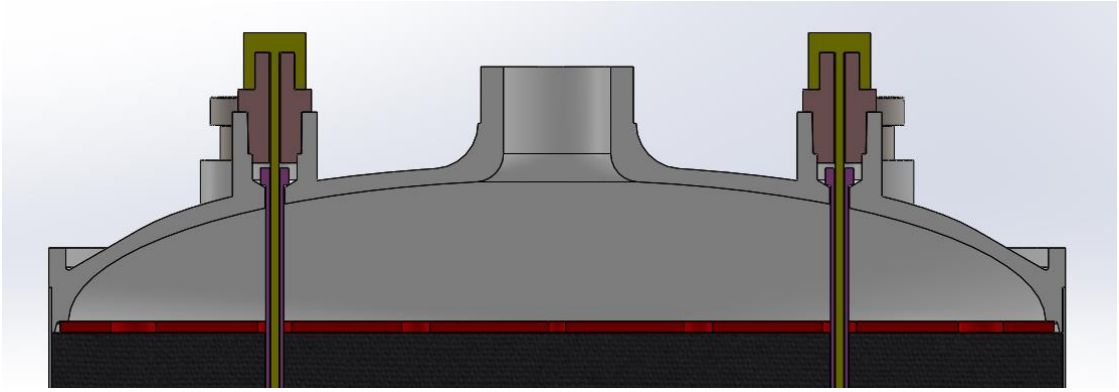

Figure 2.32 - Reactor dome middle section.

2.4.1.3 Injection Plate and Stopping Grid

The catalyst pack is kept in place by an **injection plate** at its top and a **stopping grid** at its bottom (figure 2.29).

The **injection plate** is essentially a holed disk where the oxidizer flows through to reach the catalytic material. The material used is AISI 316 stainless steel.

The **stopping grid** is placed near the lower end of the cylindrical body of the metal case. Due to H_2O_2 decomposition, temperature in that zone could potentially reach about 800 °C, so the grid is made of Inconel 718.

The grid is sustained by 12 **bracket-like inserts** fastened radially through the case wall. These brackets must sustain both the weight of the reactor (considering also the thrust acceleration) and the force caused by the pressure difference: the total force is therefore assumed equal to 13178 N. The brackets have a maximum height of 10 mm, a thickness of 6 mm and are 24° wide. They are fastened by 24 M4 screws (two for each insert). Like the grid, both screws and brackets are made of Inconel 718.

2.4.1.4 Axial Screws

The catalytic reactor is fastened to the fluidic line-motor junction by means of axial screws.

These screws have been verified considering as load the entire reactor weight, whose total mass has been estimated to be 9.36 kg. 6 class 8.8 screws have been considered. The verification has been taken for a tensile load:

Screw	σ [Pa]	Safety factor
M1.8	1.25E+07	51.29
M2	1.02E+07	62.85
M3	4.22E+06	151.62
M4	2.42E+06	264.51
M5	1.50E+06	427.42
M6	1.06E+06	606.36
M7	7.36E+05	869.63
M8	5.80E+05	1103.15
M10	3.47E+05	1844.17

Table 2.3 - Tensile verification of axial screws.

The tensile verification has produced good results for every type of screw considered. M3-type screws have been chosen.

2.4.1.5 Thermal Expansion Study

Since the metal case is subjected to a great temperature increase because of the H_2O_2 decomposition, some preliminary calculations about its thermal expansion have been made.

The dilatation of each dimension of the metal case due to temperature change has been calculated using the linear thermal expansion model; calling x a general dimension, ΔT the temperature difference and α_L the linear expansion coefficient (measured in K^{-1}), it yields:

$$\Delta x = \alpha_L \cdot x \cdot \Delta T \tag{2.8}$$

This formula has been implemented for three different dimensions of the metal case:

- Internal diameter: initial value = 179 mm.
- External diameter: initial value = 180 mm.
- Cylinder height: initial value = 191.6 mm.

For Inconel 718 a value of $1.6 \times 10^{-5} K^{-1}$ for the linear thermal expansion coefficient has been used [18]. The temperature difference implemented is 700 K.

The results of these calculations are reported in the figure below where the positions of the metal case cross section in the cold and hot cases are shown.

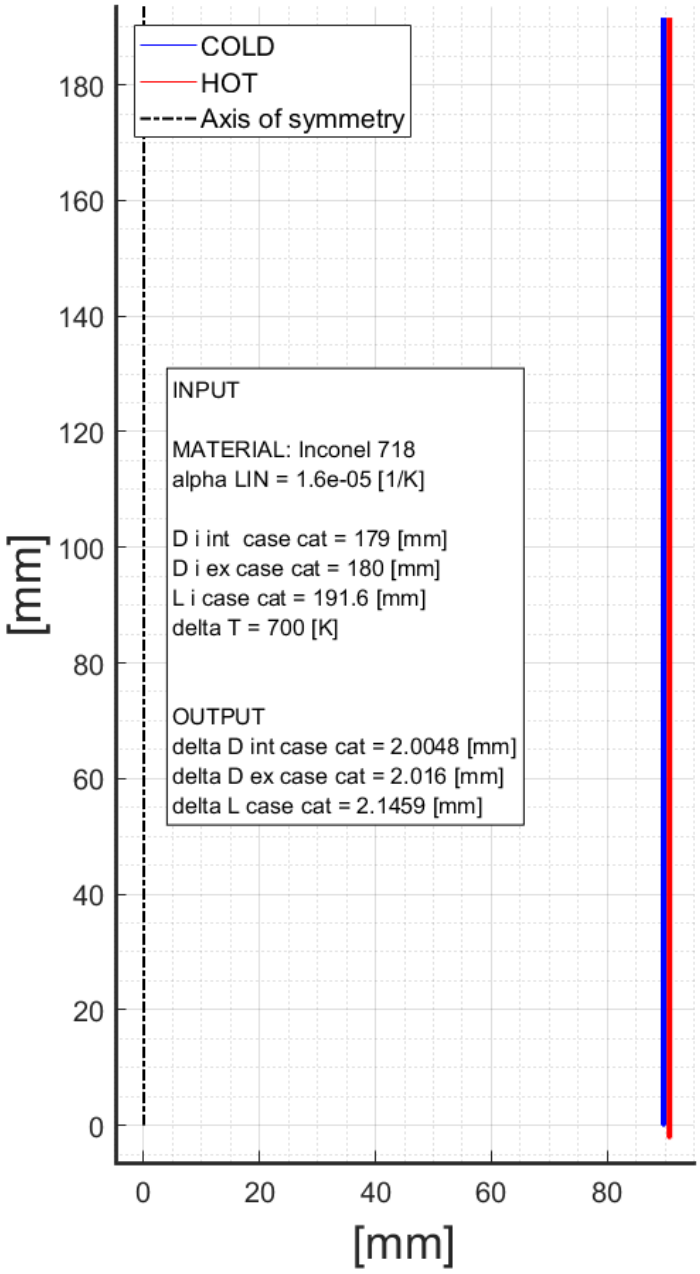

Figure 2.33 - Dilatation of the reactor metal case.

The results proved that the thermal elongation is quite limited, even with a great temperature gradient. This effect has been considered in the sizing of the cotton phenolic flange in contact with the reactor basement: a clearance (~1 mm) in the interface between the flange and the metal case has been used.

2.4.1.6 Temperature Diagnostic

The temperature of the decomposed H_2O_2 after the catalytic reactor is measured by 2 thermocouples that pass through the metal case and the catalytic material (see figure 2.29).

Previous experiences suggested to use thermocouples with a core cross section diameter of 1.5 mm.

2.5 Recovery System

The recovery system allows the rocket to be retrieved after the mission. It consists in a **main parachute**, a **drogue parachute** and a **floating system** kept inside a bay right below the nosecone. A **door** keeps the system closed and opens at the appropriate moment to allow the aforementioned devices to operate.

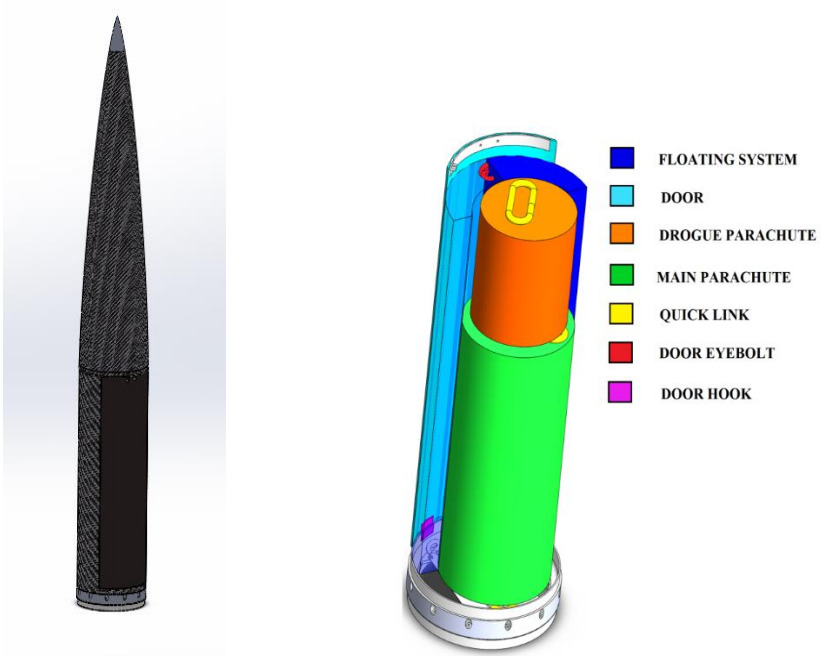

Figure 2.34 - External (left) and internal (right) view of the recovery bay.

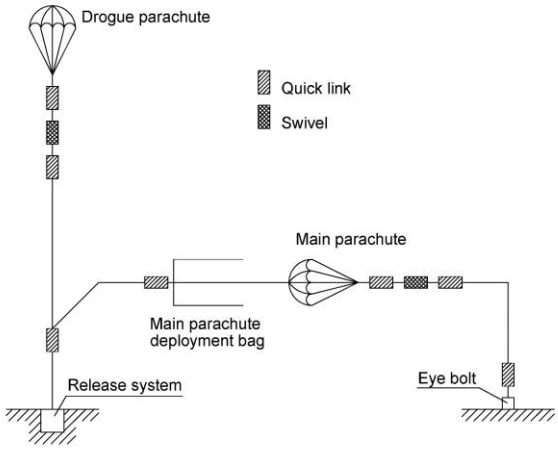

Figure 2.35 - Deployed recovery system schematic.

The system activates when the rockets reaches the apogee. The rocket is supposed to land on water. The modes of operation of the system are explained schematically as follows:

- The recovery bay is closed.

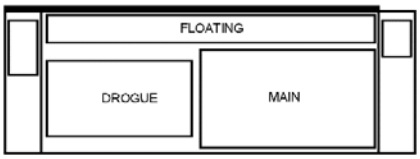

Figure 2.36 - Schematic cross section of the closed recovery bay.

- The cutter-spring system allows the opening of the door which is directly linked to the drogue parachute with a shock cord.

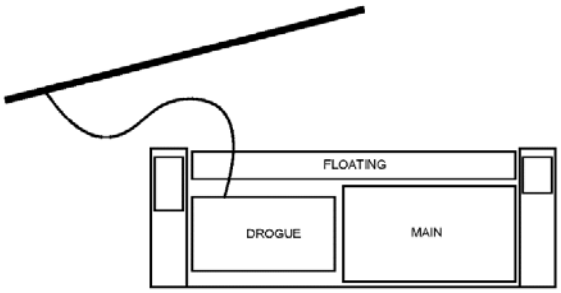

Figure 2.37 - Schematic cross section at the opening of the door.

- Once the door is removed, the floats, directly linked to the bay with a shock cord, are the first components to come out. At the same time the door pulls out the drogue parachute, which is also linked to the main parachute and the bay with a 3 loops shock cord. The opening of the secondary parachute allows the first deceleration during the free fall of the rocket.

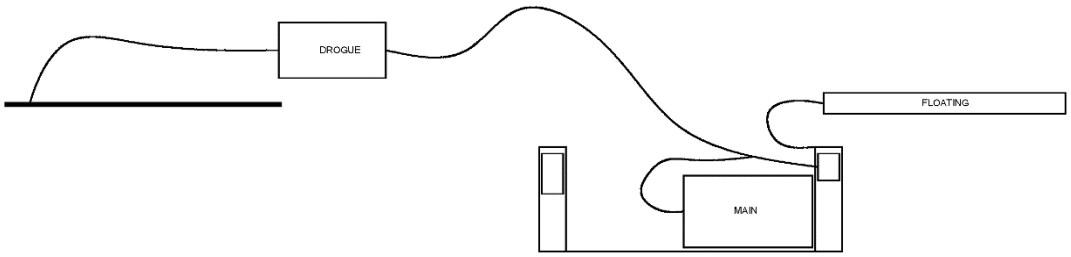

Figure 2.38 - Schematic cross section at the extraction of the components.

- At about 1 km or 2 from the ground the drogue parachute breaks away from the bay pulling out the main parachute. During the last stage of the descent the main parachute is supposed to support the whole structure and slow the rocket down until the water landing. The floats, extracted at the apogee, inflate once in contact with the water, ensuring the buoyancy.

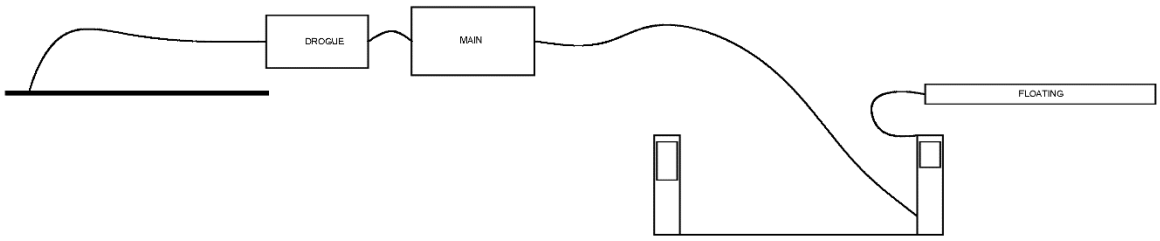

Figure 2.39 - Schematic cross section at the complete extraction of the components.

Chapter 3

Test Campaign: Goals, Requirements and Procedures

The rocket subsystems will undergo a series of tests. These tests will be of 3 kinds:

- *Vertical tests of the fluidic line.*
- *Vertical tests of the catalytic reactor.*
- *Horizontal tests of the entire propulsive system.*

The **horizontal tests** will be not treated in this thesis: there is already a functional horizontal test bench, so there is no need to design a new one.

The tests of **fluidic line** and **catalytic reactor** will be run on separate vertical benches appositely designed.

The **fluidic line test** aims to verify if the pressurization and the oxidizer discharge happen correctly.

The **catalytic reactor test** aims to verify the correct functioning of the catalytic system and measure how much thrust it provides without grain combustion.

3.1 Test Benches Requirements

Before describing the test benches in detail, it is necessary to define their functional and safety requirements.

3.1.1 Fluidic Line Test Bench

The **functional requirements** of the fluidic line test bench are:

- *Vertical layout*: the oxidizer must be discharged vertically in order to be as close as possible to the flight conditions.
- *As close as possible to the actual flight design*: the section between the oxidizer inlet and the cavitating Venturi must be identical to its counterpart in the flight configuration. The pressurizer tank must be also the same used for the mission.
- *Oxidizer flow rate measurement*: a flowmeter must be placed downstream from the oxidizer tank.
- *Commercial components*: most of the hydraulic components will be identical to the ones used for the mission. The bench must be also composed by easy-to-acquire commercial components.

The **safety requirements**, on the other hand, are:

- *The tests must be done inside a dedicated container*: collateral damages must be prevented. Because the system must fit inside the container, it cannot exceed 2.3 m in height. For this reason, the pressurizer line and tank cannot be stacked on top of the oxidizer tank but must be placed on its side. Consequently, the gas line between the pressurizer and oxidizer tanks must include some sort of bend.
- *Safety measures against overpressure*: sensors, tank venting, a by-pass line and a burst disk must be used to prevent damage from unexpected overpressure phenomena caused by pressurization and/or H_2O_2 decomposition.
- *Disposal of discharged and/or leaked* H_2O_2: hoses must be placed at every possible outlet in order to channel discharged and/or leaked H_2O_2 into containers for liquids. A large amount of water must be at disposal to dilute eventual leaked 90% H_2O_2. Protections must be used to shield the container from leaked oxidizer.

3.1.2 Catalytic Reactor Test Bench

The **functional requirements** of the catalytic reactor test bench are:

- *Vertical layout*: the thrust must be directed downwards in order to have conditions as close as possible to the ones during flight.

- *~300 kg of vertical load*: the bench must be loaded with a water tank to reach a total weight of ~300 kg in order to counterbalance the thrust exerted by the reactor (expected to be ~2500 N).
- *H_2O_2 injected in the reactor directly from storing tanks in situ*: the cavitating Venturi and the components downstream from it are the only part of the rocket fluidic system that are required for the test. The test location is already provided with the necessary H_2O_2 tanks and fluidic lines.
- *Temperature measurement*: the test reactor has 2 thermocouples inside it to measure temperature, just like the flight reactor (see section 2.4.1.9).
- *Thrust measurement*: load cells are required to measure the thrust developed by the system.

The **safety requirements**, on the other hand, are:

- *Supports capable of withstanding the loads*: the various part of the bench must be able to support all the loads, including the weight of the reactor, the thrust and the downward load.
- *The water tank must be stable and easy to empty*: the water tank must have a vent in the lower part to make it easier to empty. Perimetrical sheet-metal walls must be used to keep the tank stable.
- *Sensor redundancy*: at least 2 thermocouples and 4 load cells must be used.
- *Monitoring systems to detect anomalies*: temperature and pressure sensors must be used in the fluidic line to detect eventual oxidizer decomposition, overpressure phenomena and other anomalies.
- *Breaking fasteners for the nozzle*: the reactor used for the test must have the nozzle fastened with bolts that break in case of overpressure phenomena. In that way, only the nozzle would detach and the reactor would not explode.
- *Protections against eventual explosions and/or detachments*: the area surrounding the test location must be surrounded by an embankment. The test bench must not be higher than the bank, so it must not exceed 2 m in height. Additional protections must be used around the bench to stop eventual detached fragments.
- *Plume deflector below the nozzle*: the hot exhaust (up to ~800 °C) must be deviated sideways.
- *Disposal of leaked H_2O_2*: a large amount of water must be at disposal to dilute eventual leaked 90% H_2O_2.

3.2 Tests Procedures

In this section procedures and safety measures for both fluidic line and catalytic reactor tests are described.

3.2.1 Fluidic Line Tests

The fluidic line to test has the same components of the flight configuration (see section 2.3); only slight changes in the connections between the pressurizer line and the oxidizer tank are needed to allow the pressurizer tank and line to be placed at the side of the other tank (see section 3.1.1). For easiness of reference the process flow diagram of the entire fluidic line (see figure 2.8) is here reported again:

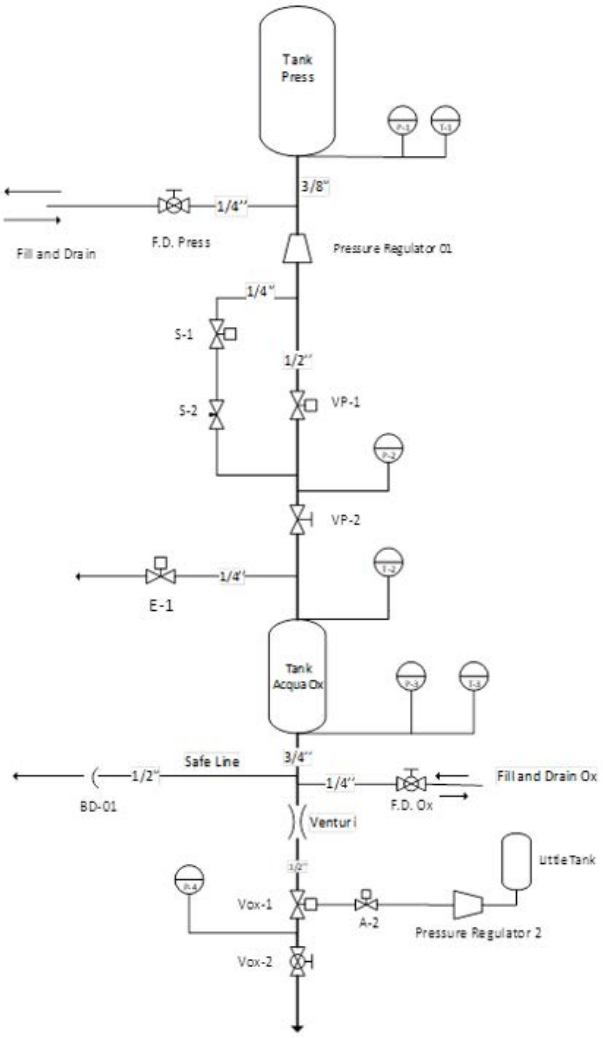

Figure 3.1 - Process flow diagram of the entire fluidic line.

The fluidic line must undergo 3 series of tests:

- *Calibration of the pressurization system*: the system without oxidizer is pressurized in order to verify the correct functioning of the pressurization system and the tightness of tanks and fluidic line components.
- *Discharge tests with distilled* H_2O: if the previous tests succeed, discharge tests are carried out using a harmless liquid, specifically distilled water. The oxidizer tank is filled with H_2O and pressurized; then the water is discharged through the oxidizer outlet in order to simulate the fluidic line functioning during flight.
- *Discharge tests with 90%* H_2O_2: if the previous tests succeed, the discharge tests are repeated using the actual oxidizer (90% hydrogen peroxide) in order to simulate flight conditions as closely as possible.

The same vertical bench will be used for all these tests (see chapter 4 for more details).

The **safety measures** adopted to meet the safety requirements (see section 3.1.1) are listed below:

- *Class 1 or 2 materials*: all materials in contact with the oxidizer have very good compatibility with the latter.
- *Oxidizer tank venting*: it ensures safety against moderate/high decomposition and overpressure.
- *Burst disk*: it is placed at the end of a safety line downstream from the oxidizer tank, ensuring safety against overpressure.
- *By-pass line*: it is placed in the pressurizer line and it is used to adjust the gas filling time in order to prevent excessively high temperatures due to compression.
- *Hose at burst disk outlet*: it channels H_2O/H_2O_2 into a container in case of disk bursting.
- *Hose at the main outlet*: it channels discharged H_2O/H_2O_2 into a container.
- *Temperature and pressure sensors*: they allow to detect anomalies such as oxidizer decomposition, that could cause overpressure or other dangerous phenomena.
- *Water tank with hose at disposal*: it is used to dilute eventual leaked H_2O_2.
- *Container*: it contains the test bench in order to prevent collateral damages in case of explosion or H_2O_2 leakage.
- *Plexiglass panels on the container walls*: they prevent eventual contact of leaked H_2O_2 with the container walls.

- *Plastic tarpaulin on the container floor*: it prevents eventual contact of leaked H_2O_2 with the container floor and rout it outside.

The following tables list all the main steps necessary for the tests. Moreover, in case of failures, it refers to which emergency procedure must be done.

Calibration of the Pressurization System

Procedure	Description	Valve	Status	Sensor	Output	Emergency
Verify that all components are clean and inside the line there is no air.						
Fill and drain pressurization tank to test the line.	Fill and drain pressurization tank to test if there are leakages.	ALL VALVES	CLOSE			
		FD PRESS	OPEN			
		FD PRESS (when tank press. is reached)	CLOSE	T-1	Temperature increasing	
				P-1	Pressure increasing	
				P-2	P_{atm}	If P-2 higher than P_{atm} follow EM-1.
				P-3	P_{atm}	If P-3 higher than P_{atm} follow EM-1.
		FD PRESS	OPEN			
		FD PRESS	CLOSE			
Test if there are leakages in the ox line by pressurizing the tank with 10 Bar.	Fill and drain ox tank with 10 Bar.	FD OX (reach 10 bar in the ox tank than depressurize).	OPEN	P-3	10 Bar	
				P-4	P_{atm}	If P-4 higher than P_{atm} then VP-1 has leakage.
		FD OX (when depressurize is complete).	CLOSE			

Table 3.1 - Procedures for calibration of the pressurization system.

Discharge Tests with Distilled H_2O

Procedure	Description	Valve	Status	Sensor	Output	Emergency
Fill ox tank with H_2O.	Create vacuum in ox tank and then fill tank with distilled water.	ALL VALVES	CLOSE			
		FD OX (create vacuum inside the tank)	OPEN	P-3	0	
		FD OX (when vacuum is reached)	CLOSE			
		FD OX (fill H_2O)	OPEN			
		FD OX (when tank ox is full)	CLOSE			
Fill pressurization tank.	Fill pressurization tank.	ALL VALVES	CLOSE			
		FD PRESS	OPEN	T-1	Temperature increasing	
				P-1	Pressure increasing	
				P-2	P_{atm}	If P-2 higher than P_{atm} follow EM-1.
				P-3	P_{atm} + weight of H_2O	If P-3 higher than P_{atm} follow EM-1.
		FD PRESS (when tank press. is reached)	CLOSE			
Removing safety.	Two main safety valves (pressurization line and oxidizer line) are opened.	VP-2	OPEN			
		VOX-2	OPEN			
		GAS HATCH	CLOSE			
		LIQUID HATCH	CLOSE			

Pressurize ox tank.	In order to prevent high temperature due to the gas compression inside the ox tank (ullage volume), a very slow pressurization ramp is required. The by-pass line has a calibrated orifice to adjust the gas filling timing.	S-1	OPEN	P-2	Pressure increasing	If S-1 fails to open, follow EM-1.
				P-3	Pressure increasing	
		VP-1 (after nominal pressure is reached in ox tank)	OPEN			If VP-1 fails to open, follow EM-2.
		S-1	CLOSE			
Discharge.	Discharge of the ox tank line.	VOX-1	OPEN			If VOX-1 fails to open, follow EM-1 and EM-4.

Table 3.2 - Procedures for discharge tests with distilled H_2O.

Discharge Tests with 90% H_2O_2

Procedure	Description	Valve	Status	Sensor	Output	Emergency
Fill ox tank with H_2O_2.	Create vacuum in ox tank and then fill tank with distilled water.	ALL VALVES	CLOSE			
		FD OX (create vacuum inside the tank)	OPEN	P-3	0	
		FD OX (when vacuum is reached)	CLOSE			
		FD OX (fill H_2O_2)	OPEN			
		FD OX (when ox tank is full)	CLOSE			

Wait 10 minutes to check if decomposition phenomena take place.	Check if there are decomposition phenomena of the H_2O_2.	ALL VALVES	CLOSE	T-2	Ambient temperature	If T-2 increases, follow EM-3.
				P-3	P_{atm} + weight of H_2O_2	If P-3 increases, follow EM-3.
Fill pressurization tank.	Fill pressurization tank.	ALL VALVES	CLOSE			
		FD PRESS	OPEN	T-1	Temperature increasing	
				P-1	Pressure increasing	
				P-2	P_{atm}	If P-2 higher than P_{atm} follow EM-1.
				P-3	P_{atm} + weight of H_2O_2	If P-3 higher than P_{atm} follow EM-1.
		FD PRESS (when tank press. is reached)	CLOSE			
Removing safety.	Two main safety valves (pressurization line and oxidizer line) are opened.	VP-2	OPEN			
		VOX-2	OPEN			
		GAS HATCH	CLOSE			
		LIQUID HATCH	CLOSE			
Pressurize ox tank.	In order to prevent high temperature due to the gas compression inside the ox tank (ullage volume), a very slow pressurization ramp is required. The by-pass line has a calibrated orifice to adjust the gas filling timing.	S-1	OPEN	P-2	Pressure increasing	If S-1 fails to open, follow EM-1.
				P-3	Pressure increasing	
		VP-1 (after nominal pressure is reached in ox tank)	OPEN			If VP-1 fails to open, follow EM-2.
		S-1	CLOSE			

Discharge.	Discharge of the ox tank line.	VOX-1	OPEN	If VOX-1 fails to open, follow EM-1 and EM-4.

Table 3.3 - Procedures for discharge tests with H_2O_2.

Emergency Procedures

Emergency	Procedure	Description	Valve	Status	Failure
EM-1	Drain pressurization tank.	Drain pressurization tank in case of VP-1, S-1 or VP-2 leakage.	VP-2	OPEN	
			VP-1	OPEN	If VP-1 fails to open, follow EM-2.
			E-1	OPEN	
EM-2	Drain pressurization tank.	Drain pressurization tank in case VP-1 fail.	VP-2	OPEN	
			S-1	OPEN	If S-1 and VP-1 fails, open FD PRESS.
			E-1	OPEN	
EM-3	Reduce the pressure in the ox tank.	Reduce the pressure in case of decomposition of H_2O_2.	ALL VALVES	CLOSE	
			E-1	OPEN	
EM-4	Drain ox tank.	Drain H_2O_2 tank.	ALL VALVES	CLOSE	
			FD OX	OPEN	

Table 3.4 - Emergency procedures for fluidic line tests.

3.2.2 Catalytic Reactor Tests

For this test a specifically made reactor is used (see section 4.2 for more details).

One of the storage tanks used in the test facility, including its fluidic line and pressurization system, will be utilized to feed the reactor. The only needed parts of the rocket fluidic system are the cavitating Venturi and the components downstream from it. Here is the process flow diagram of the system to test:

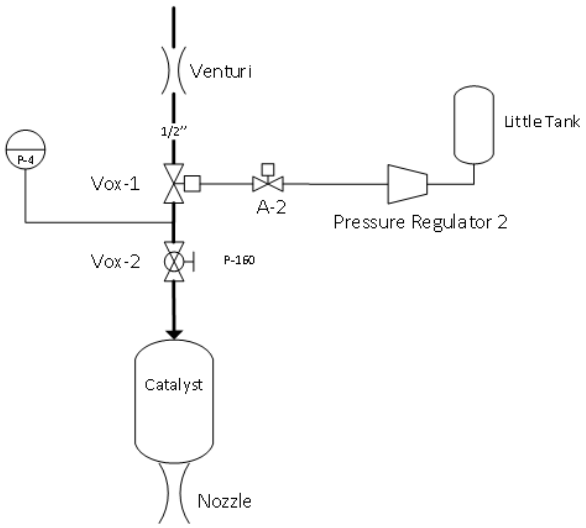

Figure 3.2 - Process flow diagram of the test reactor and its fluidic line.

The catalytic reactor tests will be carried out after the fluidic line tests. The reactor test consists in injecting 90% H_2O_2 into the catalytic bed, decomposing it and expelling the product gasses from the nozzle. Measurements of thrust will be taken. A dedicated test bench (different from the one used for the fluidic line tests) will be used (see chapter 4 for more details).

The **safety measures** adopted to meet the safety requirements (see section 3.1.2) are listed below:

- *Class 1 or 2 materials*: all materials in contact with the oxidizer have very good compatibility with the latter.
- *Breaking fasteners for the nozzle*: as already mentioned in section 3.1.2, the nozzle is fastened with bolts that break in case of overpressure phenomena. In that way, only the nozzle would detach and the reactor would not explode.
- *Temperature and pressure sensors*: they allow to detect anomalies such as oxidizer decomposition that could cause overpressure or other dangerous phenomena.
- *4 load cells and 2 thermocouples for redundancy*: as already mentioned in section 3.1.2, multiple sensors are used to ensure reliability.
- *Plume deflector below the nozzle*: as already mentioned in section 3.1.2, the hot exhaust (up to ~800 °C) is deviated sideways by a curved steel deflector.
- *Steel net and plexiglass panels around the test bench*: they prevent collateral damage s in case of explosion or detachments.

- *Water tank with hose at disposal*: it is used to dilute eventual leaked H_2O_2.
- *Surrounding embankment*: the test facility is surrounded by ~2 m tall embankment to protect the surrounding area from eventual explosions or detachments.

All the main steps necessary for the tests are listed in the following tables. Furthermore, in case of failures, it refers to which emergency procedure must be done.

Procedures for Catalytic Reactor Tests

Procedure	Description	Valve	Status	Emergency
Verify that all components are clean and inside the line there is no air.				
Removing safety.	Safety valves are opened.	ALL VALVES	CLOSE	
		VOX-2	OPEN	
Discharge.	Discharge of H_2O_2 through the reactor.	VOX-1	OPEN	If VOX-1 fail to open, follow EM-1.

Table 3.5 - Procedures for catalytic reactor tests.

Emergency Procedures

Emergency	Procedure	Description	Valve	Status
EM-1	Drain feed line.	Drain feed line from H_2O_2.	ALL VALVES	CLOSE
			RELIEF	OPEN

Table 3.6 - Emergency procedures for catalytic reactor tests.

Chapter 4

Test Benches Design

As mentioned in the previous chapter, 2 different vertical test benches have been designed, one for the **fluidic line tests** and one for the **catalytic reactor tests**.

4.1 Fluidic Line Test Bench

The fluidic line is sustained by a stainless-steel frame built with Fischer SaMontec components for plant engineering. The frame consists in 4 mounting channels stiffened by other transversal channels of the same type. Pipe clamp collars are fastened to 4 of the transversal channels and clamped around the tanks in order to keep the entire fluidic line stable and raised from the base (there are 80 mm between the lower junction and the base plate). The tanks themselves are not stacked on top of each other, but are placed side by side, with a slightly modified gas line connecting them at the top of the structure (see also section 3.1.1). The layout of the test bench is showed in detail in the following figures:

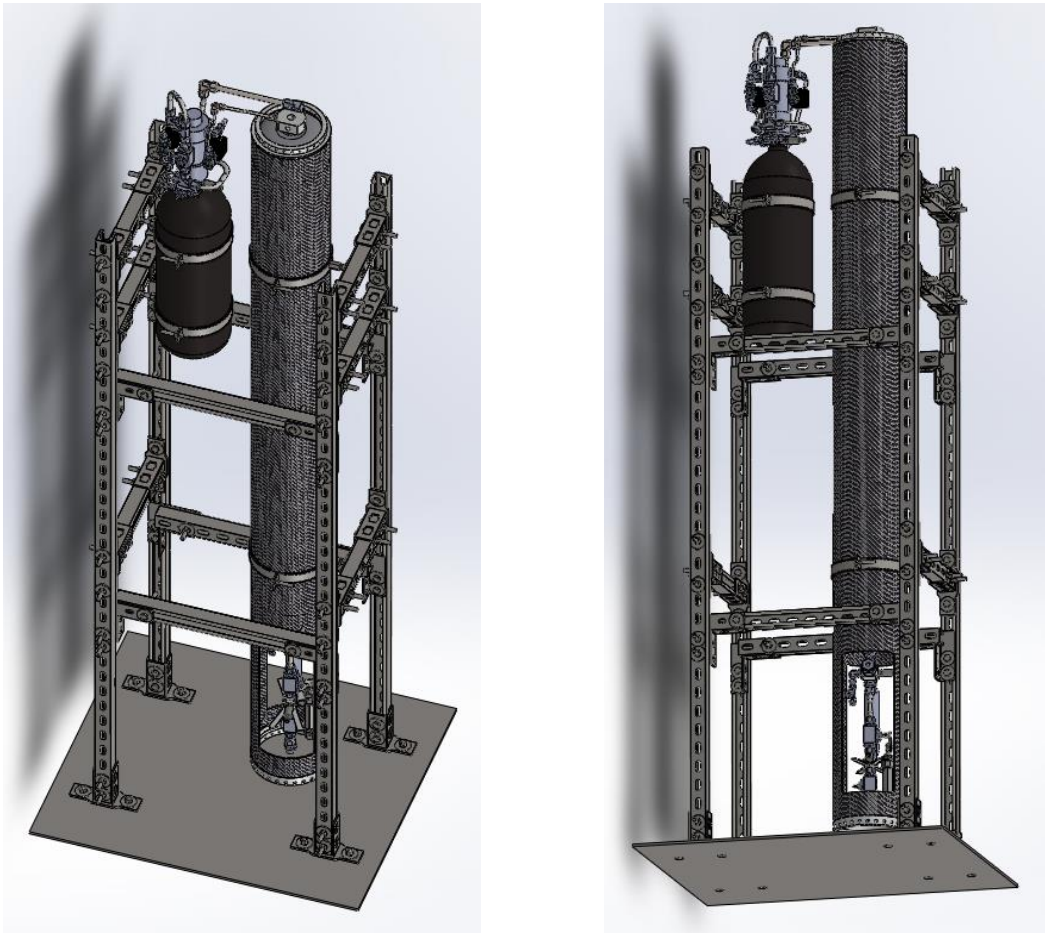

Figure 4.1 - Fluidic line test bench.

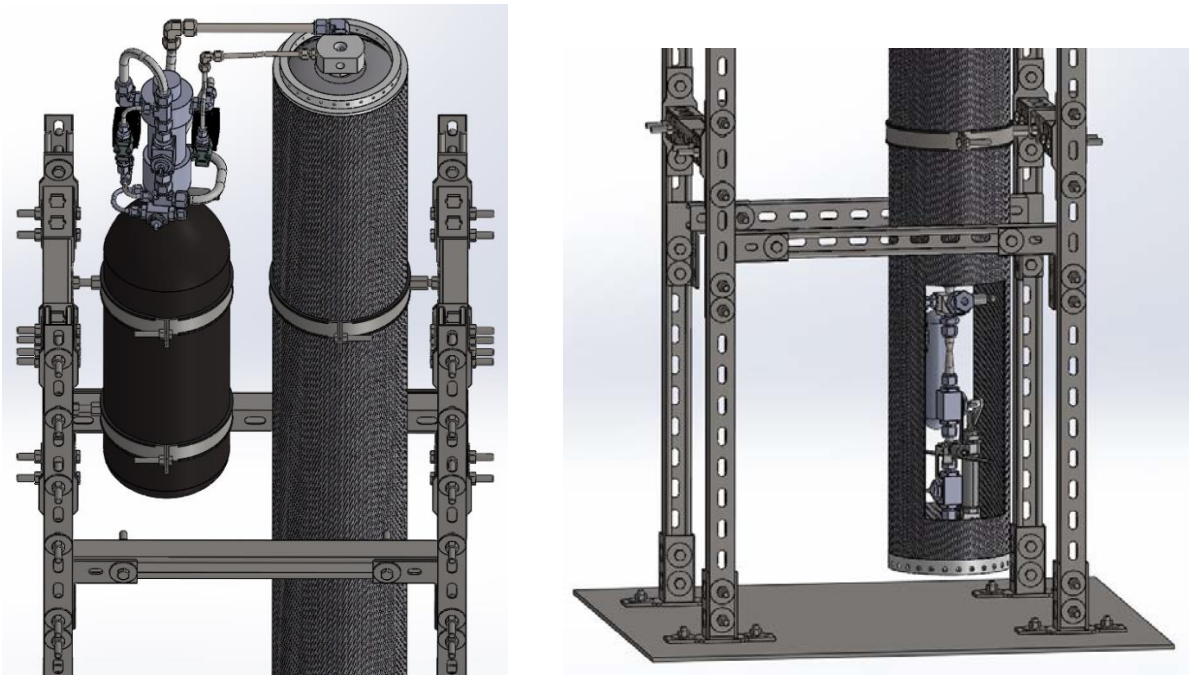

Figure 4.2 - Fluidic line test bench details: upper part (left) and lower part (right).

The vertical mounting channels are 1900 mm tall. The base plate is a 750×850 mm steel rectangle with a thickness of 7 mm. It is the only part of the bench that must be custom-made. Overall, the stand (including the fluidic line to test) is almost 2264 mm tall.

The parts of the test bench are listed below; drawings with dimensions are included:

- 4 vertical mounting channels Fischer FUS 41/41/1.5, 1900 mm long.

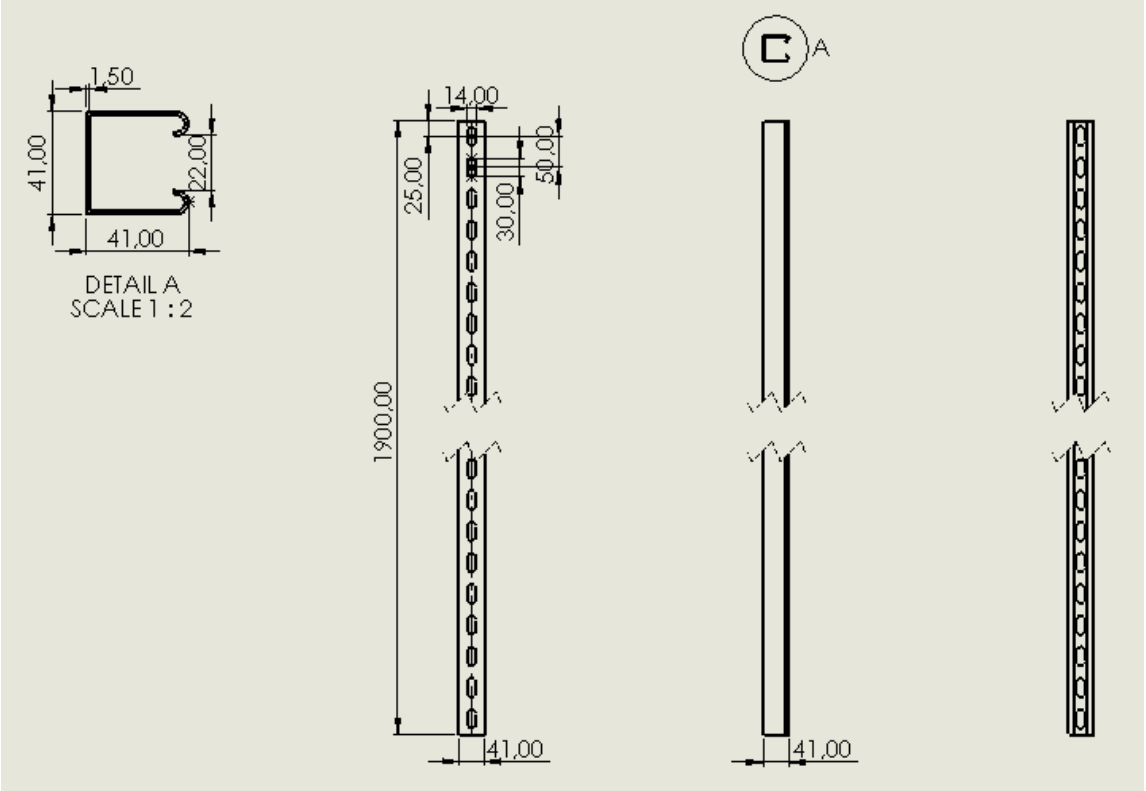

Figure 4.3 -Vertical mounting channel orthogonal projections.

- 6 transversal mounting channels Fischer FUS 41/41/1.5, 350 mm long.

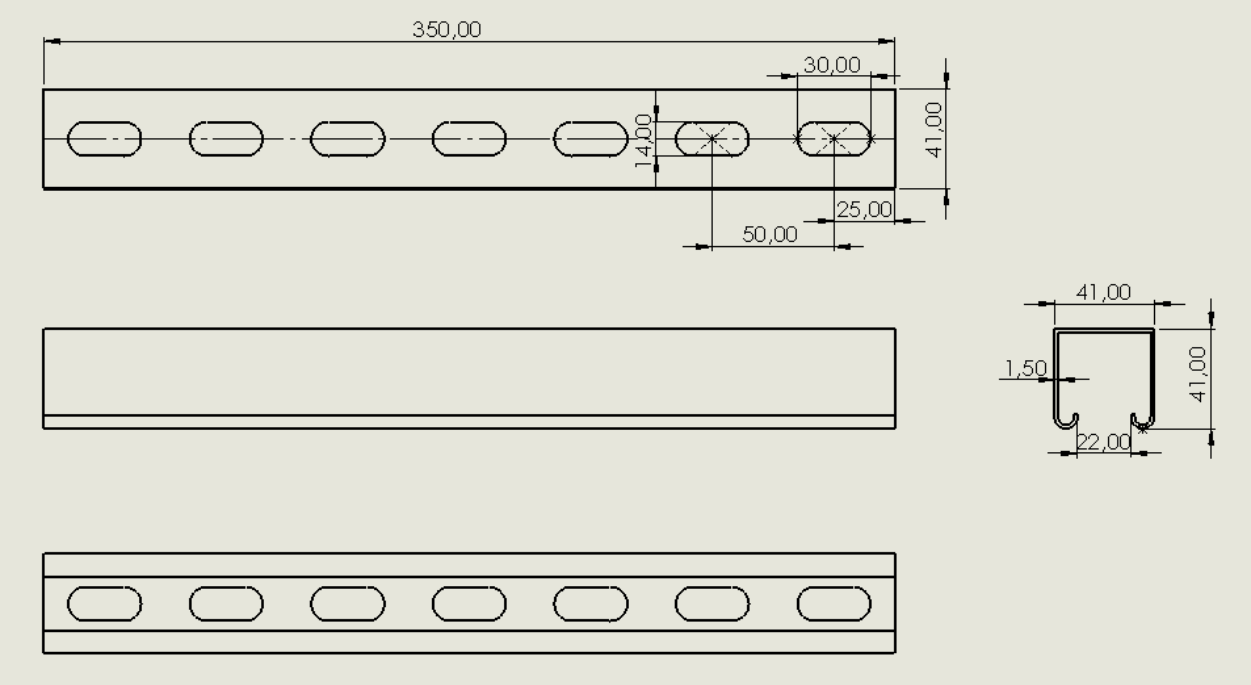

Figure 4.4 - Transversal mounting channel orthogonal projections.

- 4 stiffening mounting channels Fischer FUS 41/41/1.5, 550 mm long.

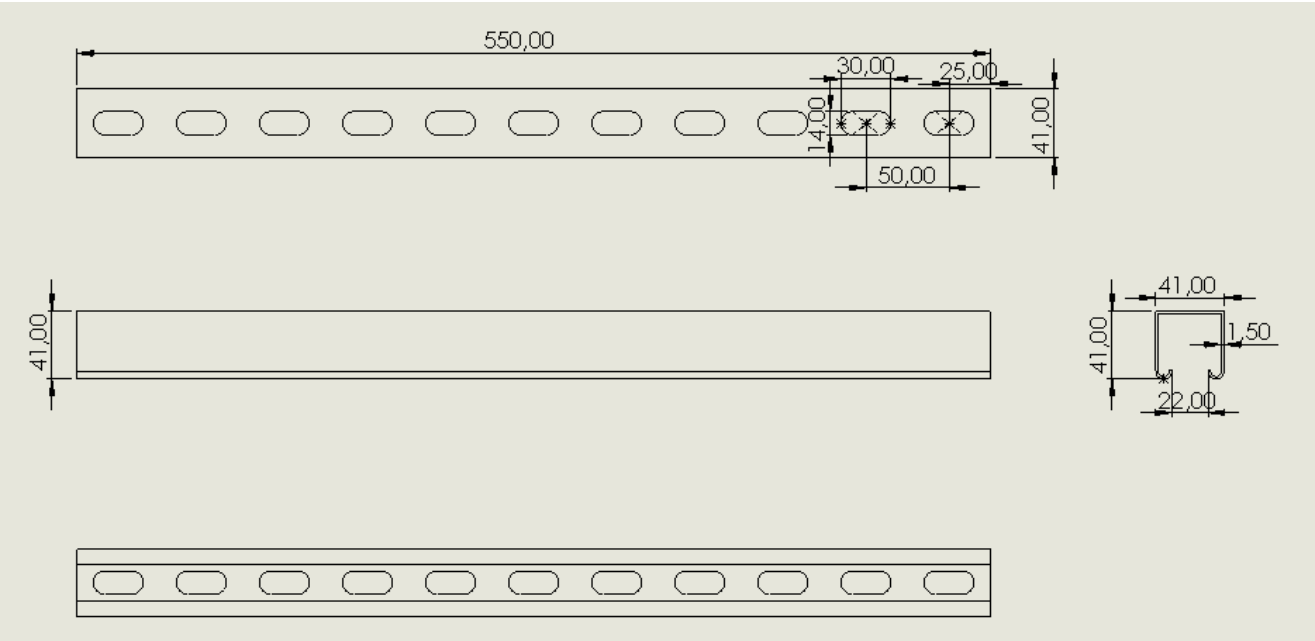

Figure 4.5 - Stiffening mounting channel orthogonal projections.

All the mounting channels are obtained cutting 4 FUS 41/41/1.5 channels with a length of 3000 mm and 1 FUS 41/41/1.5 channel with a length of 2000 mm.

- 4 saddle brackets Fischer PSFQ 41.

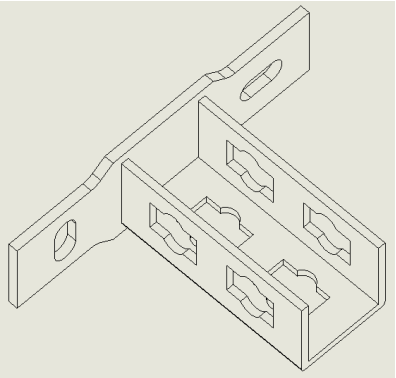

Figure 4.6 - Saddle bracket axonometry.

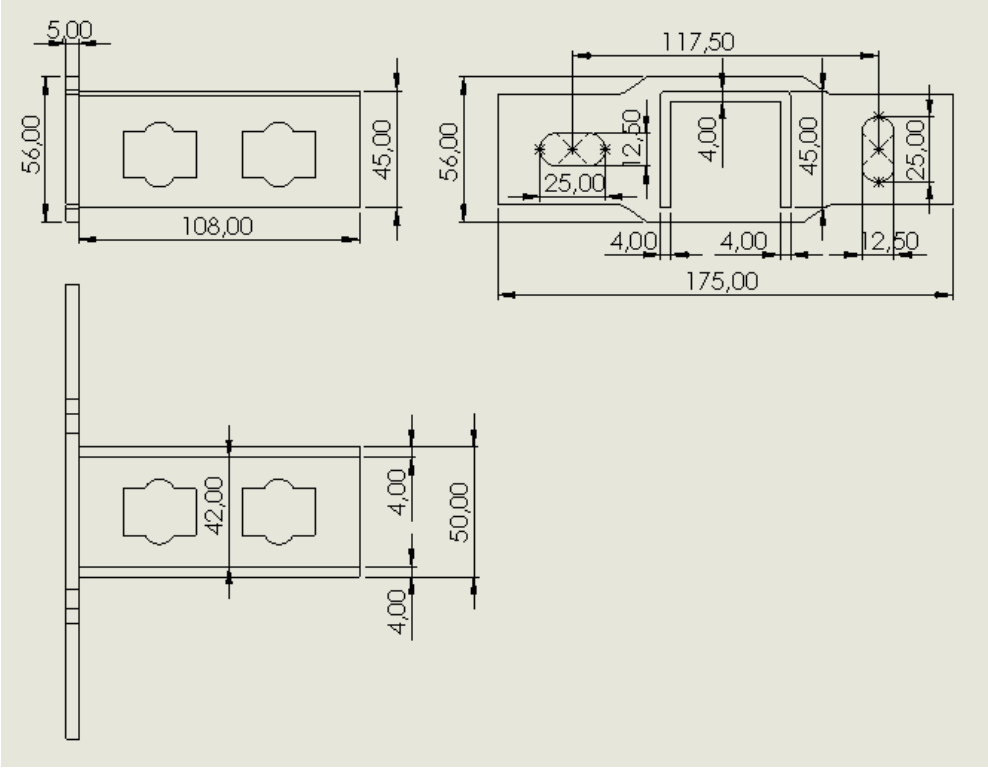

Figure 4.7 - Saddle bracket orthogonal projections.

- 8 universal angle brackets Fischer UW S.

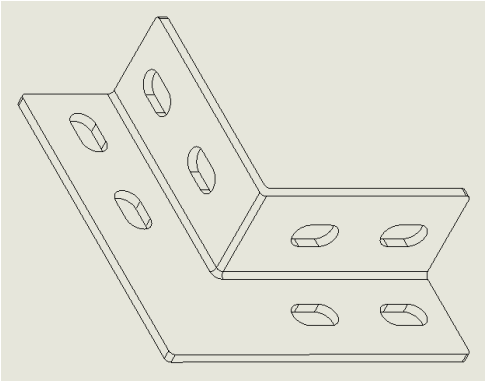

Figure 4.8 - Universal angle bracket axonometry.

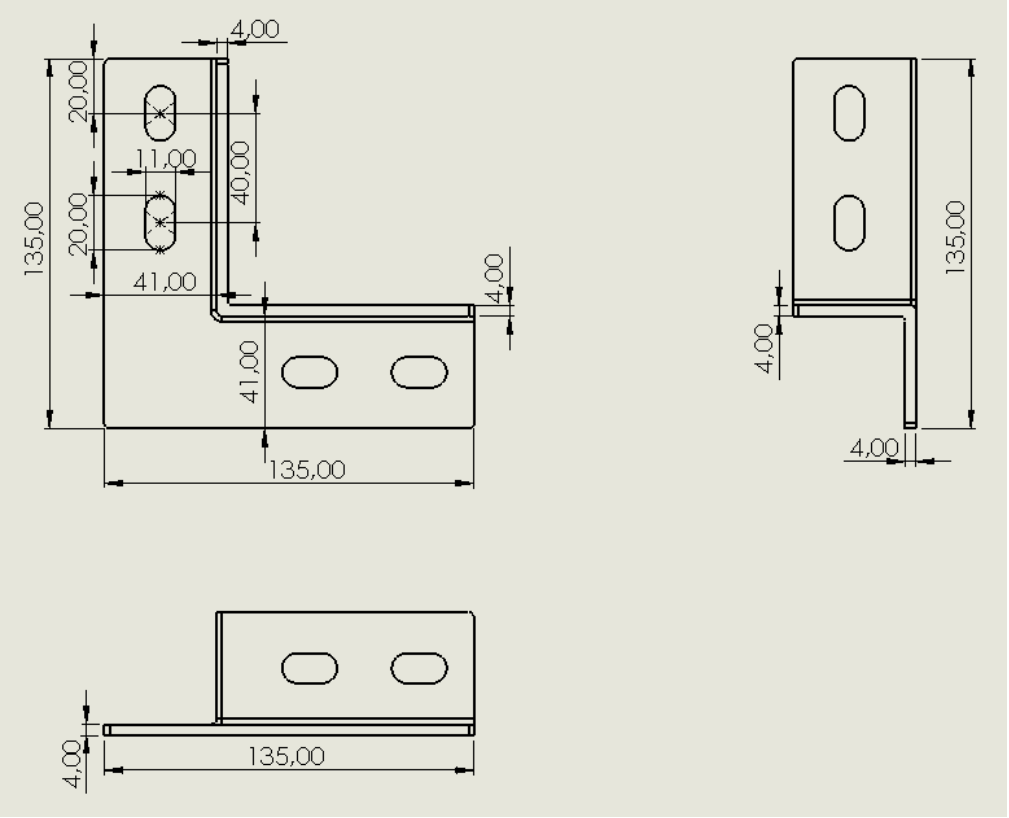

Figure 4.9 - Universal angle bracket orthogonal projections.

- 4 T-head bolts Fischer FHS Clix S 10×40.

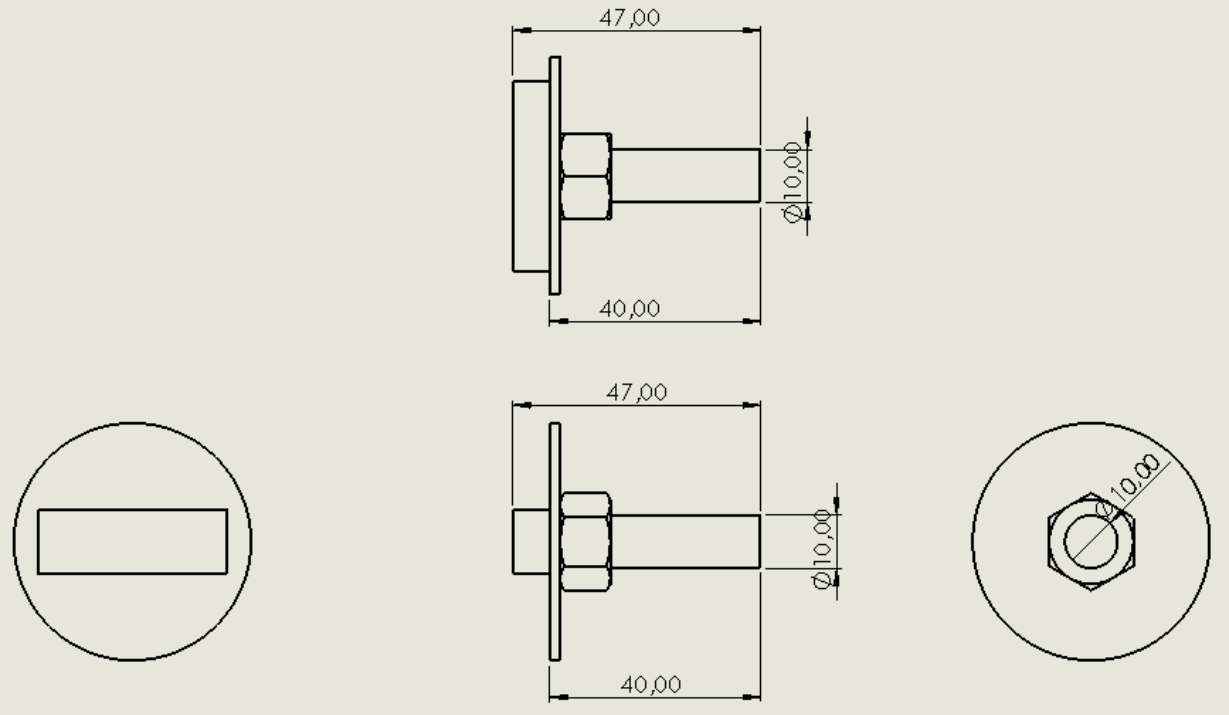

Figure 4.10 - T-head bolt orthogonal projections.

- 4 pipe clamp collars Fischer FRSM 6”-7” M10/M12 [21].

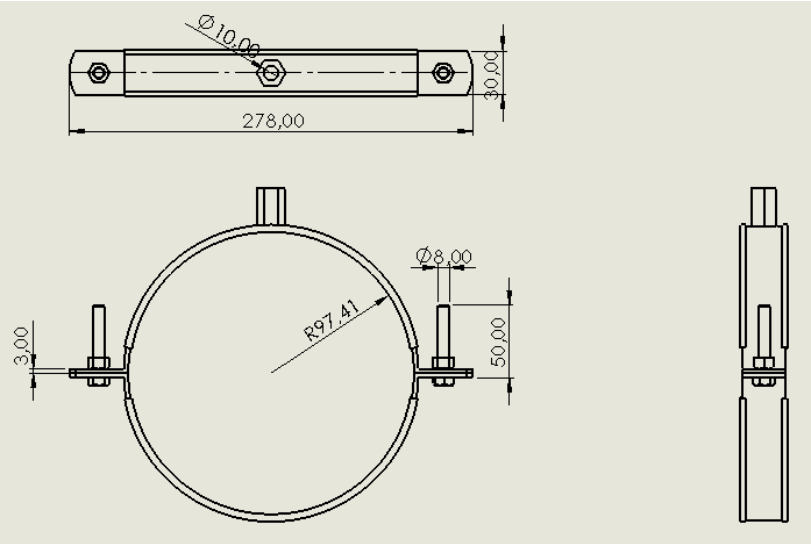

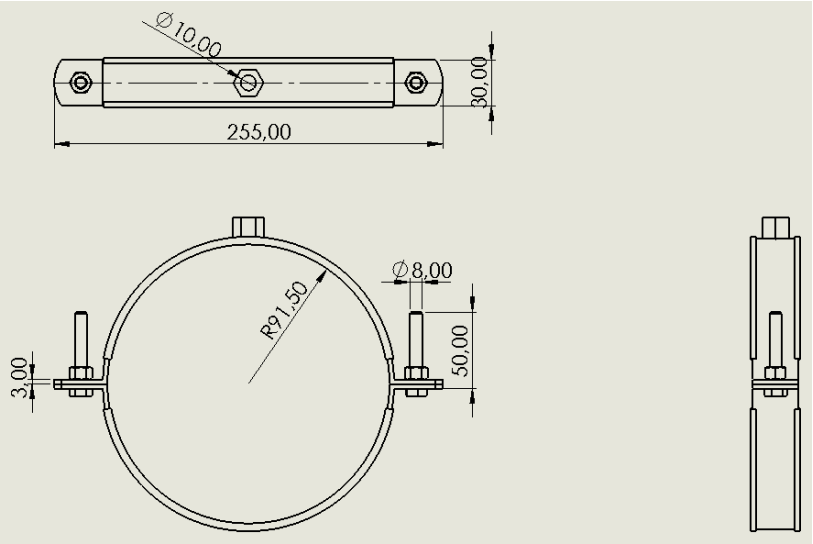

Figure 4.11 - Pipe clamp collars orthogonal projections.

- Custom-made base plate.

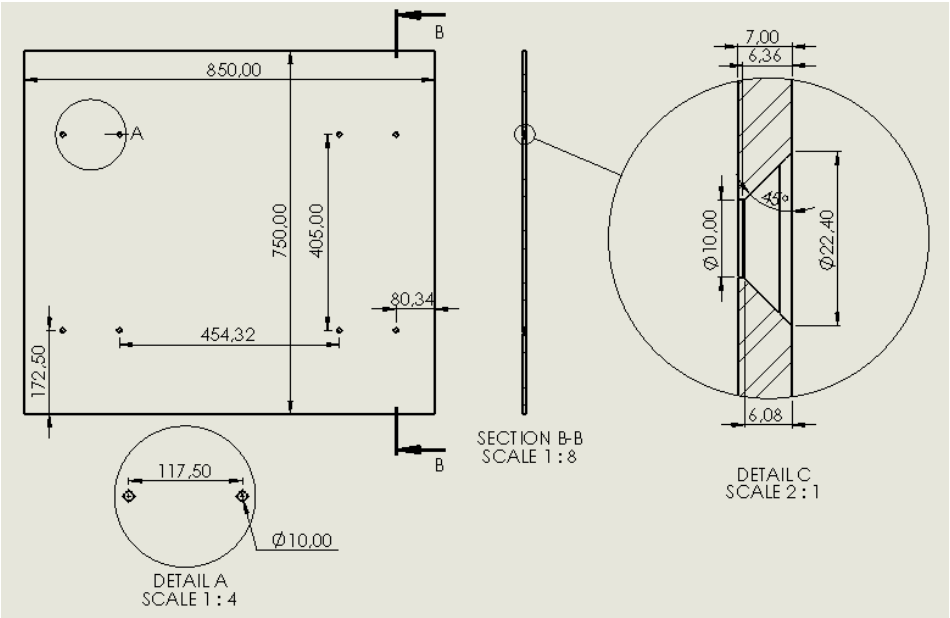

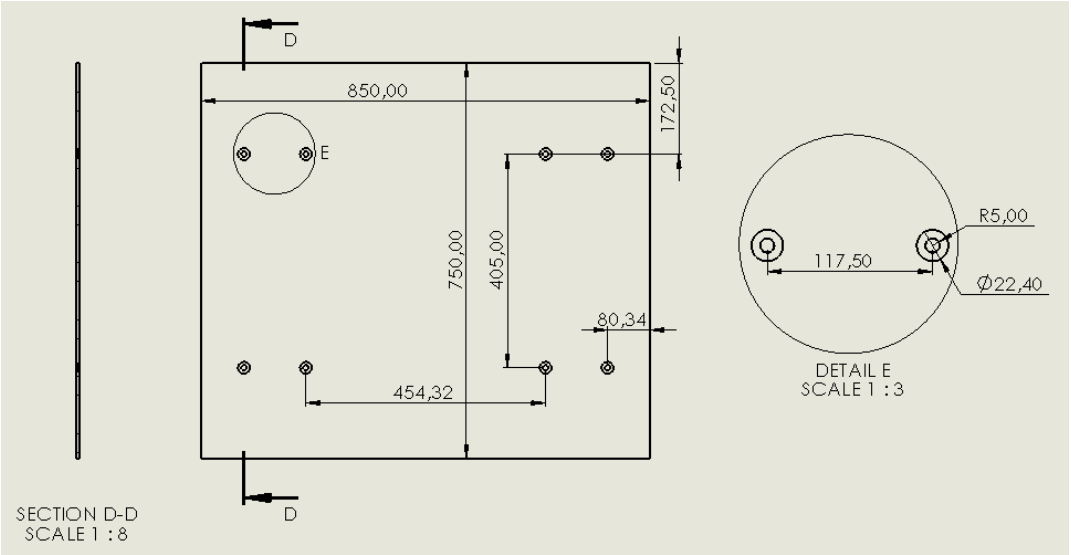

Figure 4.12 - Base plate orthogonal projections.

The drawings of the test bench assembly are shown below:

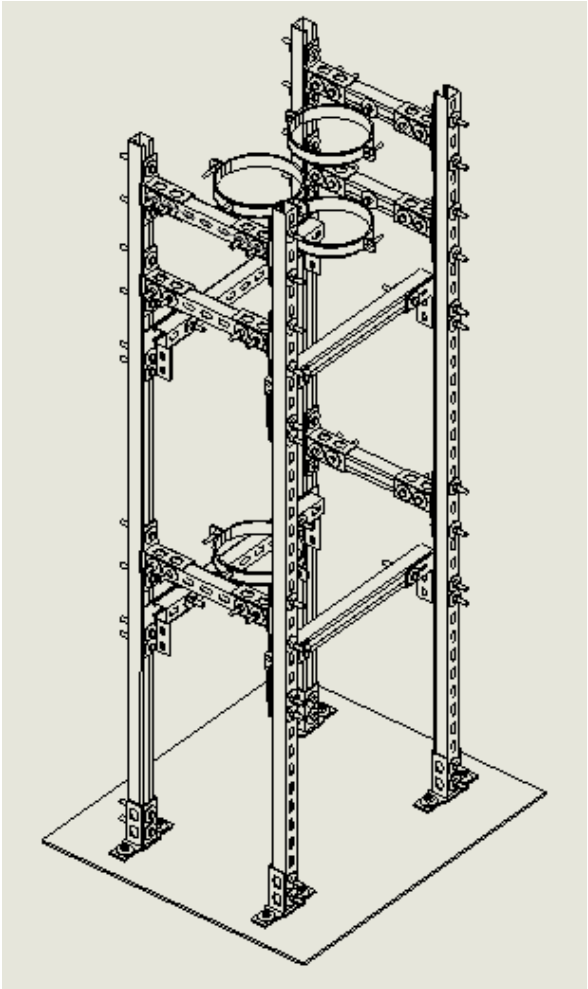

Figure 4.13 - Fluidic line test bench assembly axonometry.

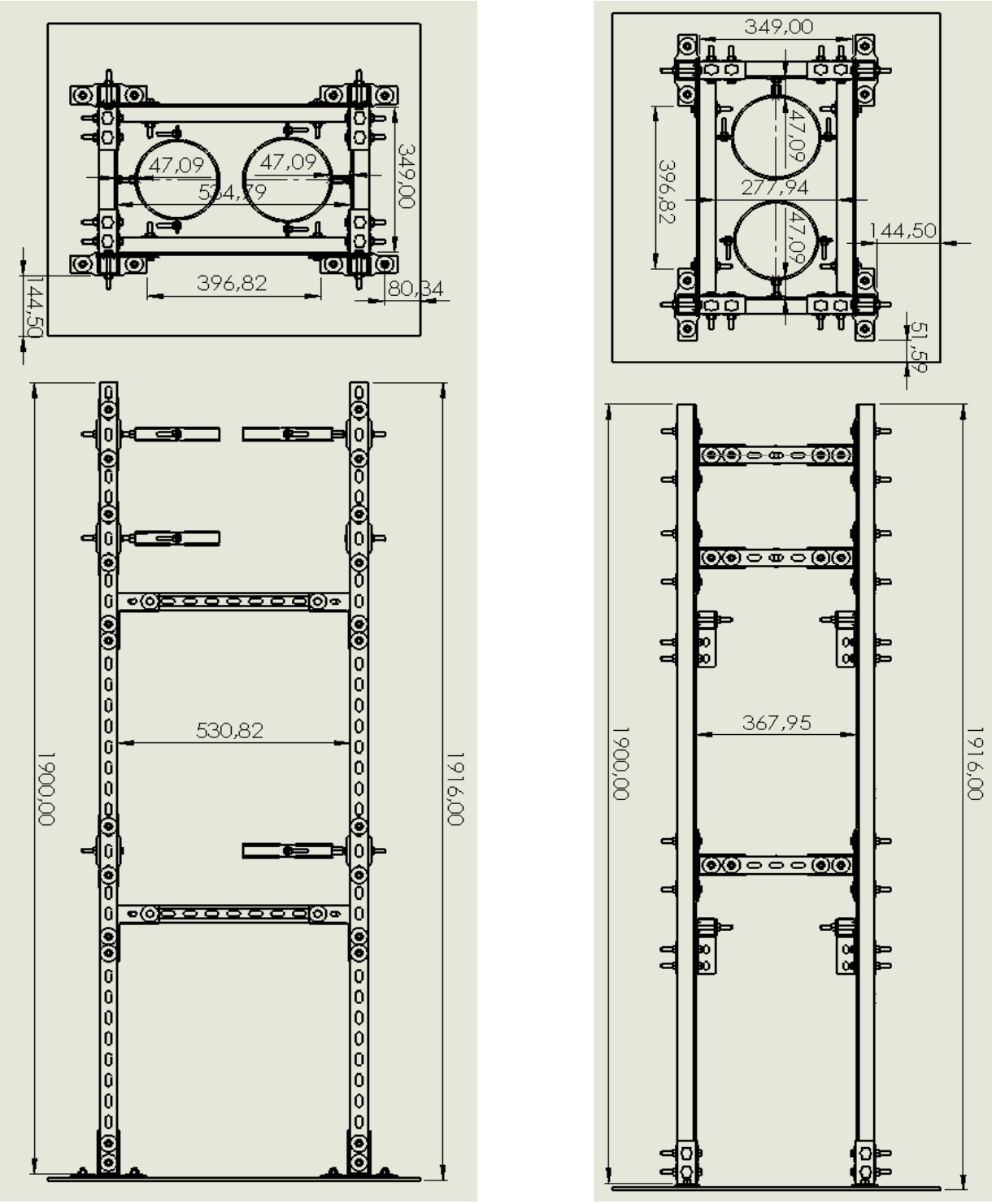

Figure 4.14 - Fluidic line test bench assembly orthogonal projections.

The estimated masses of the system are:

- Mass of the fluidic line with filled tanks: 85.7 kg.
- Mass of the fluidic line with filled tanks, including pipe clamp collars: 88.3 kg.
- Mass of the supporting frame: 79.7 kg.
- Total mass of the test stand with filled tanks: 167.9 kg.

4.1.1 Fluidic Line Test Bench Sizing

The weight of the fluidic line with filled tanks is not negligible, therefore resistance checks of the most stressed parts have been made. The critical parts that have been checked are the **T-head bolt junctions**, which connect the pipe clamp collars to the transversal mounting channels, and the **saddle bracket junctions**, which connect transversal and vertical mounting channels.

4.1.1.1 T-head Bolt Junctions Verification

The parts that needed resistance verifications were:

- Each *T-head bolt*.
- Each *center of the transversal mounting channel* (which is where the load is applied).

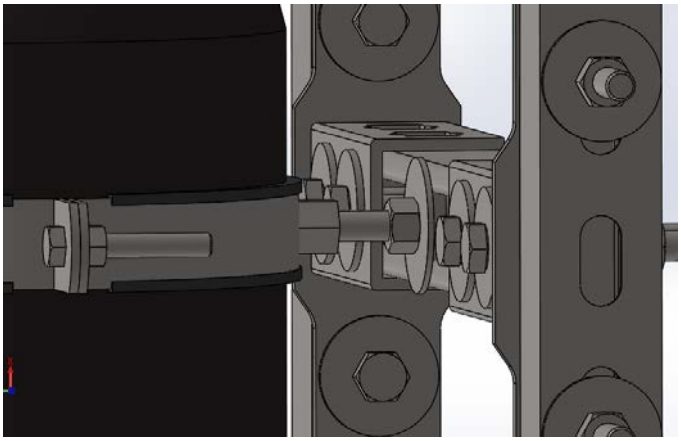

Figure 4.15 - T-head bolt junction.

The same load is applied to each one of these parts. Since there are 4 T-head bolt junctions, the load on each part should be equal to ¼ of the weight of the fluidic line with filled tanks, including pipe clamp collars. The estimated value is therefore ~216.5 N. The estimated maximum acceptable loads for the 2 aforementioned parts are:

- Maximum acceptable transversal load for the *T-head bolt*: 2000 N.
- Maximum acceptable load on the *center of the transversal mounting channel*: 4400 N [21].

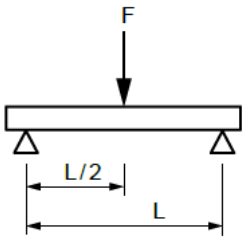

Figure 4.16 - Load condition of transversal mounting channel.

It can be noticed that the applied load is considerably lower than all the maximum acceptable loads. Margins of safety have been calculated with the following formula:

$$MoS = \frac{Maximum\ acceptable\ load}{Applied\ load} \tag{4.1}$$

The found values are respectively:

- *T-head bolt*: $MoS = 9.24$.
- *Center of the transversal mounting channel*: $MoS = 20.32$.

4.1.1.2 Saddle Bracket Junctions Verification

Because the lower walls of the saddle brackets support the transversal mounting channels, the bolted joints between the transversal channels and the brackets are not subjected to shear stresses. Therefore, only the bolted joints between the saddle brackets and the vertical mounting channels have been verified.

Figure 4.17 - Saddle bracket junction.

From the previous figure it is evident that only the lower bolt of each junction supports the load. Therefore, the load is distributed between 8 bolts. 3 verifications have been made:

- *Shear resistance of bolts*.
- *Resistance of hole-weakened parts* (i.e. saddle brackets and vertical mounting channels).
- *Bearing resistance* of saddle brackets and vertical mounting channels [22].

The assumed values of strength of the various parts are:

- Maximum acceptable shear stress of bolts (class 8.8): 264 MPa [23].
- Maximum acceptable stress of mounting channels material (S250 GD steel): 188 MPa [21].
- Yield strength of saddle brackets material (DD11 steel): 170 MPa [21] [24].

The loads on the joints have been calculated; the found margin of safety (see eq. 4.1) are:

- *Shear resistance of bolts*: $MoS = 2387.35$.
- *Resistance of hole-weakened parts*:
  - Saddle brackets: $MoS = 243.36$.
  - Vertical mounting channels: $MoS = 70.32$.
- *Bearing resistance*:
  - Saddle brackets: $MoS = 1570.09$.
  - Vertical mounting channels: $MoS = 520.90$.

It is evident that the loads on the junctions are well below the maximum acceptable values.

4.2 Catalytic Reactor Test Bench

A specifically made reactor is used for this test: it is closed by 2 flanges placed at its opposite ends and kept tight by a series of threaded bars; a graphite nozzle akin to the one at the rocket motor outlet is placed inside the lower flange.

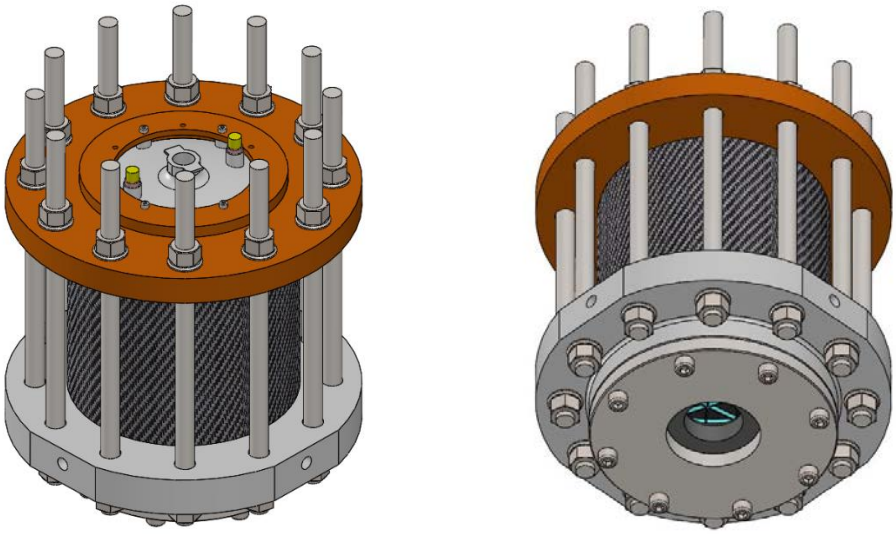

Figure 4.18 - Test reactor.

The catalytic reactor has the same internal layout of the one designed for the flight (see figure 4.19 and section 2.4.1). The distance between the external faces of both ends is about 288 mm. The diameter of the flanges is 300 mm. The threaded bars are 350 mm long. The test reactor has an estimated mass of 42.5 kg.

In the test stand, the reactor is hanged to a steel plate by means of a flange. Twelve nuts fastened on the threaded bars are used to fix the system to the flange. The plate with the hanged reactor is sustained by 4 steel tubular columns. On top of the plate, at its corners, other 4 similar columns sustain another steel plate on top of which a 220 L water tank is placed. The fluidic feeding system (see section 3.2.2) is placed over the reactor, between the two plates. Between the lower plate and the lower columns 4 load cells are placed to measure loads. A steel deflector is placed under the nozzle of the reactor in order to deviate the exhaust sideways. The layout of the test bench is showed in the following figures:

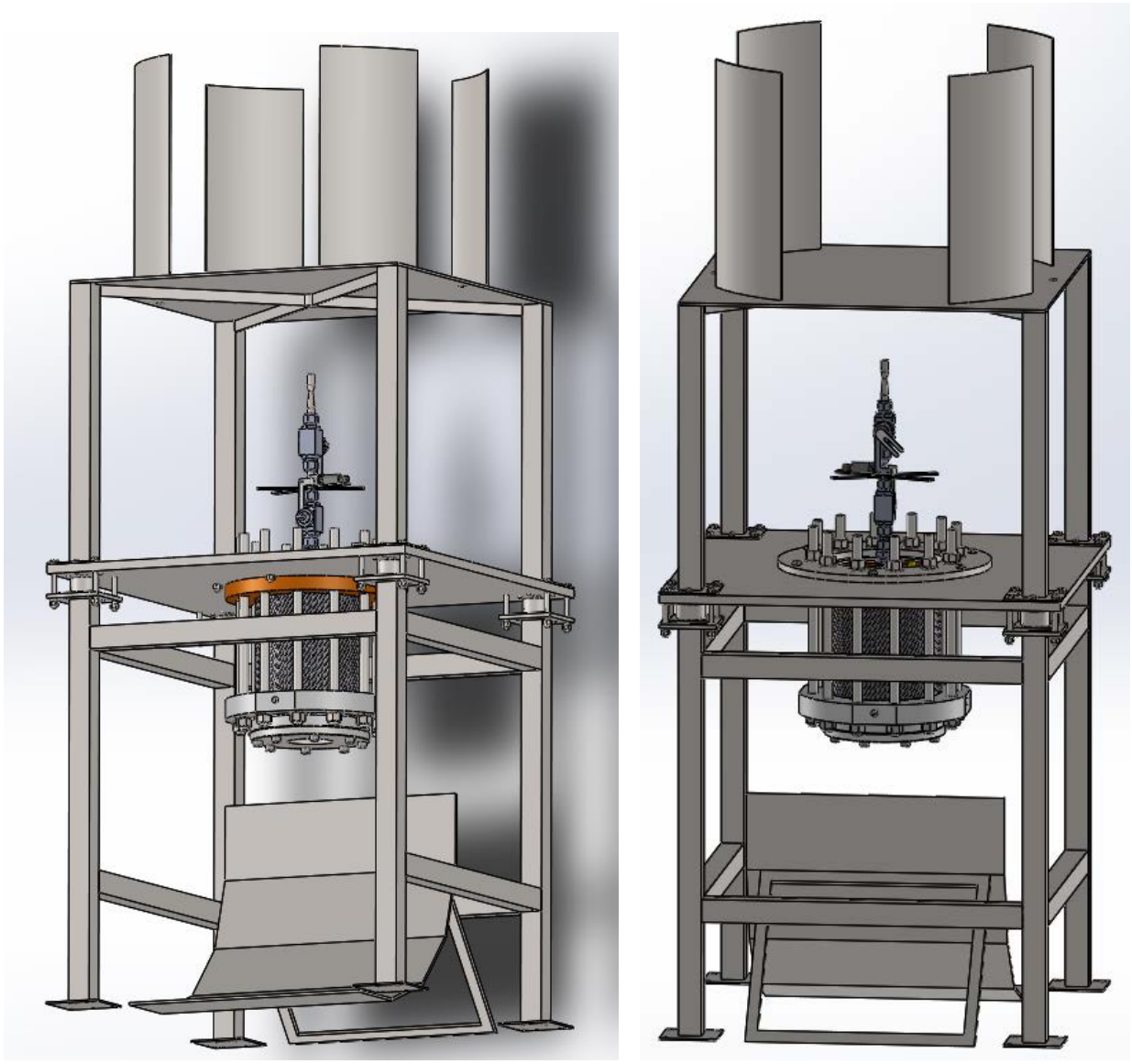

Figure 4.19 - Catalytic reactor test bench.

The tubular columns have a 40×40 mm square cross section with 3 mm thick walls. The lower plate is a 700×700 mm square with a thickness of 16 mm; its lower face is at a height of 767 mm. The nozzle is therefore about 489 mm above the ground. The upper plate is a 640×640 mm square with a thickness of 5 mm and reinforced by 2 diagonal ribs at its lower face; its upper face is at a height of almost 1291 mm, leaving between the two plates enough space (~50 cm) for the fluidic feeding system. Four perimetrical sheet-metal walls are welded on the upper plate: their height is 400 m and their purpose is to contain the water tank and keep it stable. The overall height of the stand (including the sheet-metal walls but not the water tank) is 1691 mm. The deflector is a 5 mm thick steel sheet that has been bent to deviate exhaust gasses sideways.

Its height is 400 mm and it is sustained by a simple rectangular frame welded on its back side. Its mass is 13.9 kg.

The test bench is mostly custom-made, except for the bolt joints, the feeding line components, the water tank and the sensors (notably the load cells).

The parts of the test bench are listed below; drawings with dimensions are included:

- Lower plate.

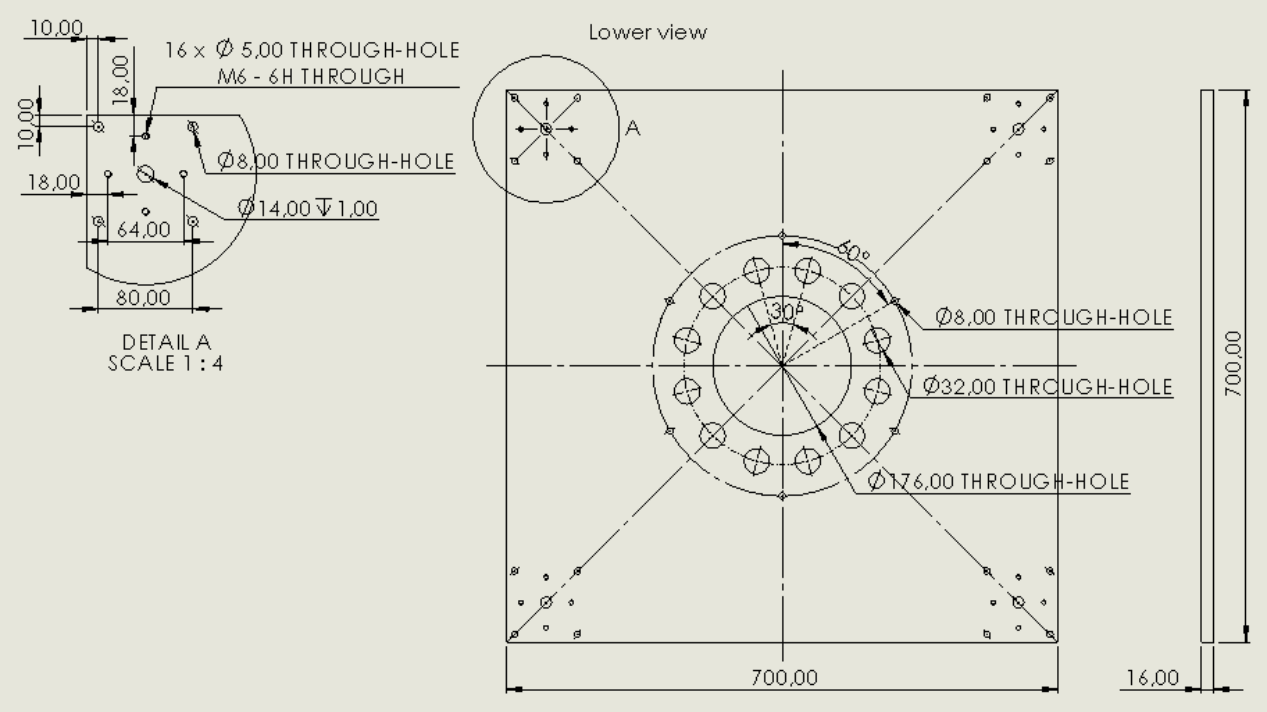

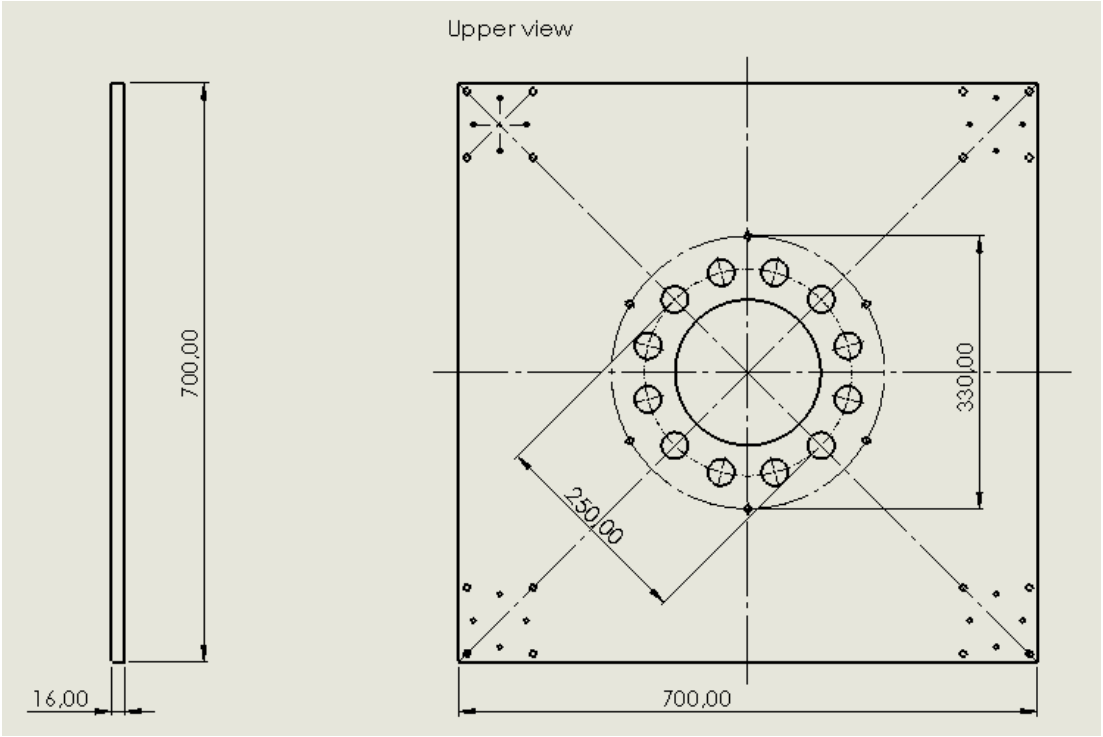

Figure 4.20 - Lower plate orthogonal projections.

- Flange.

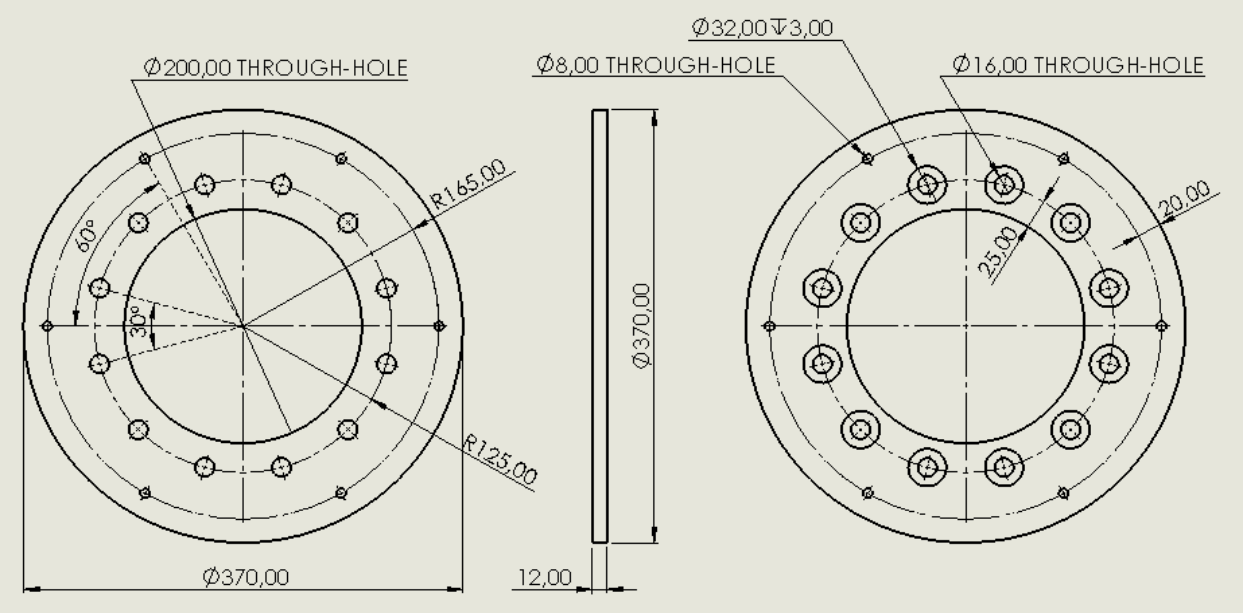

Figure 4.21 - Flange orthogonal projections.

- Upper plate.

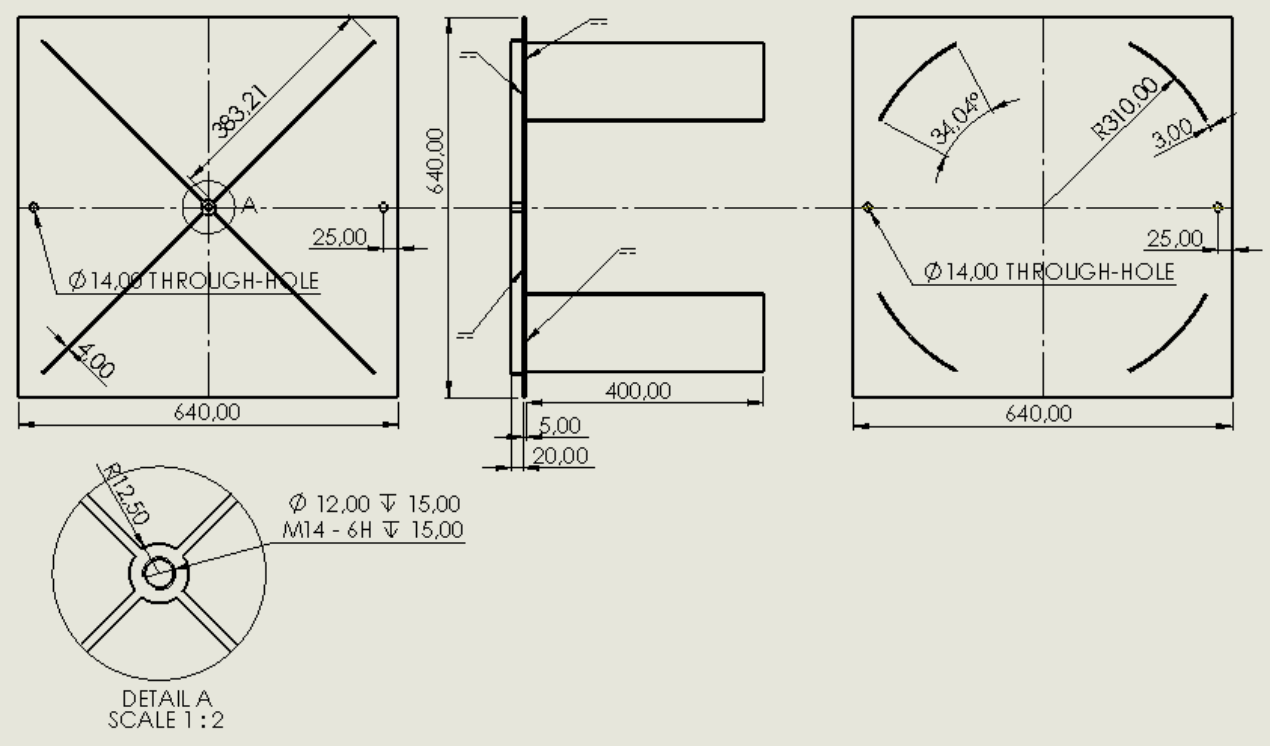

Figure 4.22 - Upper plate orthogonal projections.

- 4 lower columns.

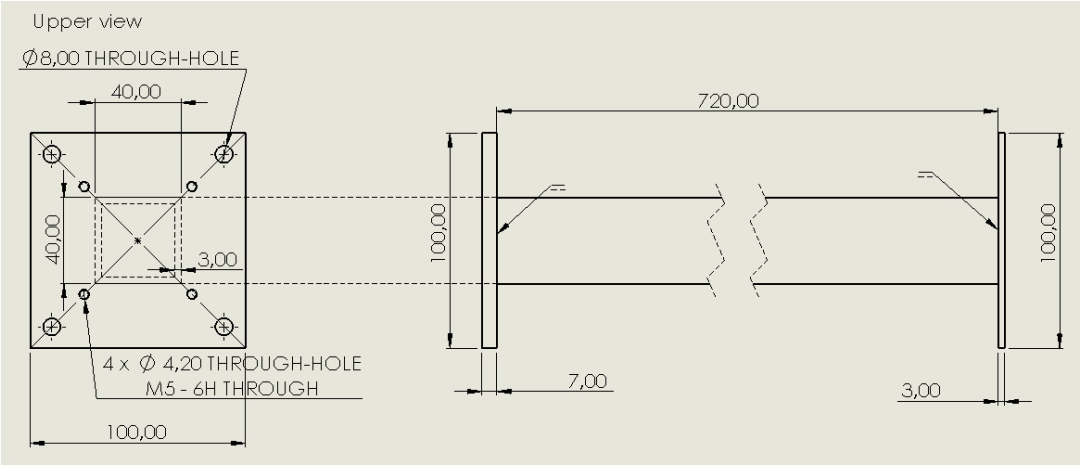

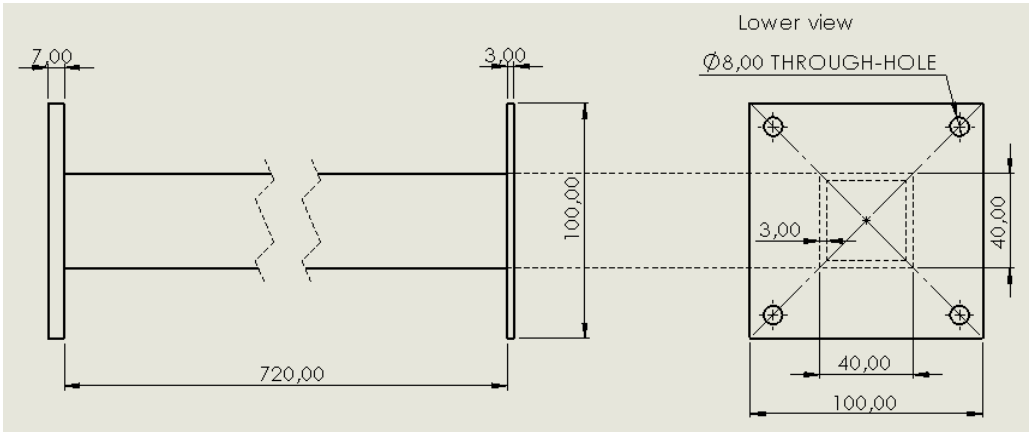

Figure 4.23 - Lower column orthogonal projections.

- 4 upper columns.

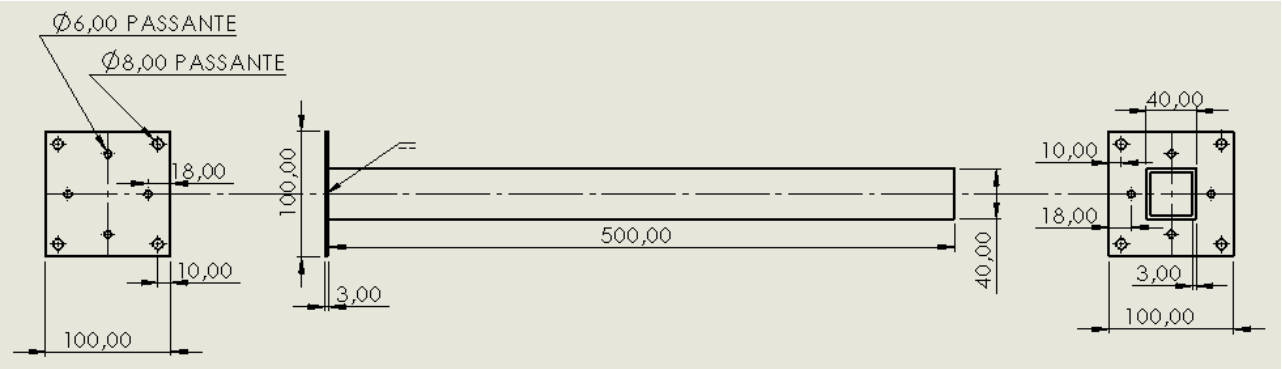

Figure 4.24 - Upper column orthogonal projections.

- 7 crossbeams.

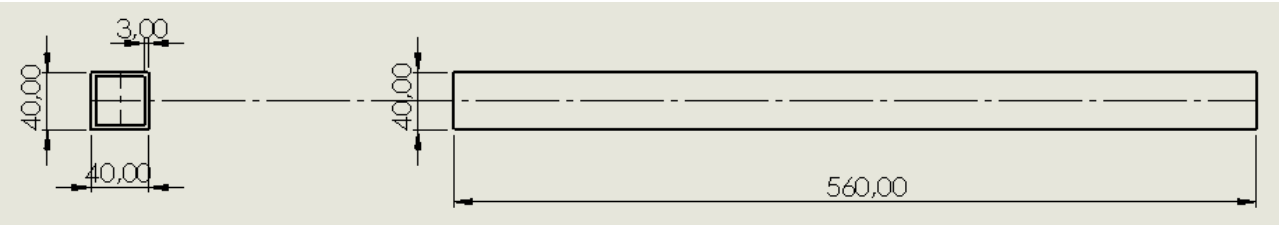

Figure 4.25 - Crossbeam orthogonal projections.

- 4 load cells Flintec MBA 250 lb.

Figure 4.26 - Load cell Flintec MBA [25].

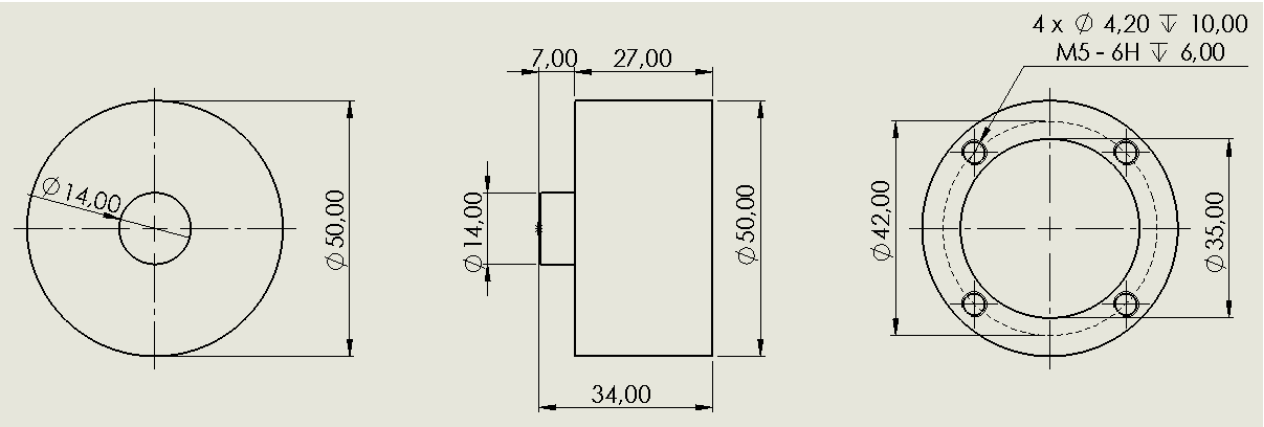

Figure 4.27 - Load cell orthogonal projections.

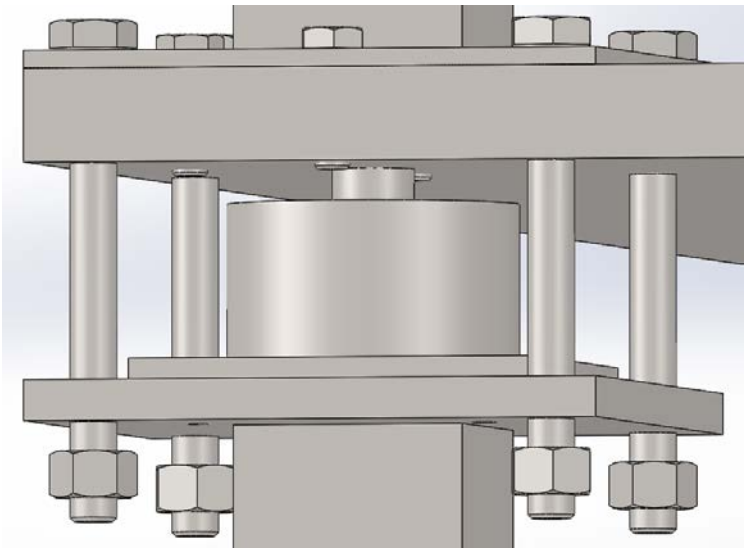

Figure 4.28 - Load cell placement.

It is evident that the upper part of the stand must not be fastened to the lower columns in order not to affect the load cells measurements. For this reason the connecting bolts shown in figure 4.29 are free to slide up and down and are used only for safety and to avoid lateral displacements.

The load cells characteristics are listed in the following table:

TECHNICAL DATA	
Accuracy	0,2%
Nominal full scale load (Ln)	50...1.000 kg
Nominal output at FSO	2mV/V
Output tolerance at Ln	<± 0,2% FSO
Combined errors: Non linearity Histeresis, Repeatibility	< ± 0,2% FSO
Creep (after 30 min. at Ln)	< ± 0,06% FSO
Zero load out of balance signal	< ± 1% FSO
Thermal drift in Sensitivity compensated Zero range Calibration	< ± 0,01% FSO°C < ± 0,01% FSO°C -
Nominal input resistance	350 Ohm
Nominal output resistance	350 Ohm
Isolation resistance	> 10 GOhm
Nominal supply voltage	10 V
Maximum supply voltage	15 V
Compensated temperature range	-10...+50°C
Maximum temperature range	-20...+60°C
Storage temperature range	-30...+80°C
Permitted static load	130% Ln
Permitted dinamic load	100% Ln
Maximum applicable load	150% Ln
Rupture load	> 300% Ln
Maximum elastic deformation at Ln	< 0,2 mm
Grade of protection (DIN40050)	IP67
Electr. connections screened cable	4x0,25 / 5 m.
Elastic element material	Stainless steel

Table 4.1 - Flintec MBA load cell characteristics.

Other details of the sensors are shown below:

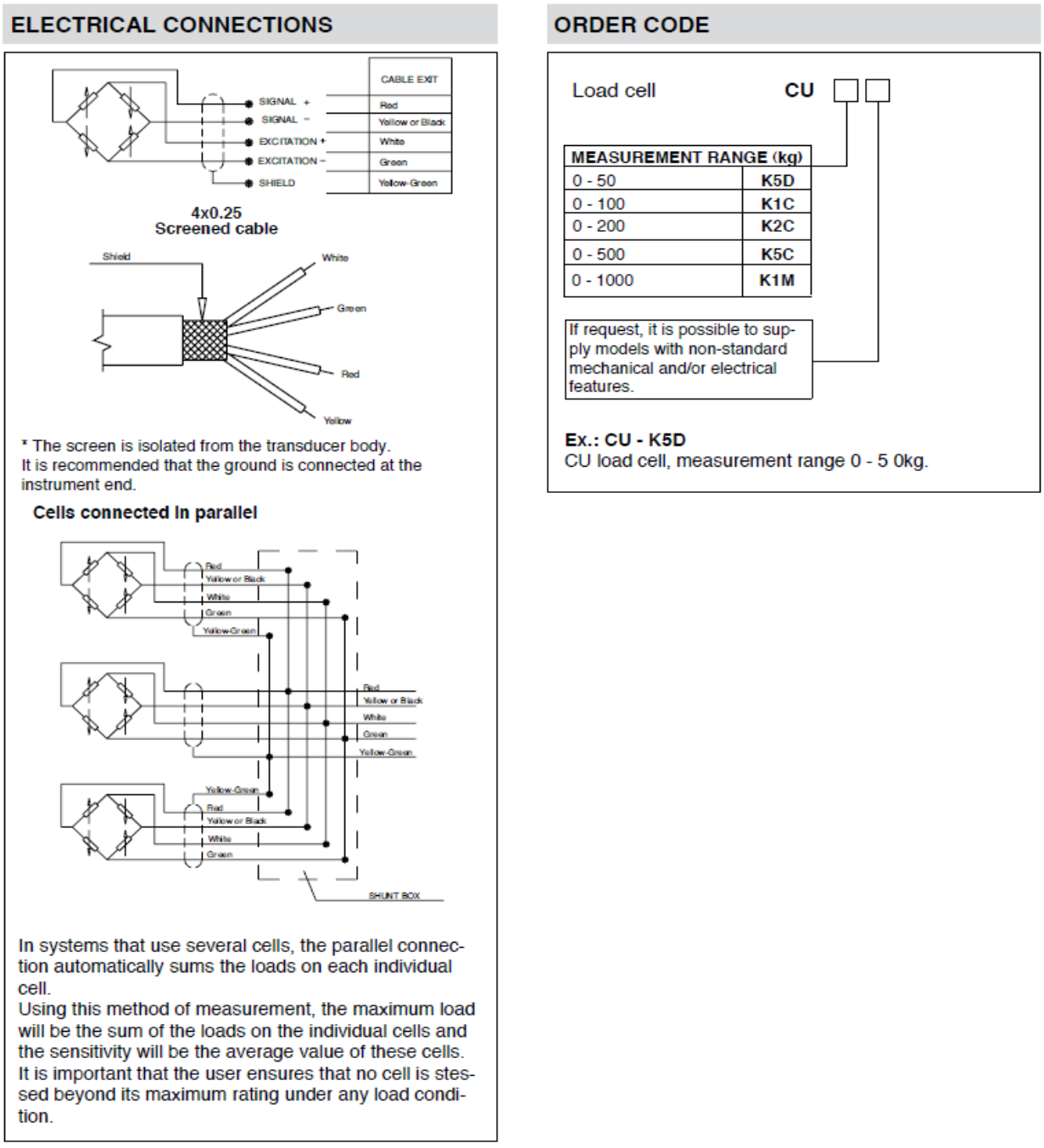

Figure 4.29 - Load cell Flintec MBA wiring and order code [25].

As mentioned in section 3.1.2, the expected thrust exerted by the catalytic reactor is ~2500 N, so the upper part of the bench must weight ~300 kg (~2943 N) to counterbalance the thrust. Therefore the load cells will measure the difference between the weight and the thrust (~440 N), so each one will measure ~110 N. However, when the system is not running, the cells will be loaded by the full weight of the above structure, so each one must withstand a load of at

least 75 kg. For these reasons, load cells with a maximum capacity of 100 kg have been chosen [25].

- 4 buffer plates.

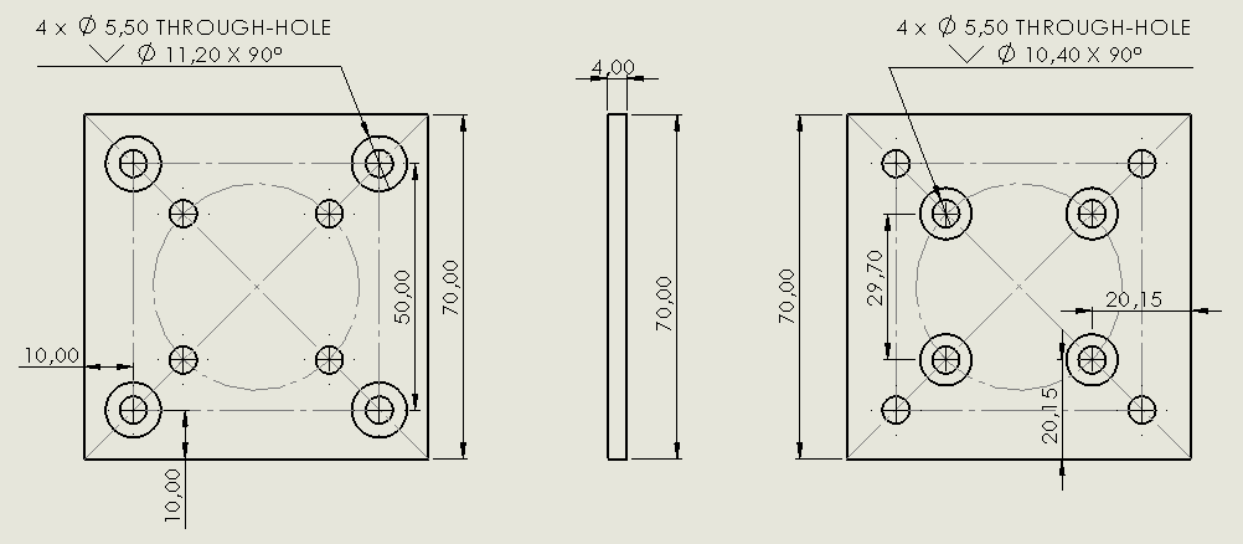

Figure 4.30 - Buffer plate orthogonal projections.

Buffer plates are placed between the load cells and the top of the lower columns. The plates are fastened onto the lower columns and the load cells are fastened onto the plates in order to avoid lateral displacements and vibrations.

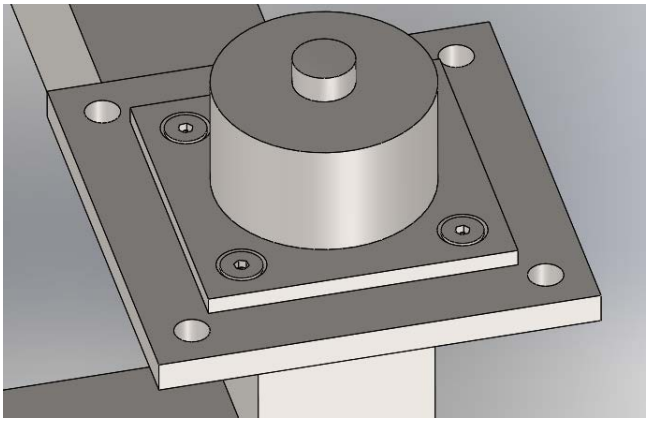

Figure 4.31 - Buffer plate placements.

- Deflector.

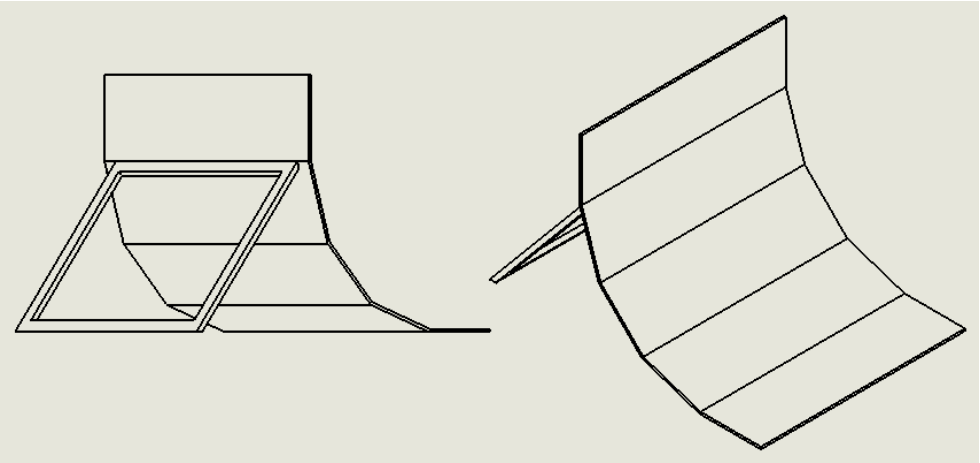

Figure 4.32 - Deflector axonometry.

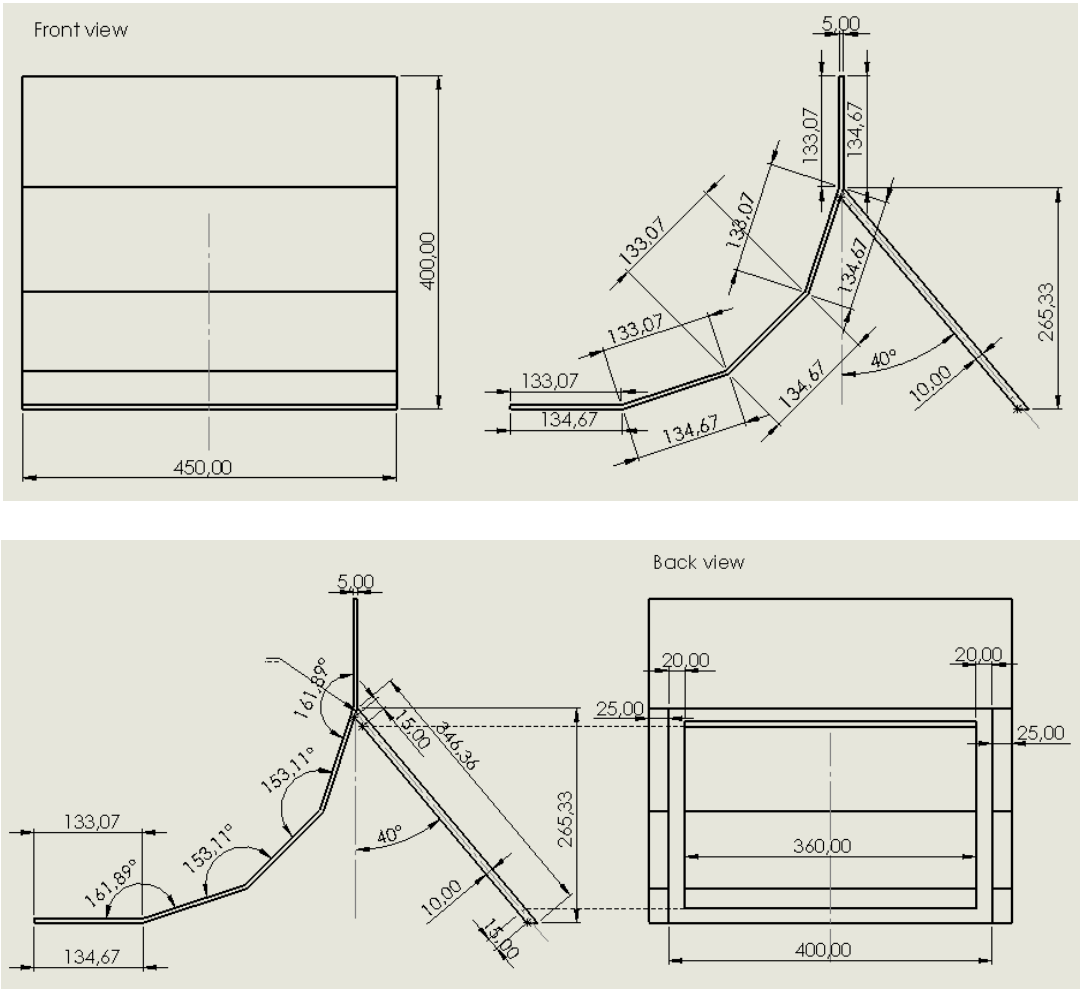

Figure 4.33 - Deflector orthogonal projections.

- Pack Services VERT-0220 (220 L) water tank [26].

Figure 4.34 - Water tank Pack Services VERT-0220.

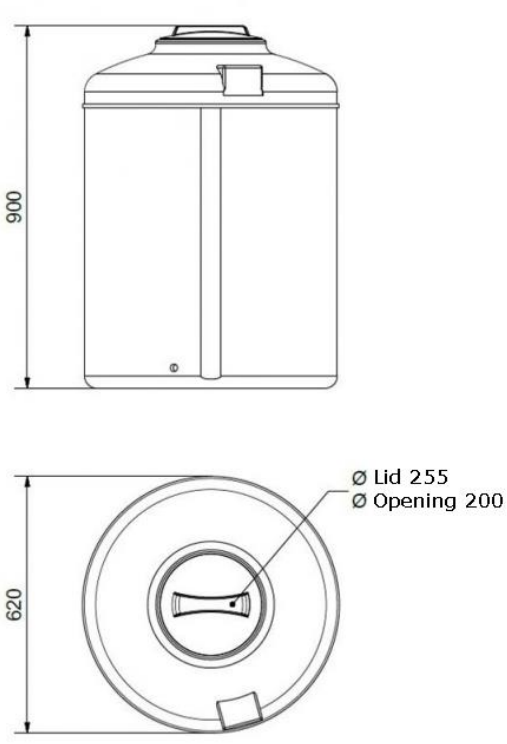

Figure 4.35 - Water tank Pack Services VERT-0220 orthogonal projections [26].

The drawings of the test bench assembly are shown below:

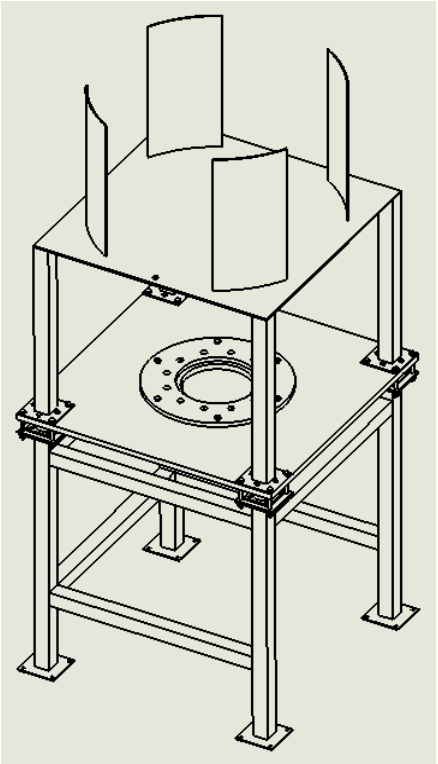

Figure 4.36 - Catalytic reactor test bench assembly axonometry.

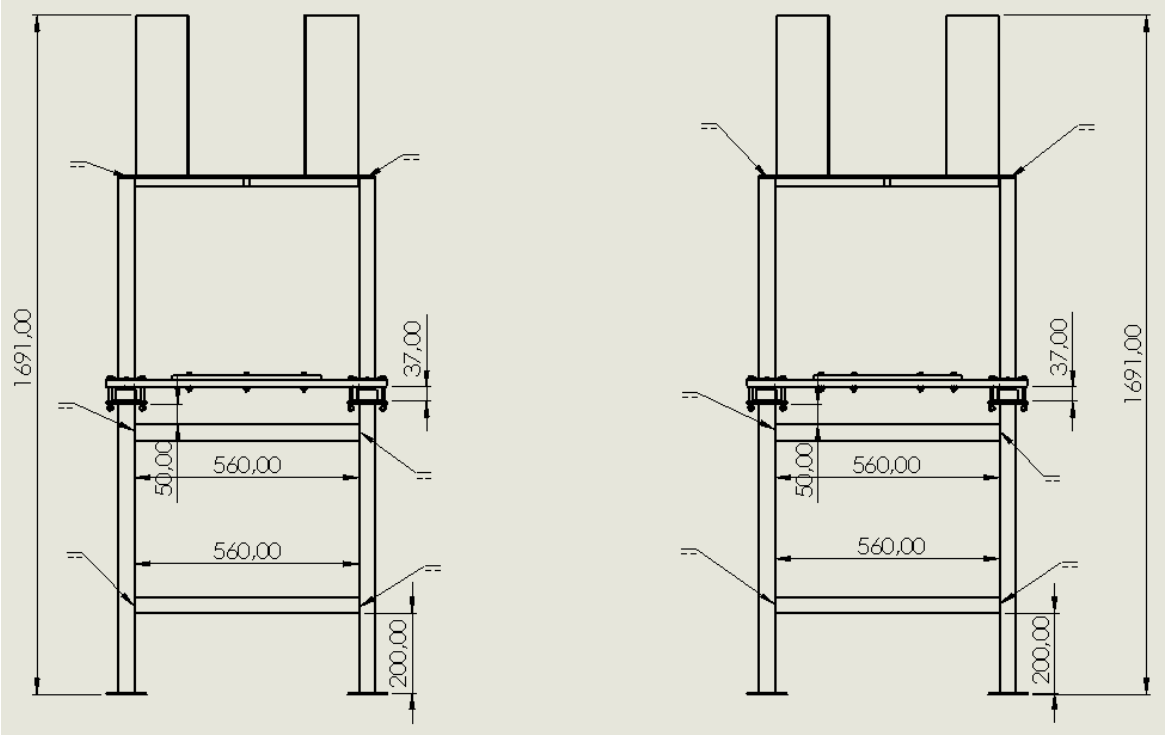

Figure 4.37 - Catalytic reactor test bench assembly orthogonal projections.

The estimated mass of the upper part of the stand (which rests on the four load cells) is 140.7 kg without the water tank. The water tank must be filled with about 159 L to reach the needed 300 kg. The mass of the entire test stand (without the water tank and the deflector) is 169.5 kg.

4.2.1 Catalytic Reactor Test Bench Sizing

Structural verifications have been made to check **columns buckling resistance** and **plates bending**. C40 steel is generally the assumed material whenever material properties are needed for calculations.

4.2.1.1 Columns Buckling Resistance Verification

Both the lower and upper columns have been verified. This check simply aimed to find the Euler's critical loads of the columns and compare it with the applied loads.

The Euler's critical load is given by the following formula:

$$P_{cr} = \frac{\pi^2 EI}{(KL)^2} \text{ [27]} \tag{4.2}$$

P_{cr} is the maximum vertical force that the column can withstand without buckling.

E is the elastic modulus of the column material. The value for C40 steel has been used (190 GPa) [28].

I is the minimum second area moment of the cross section of the column. For square tubular beams with external wall width *H* and internal wall width *h*, it is equal to:

$$I = \frac{H^2 - h^2}{12} \text{ [29]} \tag{4.3}$$

In our case, $I = 1.0197 \times 10^{-7} m^4$.

L is the length of the column (720 mm for the lower ones and 500 mm for the upper ones).

K is the effective length factor of the column. For columns with both ends fixed it is equal to 0.5.

The found value of Euler's critical load is 1.476 MN for the lower columns and 3.060 MN for the upper columns.

As mentioned in section 4.2, the maximum load on all the lower columns is 300 kg (2943 N), so 75 kg (735.35 N) for each column. On the other hand, the upper columns are loaded by the upper plate, the water tank and the thrust of the reactor, which combined exert a load of about 4300 N, so about 1075 N for each column. It is clear that the load on each column is much lower than the respective Euler's critical load. Indeed, the margins of safety are:

- Lower columns: $MoS = 2005.39$.
- Upper columns: $MoS = 2847.61$.

4.2.1.2 Plates Bending Verification

The aim of this check is to verify how the **lower** and **upper plate** behave when loaded. In both cases, as a preliminary approach, an approximated analytical model has been applied. Therefore, a more in-depth finite element analysis has been made to confirm the viability of the systems.

The **lower plate** behavior is studied both when it is loaded only by the reactor weight and when it is loaded by the thrust during discharge tests. Of the two plates, this is the more important to check because bending phenomena could cause an uneven distribution of loads on the load cells, affecting their measurements.

Navier's solution has been applied to estimate the plate bending. This model is applicable to rectangular plates simply supported along its edges and carrying a uniformly distributed load. This is quite different from our configuration: the lower plate is fixed at its corners so that no rotation or deflection is possible at those joints (meaning that it is not simply supported); on top of that, the load is not uniformly distributed on the plate and there is a large hole at its center. That said, since the corners are fixed between the upper and lower columns, it is very unlikely that bendings will occur in those zones (which are the critical ones because of the load cells presence). In comparison, Navier's solution for simply supported plates should give a much more pronounced bending at the edges, therefore it seems a very conservative approach.

The formulae used are:

$$w_{max} = \frac{16q_0}{\pi^6 D} \sum_{m=1,3,5}^{\infty} \sum_{n=1,3,5}^{\infty} \frac{sin(m\pi/2)sin(n\pi/2)}{mn[(m^2/L^2)+(n^2/L^2)]^2} \tag{4.4}$$

$$M_{max} = \frac{16q_0}{\pi^4} \sum_{m=1,3,5}^{\infty} \sum_{n=1,3,5}^{\infty} \frac{[(m^2/L^2)+\upsilon(n^2/L^2)]}{mn[(m^2/L^2)+(n^2/L^2)]^2} sin\frac{m\pi x}{L} sin\frac{n\pi x}{L} \tag{4.5}$$

$$\sigma_{x,max} = \frac{6M_{max}}{t^2} \text{ [27]} \tag{4.6}$$

w_{max} is the maximum vertical deflection (at the center of the plate).

M_{max} is the maximum bending moment per unit length (at the center of the plate).

$\sigma_{x,max}$ is the maximum stress (at the center of the plate).

q_0 is the distributed load. Its value had to be assumed by means of a simplification: first the plate has been assumed uniform and without the central hole; therefore the stress applied at the center of the plate (caused by the reactor weight and, during the test, by the thrust) has been extended to the entire surface and summed to the stress caused by the weight of plate itself. The assumed weight applied at the center before the discharge test is ~51.4 kg (which is the sum of reactor, feeding line, bolts and flange weights); the thrust exerted during the discharge test is 2500 N and, since it points down, it must be subtracted to the applied weight.

D is the flexural rigidity. In our case it is equal to:

$$D = \frac{Et^3}{12(1-\upsilon^2)} = 70.808\ kN \cdot m \text{ [27]} \tag{4.7}$$

t is the plate thickness, equal to 16 mm.

E is the elastic modulus of the column material. The value for C40 steel has been used (190 GPa).

υ is the Poisson's ratio of the plate material. The value for C40 steel has been used (0.29) [28].

L is the plate edge length, equal to 700 mm.

The found results of the Navier's model are:

- *Without thrust*:
  - $w_{max} = 0.108\ mm$
  - $M_{max} = 184\ N$
  - $\sigma_{x,max} = 4.32\ MPa$
- *With thrust*:
  - $w_{max} = 0.344\ mm$
  - $M_{max} = 586\ N$
  - $\sigma_{x,max} = 13.74\ MPa$

It is evident that the maximum vertical deflection of the plate is almost negligible for both cases: if related to the side length of the plate, it yields a deformation of only 0.015% for the

case without thrust and 0.049% for the case with thrust. Since, as previously stated, the bending at the corners of the actual plate should be even less than the one calculated with Navier's model, it is safe to assume that the loads on the lower plate should not affect the test in any significant way.

Additional checks have been made by means of finite element analyses using MSC Nastran and Patran software. These analyses have been made for configurations both with and without thrust.

In the first series of analyses the exact same assumptions used to apply Navier's model have been replicated: a rectangular steel plate without holes and simply supported along its edges has been simulated. All loads and inputs are the same used in the analytical model.

As shown in the figures below, the plate without applied thrust presented a displacement of 0.109 mm and a stress of 4.29 MPa at its center: these results are very close to the ones calculated with Navier's model.

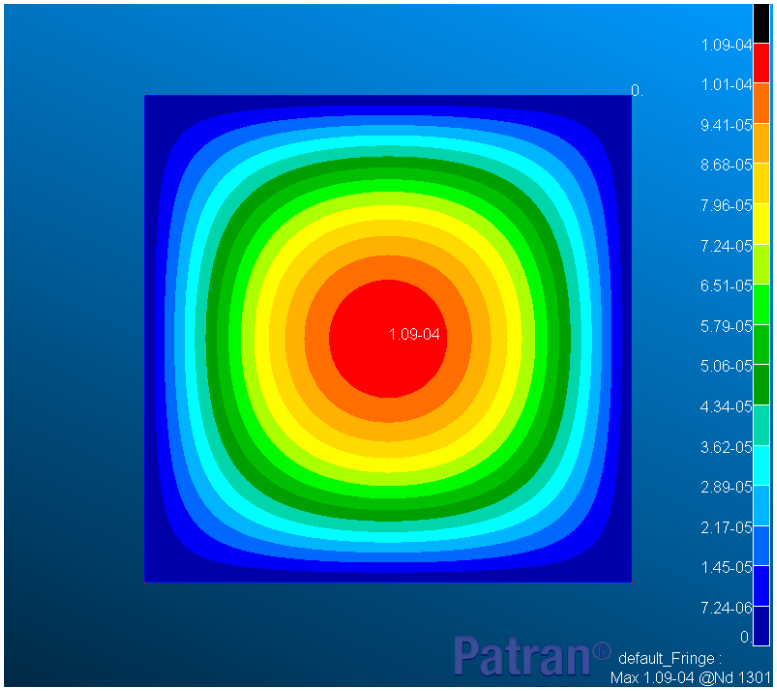

Figure 4.38 - Lower plate displacements, expressed in meters (supported edges, no hole, no thrust).

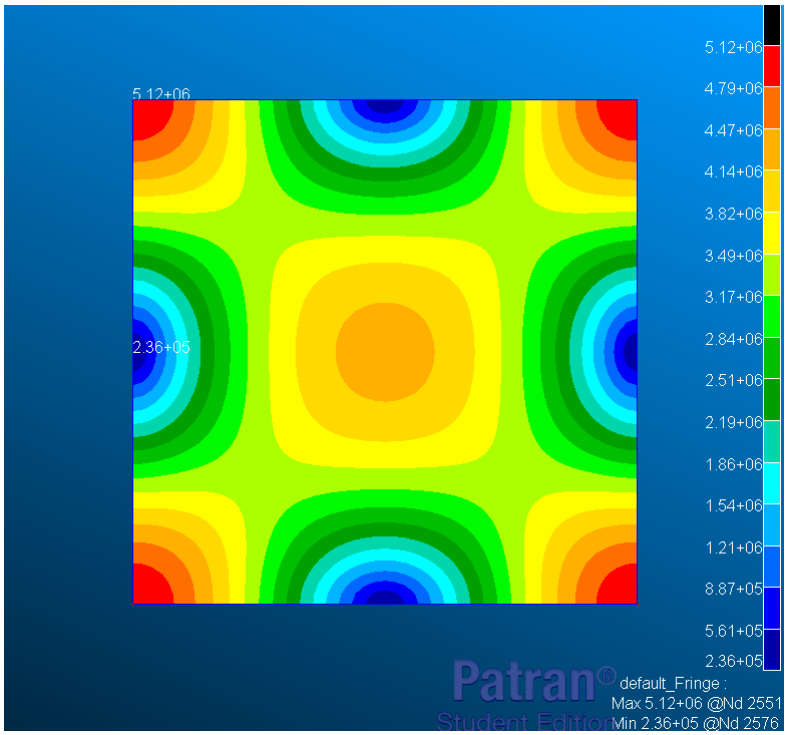

Figure 4.39 - Lower plate stresses, expressed in Pascal (supported edges, no hole, no thrust).

The analysis of the plate with applied thrust also provided results very similar to the ones found with Navier's model: 0.345 mm of displacement and 13.64 MPa of stress at the center (see figures below).

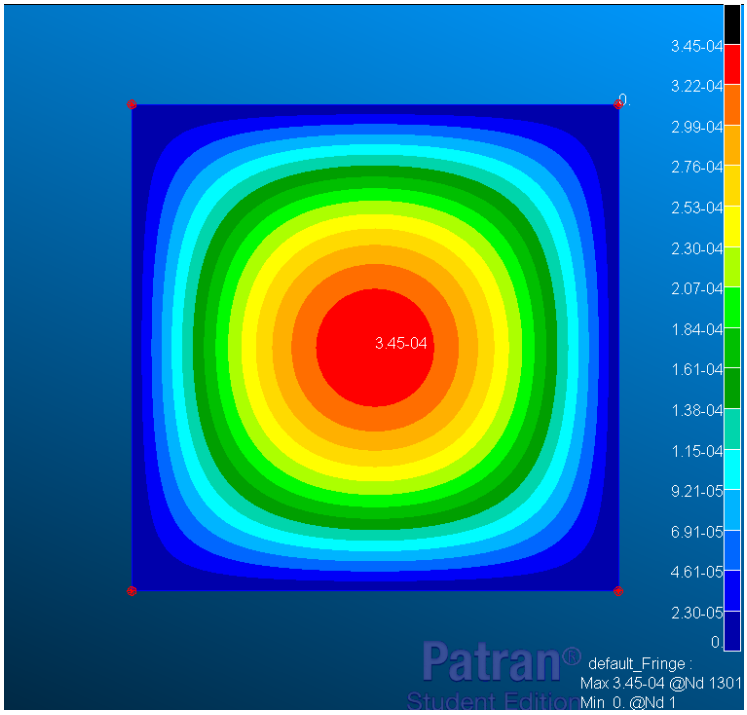

Figure 4.40 - Lower plate displacements, expressed in meters (supported edges, no hole, with thrust).

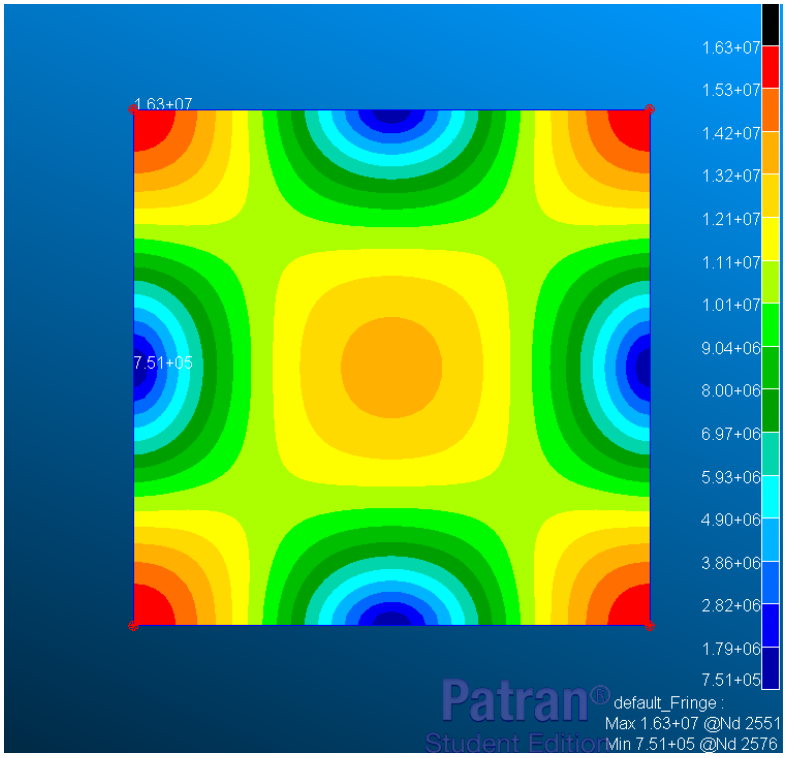

Figure 4.41 - Lower plate stresses, expressed in Pascal (supported edges, no hole, with thrust).

It is therefore evident that the analytical solution and the finite element analysis are coherent with each other; for this reason, further finite element analyses should give reliable results.

The next analyses aim to describe a system as close as possible to the actual lower plate: a square surface fixed at its corners, with a hole at its center and with two flanges applying the loads around the hole.

For the plate without applied thrust (see figures below), the maximum displacement occurs around the central hole and it is equal to 0.0132 mm, much lower than the value found with the previous models (as expected). The stresses are also less severe: they are maximum near the junctions with the upper columns at the corners, assuming values of 2.99 MPa. Still, the main aspect to notice is that there are pretty much no stresses nor displacements in the zones around the load cells at the corners, which means that their measurements should not be affected.

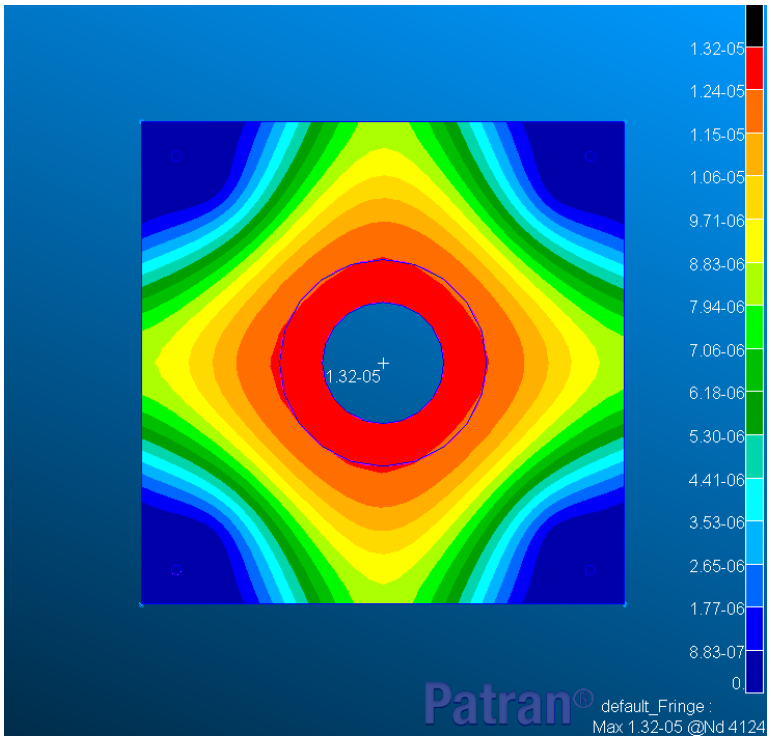

Figure 4.42 - Lower plate displacements, expressed in meters (no thrust).

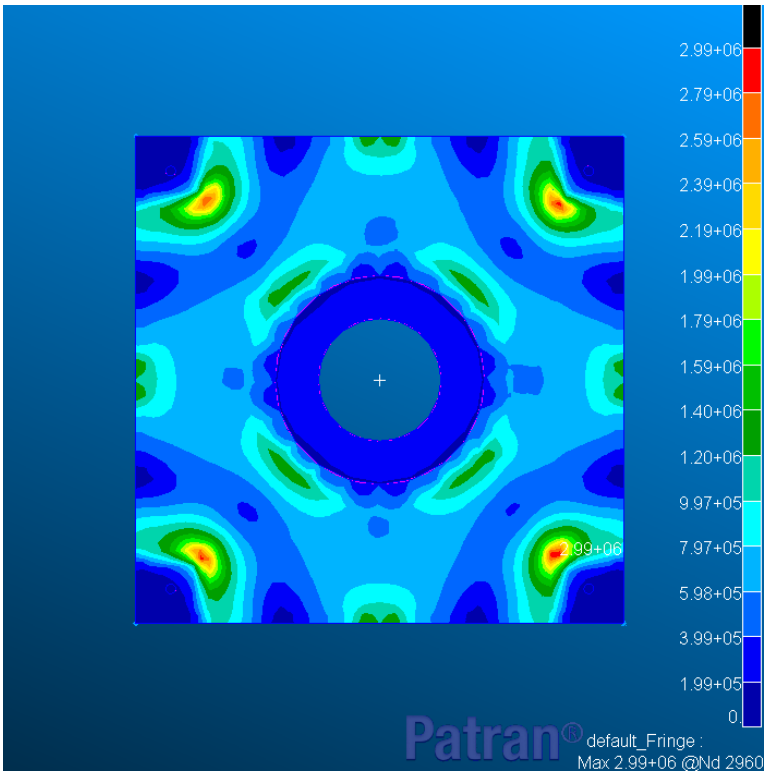

Figure 4.43 - Lower plate stresses, expressed in Pascal (no thrust).

Similar conclusions can be also drawn for the plate with applied thrust (see figures below): only the absolute values and directions of displacements and stresses are different. The maximum displacement is equal to 0.295 mm and the maximum stresses are equal to 5.55 MPa. Just like the previous case, the load cells are not affected.

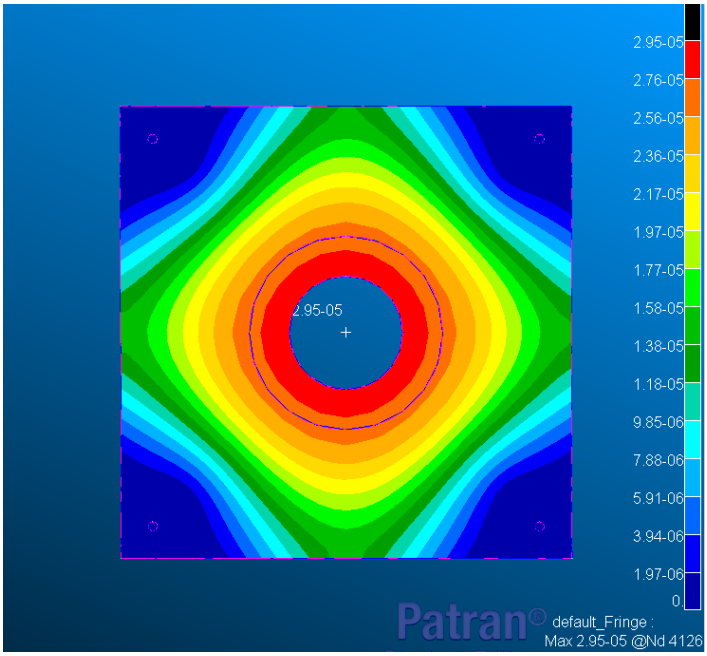

Figure 4.44 - Lower plate displacements, expressed in meters (with thrust).

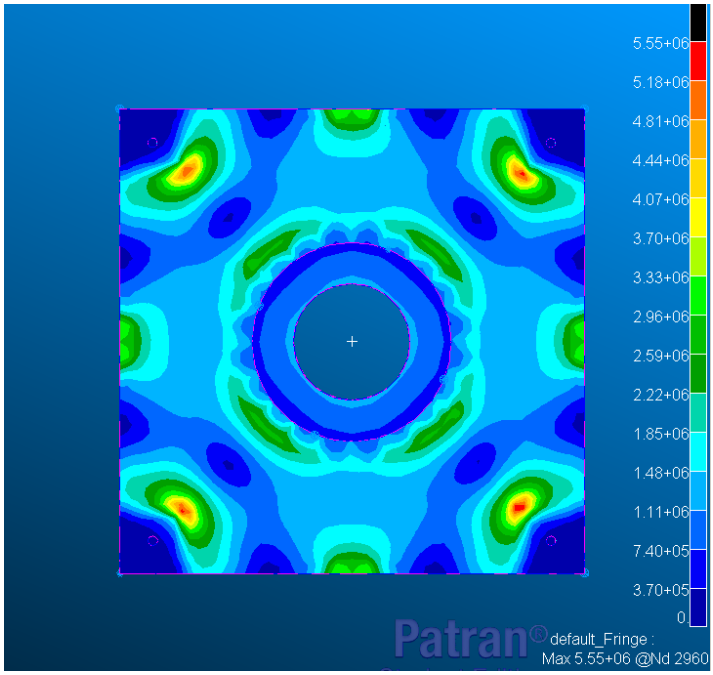

Figure 4.45 - Lower plate stresses, expressed in Pascal (with thrust).

Similar considerations have been also made for the **upper plate** with the filled water tank on top of it. In this other instance, the results found with Navier's model are:

- $w_{max} = 1.815\ mm$
- $M_{max} = 113\ N$
- $\sigma_{x,max} = 27.07\ MPa$

This time the bending found with Navier's model is a bit higher, but still very low: if related to the side length of the plate, it yields a deformation of 0.284%, which is still negligible. Bending is also not very consequential for the upper plate because it does not affect the load cells.

Just like the lower plate case, the first analysis replicates layout, loads and inputs of the Navier's model: a uniformly loaded rectangular steel plate without ribs and simply supported along its edges has been simulated (see figures below). The found displacement and stress at the center are respectively 1.82 mm and 26.86 MPa, which are both very close to the ones calculated with the analytical model.

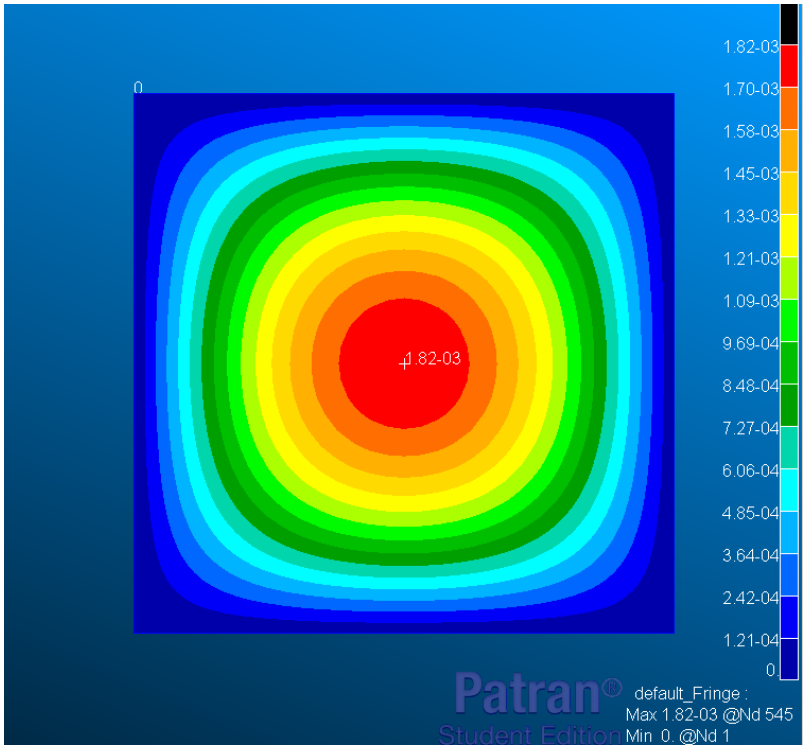

Figure 4.46 - Upper plate displacements, expressed in meters (supported edges, no ribs).

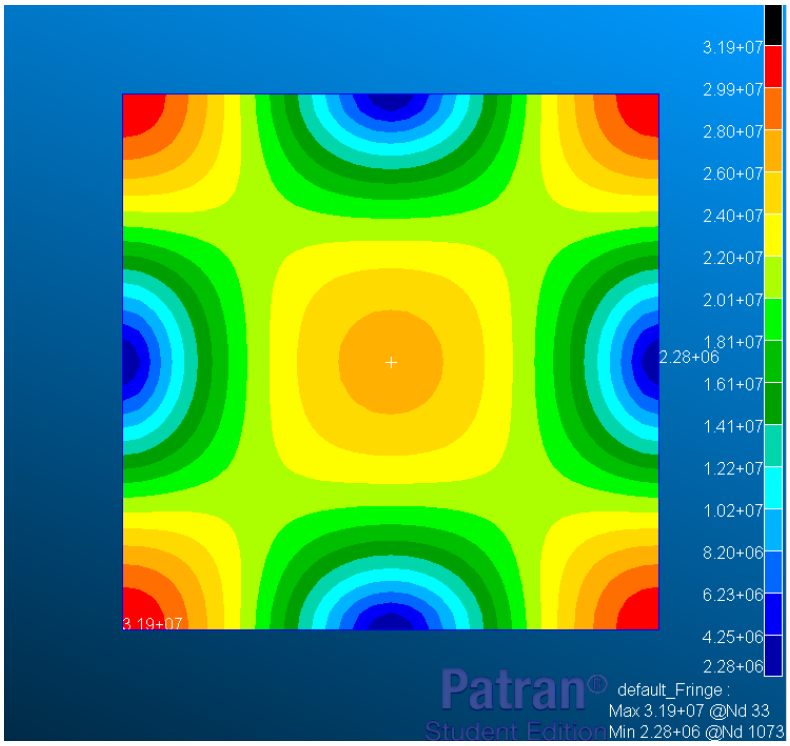

Figure 4.47 - Upper plate stresses, expressed in Pascal (supported edges, no ribs).

Again, Navier's model and the finite element analysis produce coherent results, confirming the reliability of further simulations.

Thus, a system as close as possible to the actual upper plate is then simulated: a square surface fixed at its corners, with an applied load equal to the weight of the filled water tank and with 2 crossed ribs on the bottom face (see also figures below).

Unlike the lower plate case, the found displacement at the center (equal to 1.87 mm) is very close to the one found with the approximated models, even slightly larger. Its value is still low though and should not cause issues. The stresses are also higher than those found in the previous analysis: in the plate they reach their maximum near the corners (64.07-68.65 MPa), while the absolute maximum values are reached at the lower edges of the ribs (up to 91.7 MPa).

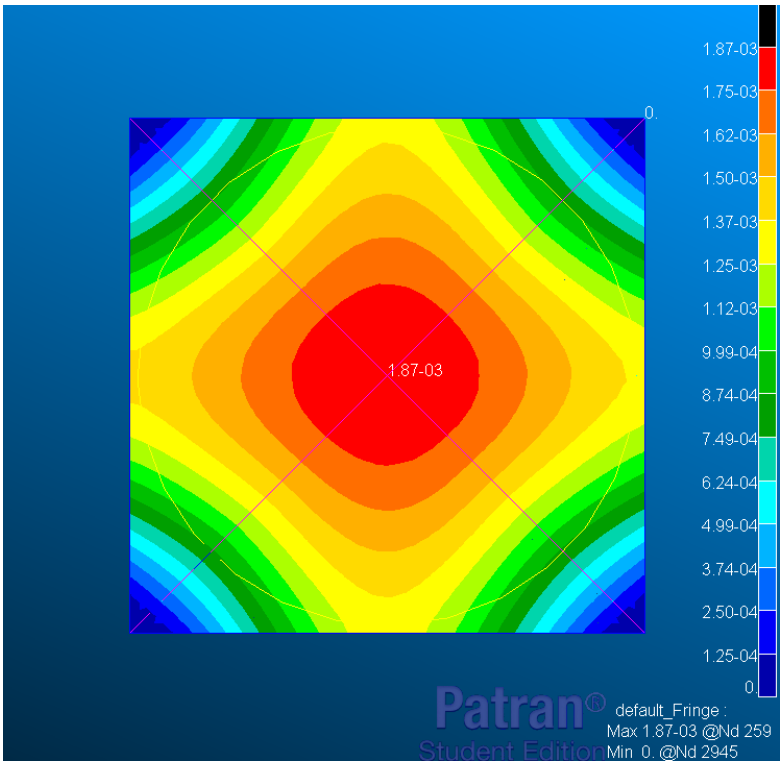

Figure 4.48 - Upper plate displacements, expressed in meters.

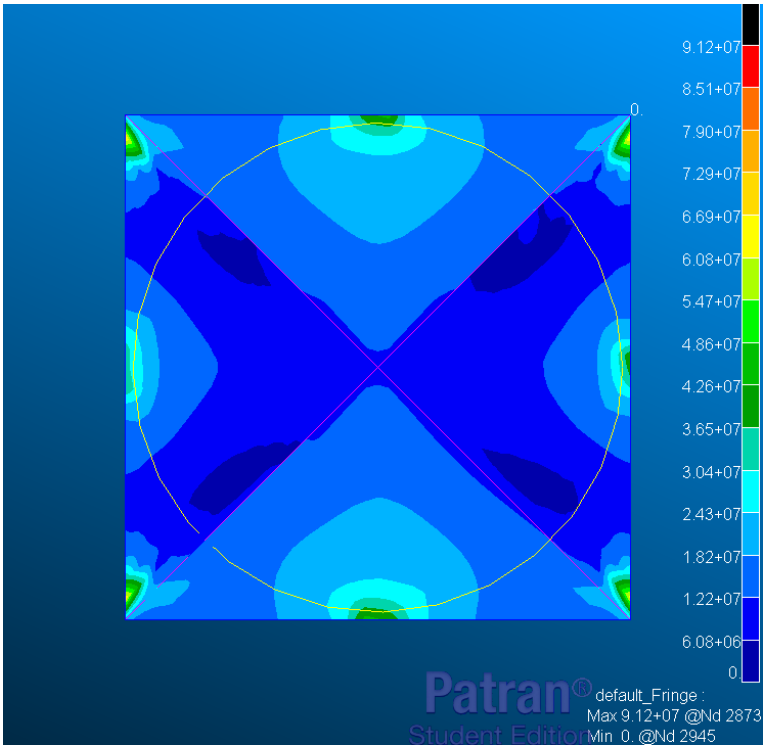

Figure 4.49 - Upper plate stresses, expressed in Pascal.

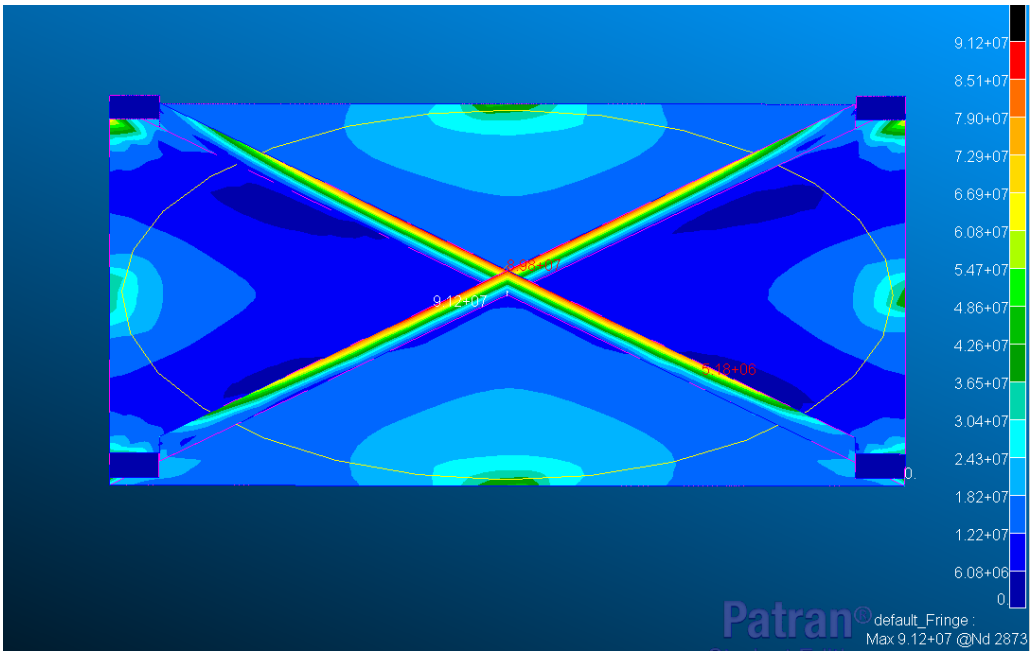

Figure 4.50 - Upper plate ribs stresses, expressed in Pascal.

The reason for the larger values of displacements and stresses found in the last analysis must be the use of constraints at the corners instead of simple support along the edges. The ribs cannot be the cause because they are meant to reinforce the structure, not to make it bend more. The following analysis aims to verify the hypothesis: the same layout of the previous simulation is used, only with simply supported edges instead of constraints at the corners (see also figures below). The found displacement at the center is 0.840 mm, lower than both the previous cases. The maximum stresses on the plate are also lower, reaching their maximum values at the corner zones (25.45-26.72 MPa). Lastly, the stresses in the ribs are lower compared to the previous analysis, reaching a maximum of about 55.4 MPa. Therefore, these results confirm the hypothesis: corner constraints cause an increase of displacements and stresses compared to simply supported edges. The results of the previous analyses are therefore coherent.

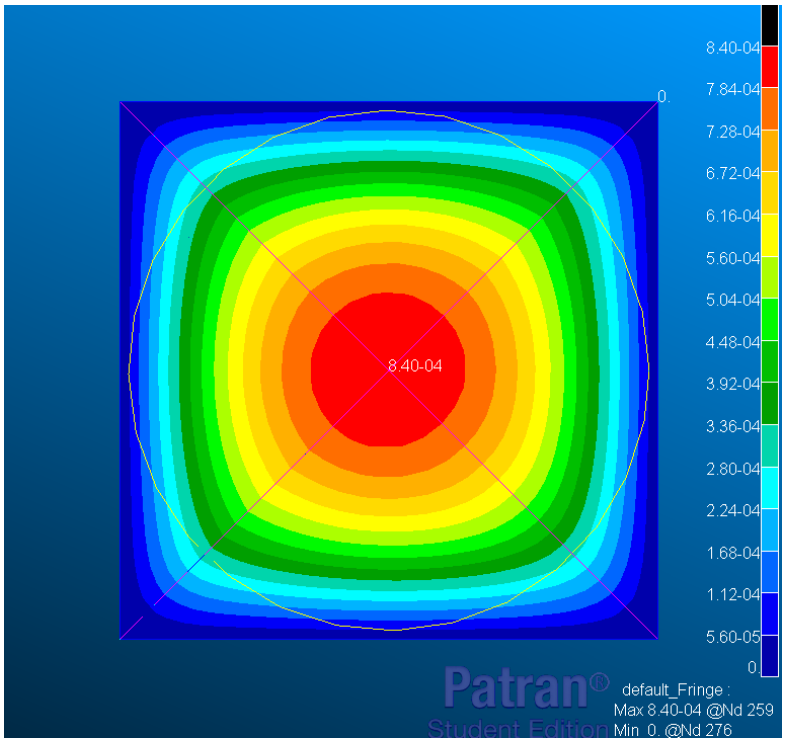

Figure 4.51 - Upper plate displacements, expressed in meters (supported edges, with ribs).

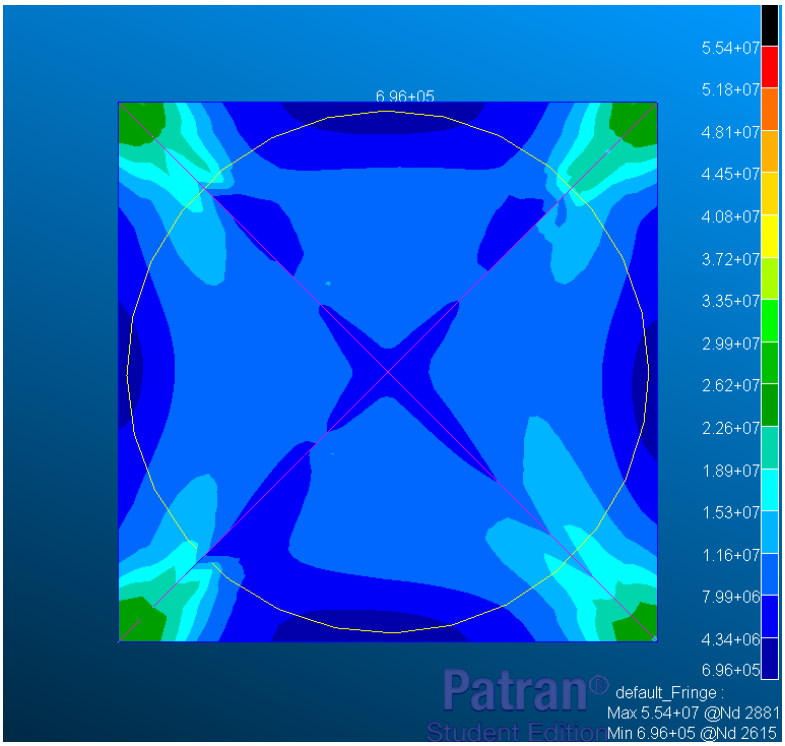

Figure 4.52 - Upper plate stresses, expressed in Pascal (supported edges, with ribs).

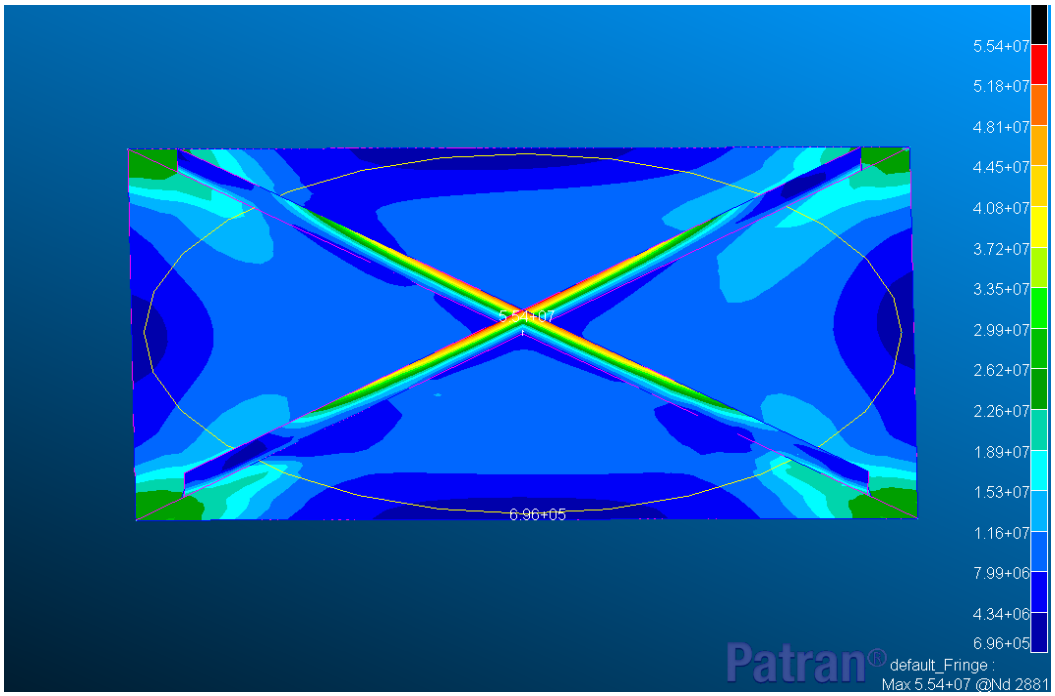

Figure 4.53 - Upper plate ribs stresses, expressed in Pascal (supported edges, with ribs).

In conclusion, it is worth to notice that not only the displacements of the plates are almost negligible, but that the stresses are also well below the yield strength of the plates material (540 MPa for C40 steel [30]).

Chapter 5

Status of the Project and Future Development

At the time when this thesis is submitted, the sounding rocket development is still in progress: its general layout and most of its parts are already defined, but it still requires refinements of some components (such as structures and fins). That said, it is complete enough to allow a definitive design of the test benches. The latter are almost ready: the components to purchase have been already ordered and the custom ones are being manufactured. Within a few days or weeks, the benches are expected to be assembled. The actual tests will require a bit more though: first the systems need to be refined and reach a definitive configuration. For the fluidic line, which should be tested before the catalytic reactor (see chapter 3), the only ready parts are the composite cylinder and the end domes of the oxidizer tank; the commercial components (pressurizer tank, valves, tubes, connectors, regulators, burst disk, cavitating Venturi, actuators and sensors) have been purchased and should be soon available. The catalytic reactor has reached a definitive configuration, but most of its parts have not been manufactured yet. When the needed components are ready, the fluidic line tests can start (see chapter 3); after them the oxidizer tank will undergo a breaking test: it will be pressurized until it bursts in order to find its exact failure point. Because the first tank will be broken, another one must be built. Other structural tests will be performed to verify the resistance of bonded and screwed joints. After the fluidic line tests, the catalytic reactor tests will be carried out (see chapter 3). Therefore, test firings of the entire motor will be performed on the horizontal bench. The recovery system must also be tested: tests for the floats have been already done, others are planned for the other parts (i.e. parachutes). The launch ramp for the rocket has been already designed, however it requires refinements and must be built. When all the tests are completed successfully, when all

the remaining refinements are done, when the launch ramp is ready and when avionics and payload are ready (see section 2.1), the rocket can be launched. The launch is planned for the beginning of 2020. The launch site will likely be in Sardinia.

Chapter 6

Conclusions

The work started with a dissertation about the characteristics of sounding rockets, hybrid rocket systems and test benches.

Then, a description of the sounding rocket has been provided.

It is 5.450 m long and with an external diameter of 195.82 mm. The nosecone is 917 mm long and has a Von Karman profile. The rocket has 4 tail fins with a symmetrical diamond profile; each fin has a span from tip to root of 160 mm, a root chord of a 200 mm, a tip chord of 100 mm and a sweep back angle of the trailing edge of 0°. The exterior is almost entirely made of carbon fiber reinforced epoxy composite.

The rocket is propelled by a hybrid system using hydrogen peroxide as oxidizer and a paraffin grain as fuel; it exerts a thrust of about 5 kN and has burning time of 20-30 s. The oxidizer is stored inside a 45 L tank whose perimetral wall is integrated into the external composite cylinder. A fluidic line injects the oxidizer into the motor by means of a pressure-fed pressurization system using N_2 as pressurizer. The motor is composed by a catalytic reactor, which decomposes the hydrogen peroxide into oxygen and water, a combustion chamber, where the decomposed oxidizer reacts with the fuel grain, and a convergent-divergent nozzle, which accelerates the exhaust gas to supersonic speed.

A recovery system is kept inside a bay right below the nosecone: it consists in a main parachute, a drogue parachute and a floating system; its function is to ensure the retrieval of the rocket at the end of the mission.

Overall the rocket has an estimated dry mass of about 75 kg. It reaches about 135 kg when the tanks are filled.

Then goals, requirements and procedures of the test campaign have been described.

First the fluidic line tests must be performed: they start with a calibration of the pressurization system that should verify the correct functioning of the pressurization system and the tightness of tanks and fluidic line components. Then discharge tests with distilled water are carried out in order to simulate the fluidic line functioning during flight. Lastly, discharge tests are repeated using the actual oxidizer (hydrogen peroxide). All these tests are performed on a vertical bench kept inside a container.

The second part of the campaign consists in testing the catalytic reactor on another vertical bench: hydrogen peroxide is injected into the catalytic bed, which decomposes it; the product gasses are then expelled from a nozzle identical to the one of the actual motor. 4 load cells measure the thrust developed by the system, which is expected to be about 2500 N. Safety measures and procedures are detailed for both tests.

Afterwards, the design and sizing processes of both test benches have been explained.

The fluidic line test bench consists in a stainless-steel frame built with Fischer SaMontec components for plant engineering. The frame consists in 4 mounting channels stiffened by other transversal channels of the same type. The vertical channels are 1900 mm tall. Pipe clamp collars are fastened to 4 of the transversal channels and clamped around the tanks in order to keep the entire fluidic line stable and raised from the base. The tanks themselves are not stacked on top of each other, but are placed side by side, with a slightly modified gas line connecting them at the top of the structure. The base plate is a 750×850 mm steel rectangle that must be custom-made. Overall, the stand with the fluidic line is almost 2264 mm tall and with an estimated mass of about 167.9 kg when the tanks are filled. All the loaded junctions have been verified and are expected to support the applied weights without issues; indeed, the most

stressed parts are the T-head bolts connecting the tanks to the transversal channels and they withstand the loads with an estimated margin of safety of 9.24.

The catalytic reactor test bench uses a specifically made reactor closed by two flanges kept tight by 12 threaded bars; a nozzle akin to the one of the rocket motor is placed inside the lower flange. In the test stand, the reactor is hanged to a steel plate by means of a flange. Twelve nuts fastened on the threaded bars are used to fix the system to the flange. The plate with the hanged reactor is a 700×700 mm square and it is sustained by 4 steel tubular columns. On top of the plate, at its corners, other 4 similar columns sustain another steel plate on top of which a 220 L water tank is placed. All the columns have a 40×40 mm square cross section. The upper plate is a 640×640 mm square reinforced by 2 diagonal ribs at its lower face. The fluidic feeding system is placed over the reactor, between the two plates. Between the lower plate and the lower columns 4 load cells are placed to measure loads. A steel deflector is placed under the nozzle of the reactor in order to deviate the exhaust sideways. The overall height of the stand (without the water tank) is 1691 mm and its estimated mass is 169.5 kg. The estimated mass of the upper part of the stand (which rests on the four load cells) is 140.7 kg without the water tank. The water tank must be filled with about 159 L to reach 300 kg: this extra weight is needed to counterbalance the 2500 N thrust of the reactor. The load cells measure the difference between the thrust and the weight of the structure resting on top of them (including the water tank).

The columns have been verified by finding their Euler's critical loads; all of them withstand the applied loads with very large margins of safety: 2005.39 for the lower columns and 2847.61 for the upper columns. The plates have been first verified using an approximated analytical model (Navier's solution); then a more in-depth finite element analysis has been made. Both plates withstand the stresses and do not bend by a significant amount: the maximum found displacement is 0.295 mm for the lower plate and 1.82 mm for the upper plate. In particular, the lower plate does not exhibit bending in the zones where the load cells are placed, which is important because it could negatively affect their measurements.

Lastly, the status of the project and its future development are discussed.

The test benches will be ready within a few days or weeks. Most of the components to test have reached a definitive design and some of them (i.e. the oxidizer tank and most fluidic line parts)

have been already purchased. Tests are expected to be carried out within 1 or 2 months. The rocket is expected to fly at the beginning of 2020.

References

[1] P. Zanella, *Sviluppo di un Codice per la Simulazione ed Ottimizzazione di Sounding Rockets,* Padova, Italia, Università degli Studi di Padova, 2012.

[2] E. Ceglia, *European Users Guide to Low Gravity Platform,* ESA, 2005.

[3] F. Barato, *Numerical and Experimental Investigation of Hybrid Rocket Motors Transient Behavior,* Padova, Italia, Università degli Studi di Padova, 2013.

[4] E. Lunde, *https://www.mynewsdesk.com/no/nammo/pressreleases/nucleus-completes-successful-first-launch-2721547*, 27 September 2018.

[5] *https://www.esa.int/Our_Activities/Space_Transportation/Norway_takes_the_lead_in_hybrid_propulsion*, 27 September 2018.

[6] *https://www.esa.int/Our_Activities/Space_Transportation/Norway_s_hybrid_rocket_motor_sets_new_record*, 6 July 2018.

[7] *http://www.aeroconsystems.com/ts_pics/ts_pics.htm*.

[8] *https://aeroconsystems.com/cart/test-stand-pictorial*.

[9] J.-Y. Lestrade, P. Prévot, J. Messineo, J. Anthoine, S. Casu and B. Geiger, *Development of a Catalyst for Highly Concentrated Hydrogen Peroxide,* 2016.

[10] A. Cervone, L. Torre, L. d'Agostino, A. J. Musker, G. T. Roberts, C. Bramanti and G. Saccoccia, *Rockets, Development of Hydrogen Peroxide Monopropellant.*

[11] R. J. Kenny, M. D. Mose, J. Hulka and G. Jones, *Cold Flow Testing for Liquid Propellant Rocket Injector Scaling and Throttling,* Sacramento, 2006.

[12] J. F. M. Demoly, O. Vielpeau, A. Treilhes, N. Rizzo, J. Rèbre, J. Mulpas, V. Jacaranda-Lakiss-Marques, E. Jean-Bart, R. Mercier, B. Fiorina and O. Gicquel, *Design of the Feed System of a Hybrid Rocket Engine,* 2013.

[13] M. Guerra, *Development of a Hydrogen Peroxide Catalytic Bed Numerical Model Supported by Experimental Data.*

[14] G. Broggiato, *Serbatoi a Parete Sottile.*

[15] AK Steel, *316/316L Stainless Steel.*

[16] Extreme Bolt & Fastener, *https://www.extreme-bolt.com/inconel-button-head-cap-screws.html*.

[17] L. Bertini, *Lezioni su "Boiler and Pressure Vessel" - Introduzione al Dimensionamento ed alla Verifica di Recipienti in Pressione (Boiler and Pressure Vessel)*.

[18] High Temp Metals, *https://www.hightempmetals.com/techdata/hitempInconel718data.php*.

[19] Dilanda, *Catalogo Dimensionale O-Ring.*

[20] Parker Praedifa, *O-Ring Handbook.*

[21] Fischer SaMontec, *Catalogo Generale Sistemi di installazione SaMontec.*

[22] S. Baragetti, *Progettazione dei Sistemi Meccanici - Calcolo delle Unioni Bullonate: Verifiche al Taglio.*

[23] P. Gelfi, *Teoria e Progetto delle Costruzioni in Acciaio.*

[24] Sidastico Spa, *https://www.sidastico.com/en/steels-for-construction-special-steels-structural-steel-construction-steel/dd11-mechanical-properties/*.

[25] Gefran, *Gefran CU - Compact Load Cell for Compression Applications*.

[26] Pack Services, *https://www.packservices.it/serbatoi-acqua/43812-40565-serbatoi-per-acqua-in-plastica-pe-cilindrici-verticali-alti-vert.html#/9328-capacita-220_lt*.

[27] T. H. G. Megson, *Aircraft Structures for Engineering Students*, 4th ed., Elsevier Aerospace Engineering Series, 2007.

[28] *https://www.makeitfrom.com/material-properties/EN-1.0511-C40-Non-Alloy-Steel*.

[29] *https://www.oppo.it/tabelle/aree_mom_inerzia.htm*.

[30] Trafileria A.Mauri e Figli S.p.A., *C40 Non-alloy High Grade Steel.*